Lateral Torsional Buckling of Wood Beams

by

Qiuwu Xiao

Thesis submitted to the
Faculty of Graduate and Postdoctoral Studies
in partial fulfillment of the requirements for the degree of
Master of Applied Science
in Civil Engineering

Under the auspices of the Ottawa-Carleton Institute for Civil Engineering

Departments of Civil Engineering
University of Ottawa
April 2014

Abstract

Structural wood design standards recognize lateral torsional buckling as an important failure mode, which tends to govern the capacity of long span laterally unsupported beams. A survey of the literature indicates that only a few experimental programs have been conducted on the lateral torsional buckling of wooden beams. Within this context, the present study reports an experimental and computational study on the elastic lateral torsional buckling resistance of wooden beams.

The experimental program consists of conducting material tests to determine the longitudinal modulus of elasticity and rigidity modulus followed by a series of 18 full-scale tests. The buckling loads and mode shapes are documented. The numerical component of the study captures the orthotropic constitutive properties of wood and involves a sensitivity analysis on various orthotropic material constants, models for simulating the full-scale tests conducted, a comparison with experimental results, and a parametric study to expand the experimental database.

Based on the comparison between the experimental program, classical solution and FEA models, it can be concluded that the classical solution is able to predict the critical moment of wood beams. By performing the parametric analysis using the FEA models, it was observed that loads applied on the top and bottom face of a beam decrease and increase its critical moment, respectively. The critical moment is not greatly influenced by moving the supports from mid-span to the bottom of the end cross-section.

Acknowledgement

Special thanks go to my supervisors, Drs. Ghasan Doudak and Magdi Mohareb. Without their great support, time, patience and advice, I would never have been able to complete this project.

I would also like to thank my fellow graduate students, Mr. Daniel Lacroix and Ms. Ghazanfarah Hafeez for the guidance and help, especially in conducting the experimental work. Also, thank you to Mr. Kevin Rocchi, Mr. Kenny Kwan. Mr. Christian Viau and Mr. Mohammadmehdi Ebadi for their support.

My deepest thanks go to my parents for financial and moral supports, and for always encouraging and believing in me to accomplish my academic goals.

Table of Contents

List of Tables

List of Figures

Chapter 1

Introduction

1.1. General

In modern day design, engineered wood products have allowed for larger spans than those obtained from traditional solid sawn joists or beams. This, coupled with the fact that economy in beam designs favors narrow and deep beams, have led to an increased probability of failure in lateral buckling. Traditionally, these types of failure modes have been prevented by limiting the depth to width aspect ratios and by providing restraints at the boundary conditions. Such prescriptive provisions do not, for example, include information about the length of the member and can therefore only be applicable in limited design cases. The Canadian Standard on engineering design in wood (CSA, 2009) includes provisions for beam lateral stability. Those provisions are provided for glulaminated (glulam) beams but the provisions are extended to solid sawn lumber and timber beams even though no research studies have been conducted to verify the validity of these provisions. The current study aims to investigate the behavior of timber beams with dimensions that makes them vulnerable to lateral torsional buckling failures, and explores whether existing theories for lateral torsional buckling are applicable to a non-isotropic material such as wood.

1.1.1. Wood Material Properties

Due to the tree's growth pattern, wood is an anisotropic material but can generally be considered as an orthotropic material (Isopescu, 2012). Properties in a wood member are given in the longitudinal, radial and tangential directions with distinctly different mechanical properties in each direction. The longitudinal axis is a direction which is parallel to the wood grain, the radial axis in perpendicular to the longitudinal axis and normal to the growth rings, the tangential axis is perpendicular to the grain and tangential to the growth rings (FPL, 2010), as shown in Figure 1.1. The mechanical properties along the longitudinal axis are generally stronger than the other two axes, however, the differences between radial and tangential axis can be considered insignificant (Isopescu, 2012).

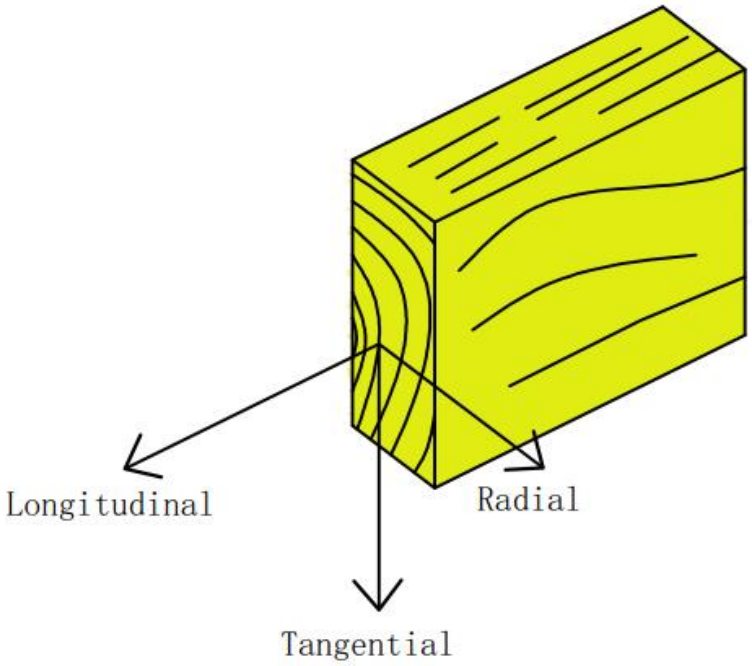

Figure 1.1 Three principle axes of wood member

In order to describe the material properties of wood, twelve constants need to be defined, namely, three Moduli of elasticity (E), three Shear moduli (G) and six Poisson's ratios (v) (FPL, 2010). The relationship between strain and stress parameters of isotropic, orthotropic and anisotropic materials are presented in the following Equations (1.1), (1.2) and (1.3), respectively (Simulia, 2011).

$$\begin{Bmatrix} \varepsilon_{LL} \\ \varepsilon_{RR} \\ \varepsilon_{TT} \\ \gamma_{LR} \\ \gamma_{LT} \\ \gamma_{RT} \end{Bmatrix} = \begin{bmatrix} \frac{1}{E} & -\frac{v}{E} & -\frac{v}{E_T} & 0 & 0 & 0 \\ -\frac{v}{E} & \frac{1}{E} & -\frac{v}{E} & 0 & 0 & 0 \\ -\frac{v}{E} & -\frac{v}{E} & \frac{1}{E} & 0 & 0 & 0 \\ 0 & 0 & 0 & \frac{1}{G} & 0 & 0 \\ 0 & 0 & 0 & 0 & \frac{1}{G} & 0 \\ 0 & 0 & 0 & 0 & 0 & \frac{1}{G} \end{bmatrix} \begin{Bmatrix} \sigma_{LL} \\ \sigma_{RR} \\ \sigma_{TT} \\ \tau_{LR} \\ \tau_{LT} \\ \tau_{RT} \end{Bmatrix} \tag{1.1}$$

$$\begin{Bmatrix}\sigma_{LL}\\ \sigma_{RR}\\ \sigma_{TT}\\ \sigma_{LR}\\ \sigma_{LT}\\ \sigma_{RT}\end{Bmatrix}=\begin{bmatrix}D_{LLLL} & D_{LLRR} & D_{LLTT} & 0 & 0 & 0\\ D_{LLRR} & D_{RRRR} & D_{RRTT} & 0 & 0 & 0\\ D_{LLTT} & D_{RRTT} & D_{TTTT} & 0 & 0 & 0\\ 0 & 0 & 0 & D_{LRLR} & 0 & 0\\ 0 & 0 & 0 & 0 & D_{LTLT} & 0\\ 0 & 0 & 0 & 0 & 0 & D_{RTRT}\end{bmatrix}\begin{Bmatrix}\varepsilon_{LL}\\ \varepsilon_{RR}\\ \varepsilon_{TT}\\ \gamma_{LR}\\ \gamma_{LT}\\ \gamma_{RT}\end{Bmatrix} \tag{1.2}$$

$$\begin{Bmatrix}\sigma_{LL}\\ \sigma_{RR}\\ \sigma_{TT}\\ \sigma_{LR}\\ \sigma_{LT}\\ \sigma_{RT}\end{Bmatrix}=\begin{bmatrix}D_{LLLL} & D_{LLRR} & D_{LLTT} & D_{LLLR} & D_{LLLT} & D_{LLRT}\\ D_{LLRR} & D_{RRRR} & D_{RRTT} & D_{RRLR} & D_{RRLT} & D_{RRRT}\\ D_{LLTT} & D_{RRTT} & D_{TTTT} & D_{TTLR} & D_{TTLT} & D_{TTRT}\\ D_{LLLR} & D_{RRLR} & D_{TTLR} & D_{LRLR} & D_{LRLT} & D_{LRRT}\\ D_{LLLT} & D_{RRLT} & D_{TTLT} & D_{LRLT} & D_{LTLT} & D_{LTRT}\\ D_{LLRT} & D_{RRRT} & D_{TTRT} & D_{LRRT} & D_{LTRT} & D_{RTRT}\end{bmatrix}\begin{Bmatrix}\varepsilon_{LL}\\ \varepsilon_{RR}\\ \varepsilon_{TT}\\ \gamma_{LR}\\ \gamma_{LT}\\ \gamma_{RT}\end{Bmatrix} \tag{1.3}$$

Where the definition of variables are shown as:

$$D_{LLLL}=E_L\left(1-\nu_{RT}\nu_{TR}\right)\Upsilon,$$

$$D_{RRRR}=E_R\left(1-\nu_{LT}\nu_{TL}\right)\Upsilon,$$

$$D_{TTTT}=E_T\left(1-\nu_{LR}\nu_{RL}\right)\Upsilon,$$

$$D_{LLRR}=E_L\left(\nu_{RL}+\nu_{TL}\nu_{RT}\right)\Upsilon=E_R\left(\nu_{LR}+\nu_{TR}\nu_{LT}\right)\Upsilon,$$

$$D_{LLTT}=E_L\left(\nu_{TL}+\nu_{RL}\nu_{TR}\right)\Upsilon=E_T\left(\nu_{LT}+\nu_{LR}\nu_{RT}\right)\Upsilon,$$

$$D_{RRTT}=E_R\left(\nu_{TR}+\nu_{LR}\nu_{TL}\right)\Upsilon=E_T\left(\nu_{RT}+\nu_{RL}\nu_{LT}\right)\Upsilon,$$

$$D_{LRLR}=G_{LR},\ D_{LTLT}=G_{LT},\ D_{RTRT}=G_{RT},$$

And where $\Upsilon=1/\left(1-\nu_{LR}\nu_{RL}-\nu_{RT}\nu_{TR}-\nu_{TL}\nu_{LT}-2\nu_{RL}\nu_{TR}\nu_{LT}\right)$, E_i are moduli of elasticity, ν_{ij} are Poisson's ratios, G_{ij} are shear modulus, ε_{ij} are strains, γ_{ij} are engineering shear strains, σ_{ij} are stresses, and τ_{ij} are shear stresses, and where i and j are L, R and T directions. For example, E_L is the moduli of elasticity along the longitudinal direction, G_{LR} is the shear moduli about longitudinal and radial direction.

Linear elastic mechanical properties of orthotropic materials can be simplified as shown in Equation (1.4):

$$\begin{Bmatrix} \varepsilon_{LL} \\ \varepsilon_{RR} \\ \varepsilon_{TT} \\ \gamma_{LR} \\ \gamma_{LT} \\ \gamma_{RT} \end{Bmatrix} = \begin{bmatrix} \frac{1}{E_L} & -\frac{\nu_{RL}}{E_R} & -\frac{\nu_{TL}}{E_T} & 0 & 0 & 0 \\ -\frac{\nu_{LR}}{E_L} & \frac{1}{E_R} & -\frac{\nu_{TR}}{E_T} & 0 & 0 & 0 \\ -\frac{\nu_{LT}}{E_L} & -\frac{\nu_{RT}}{E_R} & \frac{1}{E_T} & 0 & 0 & 0 \\ 0 & 0 & 0 & \frac{1}{G_{LR}} & 0 & 0 \\ 0 & 0 & 0 & 0 & \frac{1}{G_{LT}} & 0 \\ 0 & 0 & 0 & 0 & 0 & \frac{1}{G_{RT}} \end{bmatrix} \begin{Bmatrix} \sigma_{LL} \\ \sigma_{RR} \\ \sigma_{TT} \\ \tau_{LR} \\ \tau_{LT} \\ \tau_{RT} \end{Bmatrix} \tag{1.4}$$

Due to the similarities in the material properties in the perpendicular-to-grain direction, the number of variables can be reduced to seven, where only moduli of elasticity along longitudinal direction, shear moduli along transverse are needed to obtain a reasonable description of the material. This is not only done to simplify the analysis but also because it is impossible to determine how the wood element is cut from the tree and how it will be oriented relative to the annual rings prior to its installation (Figure 1.2).

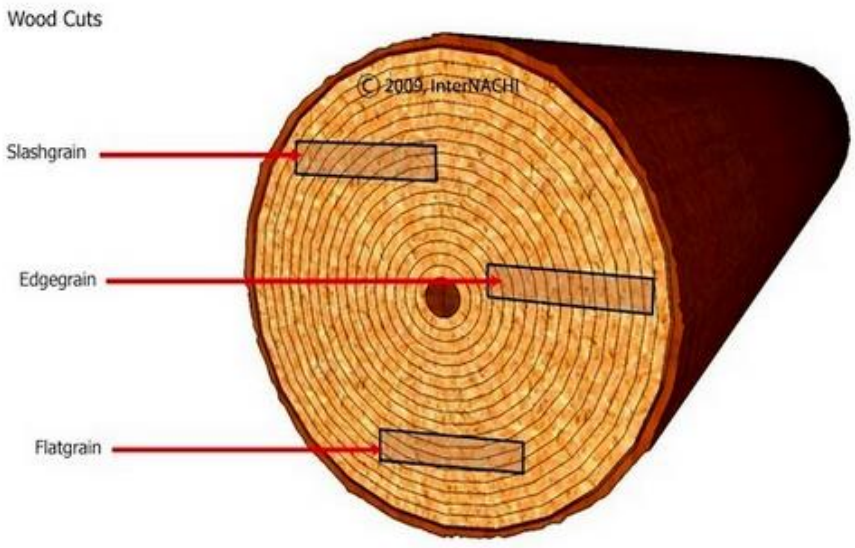

Figure 1.2 The three basic grain exposures of wood cuts
(Shepard and Gromicko, 2009)

1.1.2 The Classical Solution Lateral Torsional Buckling Failure

The lateral torsional buckling is the phenomena where an unrestrained beam or beam-column experiences simultaneous in-plane displacement, lateral displacement and twisting. A beam that is prone to a lateral torsional buckling failure would deform under an applied load or moment until a critical moment (M_{cr}) is reached, after which, a slight increment in the applied moment beyond the critical moment will create large lateral deformations.

The critical moment is a function of lateral and torsional stiffness, and is also affected by the boundary conditions, unbraced length, load patterns, and the dimension of the cross section. Figure 1.3 shows the buckling of a prismatic beam under the action of equal moments with simply-supported end conditions about the major axis, and Figure 1.4 shows the deformation of the internal cross-section.

Figure 1.3 Lateral torsional buckling of beam

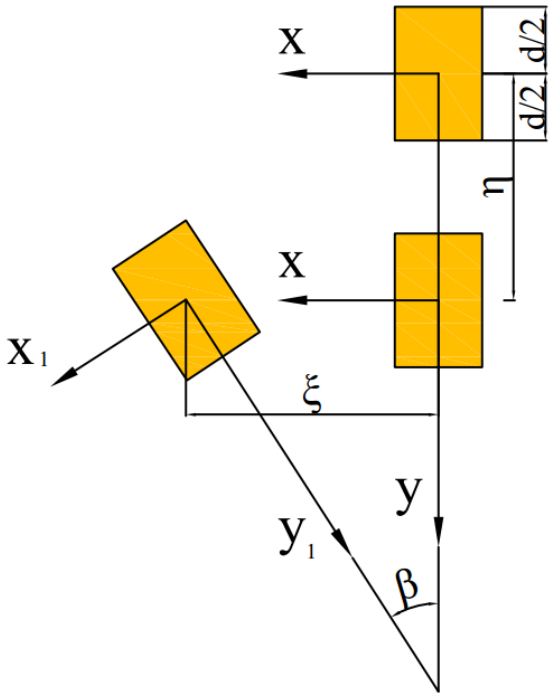

Figure 1.4 The deformation of internal cross-section in lateral torsional buckling

The lateral torsional buckling solution can be obtained from the energy expression (e.g. Trahair, 1993), as shown in Equation (1.5)

$$\pi_p = U + V \tag{1.5}$$

Where U is the internal strain energy due to the lateral buckling and twisting action of the beam, and V is the load potential energy gain. The expressions are presented in Equation (1.6) and (1.7) for a prismatic cross-section that is doubly symmetric and where the member is subjected to bending about the strong axis, and where the shear center is located at the same point as the centroid.

$$U = \frac{1}{2}\int_0^L EI_y \xi''^2 dz + \frac{1}{2}\int_0^L EC_w \beta''^2 dz + \frac{1}{2}\int_0^L GJ\beta'^2 dz \tag{1.6}$$

$$V = \int_0^L M_x(\mathrm{z})\beta(\mathrm{z})\xi''(\mathrm{z})\,\mathrm{dz} \tag{1.7}$$

Where ξ is the centroidal displacement along the x axis, and β is the rotation about the z axis,

C_w is the warping constant, J is Saint Venant Torsion constant, I_y is the moment of inertia in weak axis. Substituting Equation (1.6) and (1.7) into (1.5), results in the expression shown in Equation (1.8):

$$\pi_p = \frac{1}{2}\int_0^L EI_y \xi''^2 dz + \frac{1}{2}\int_0^L EC_w \beta''^2 dz + \frac{1}{2}\int_0^L GJ\beta'^2 dz + \int_0^L M_x \beta \xi'' \,\mathrm{dz} \tag{1.8}$$

There are two methods to calculate the classical solution, one of which assumes that $\delta\pi_p\left(\xi, \beta, \beta', \beta''\right) = 0$, resulting in the expression shown in Equation (1.9):

$$\begin{aligned}
\delta\pi_p = &\int_0^L \left(EI_y\xi'' + M\beta\right)'' \delta\xi dz + \int_0^L \left[\left(EC_w\beta''\right)'' - \left(GJ\beta'\right)' + M\xi''\right]\delta\beta dz \\
&+ \left[\left(EI_y\xi'' + M\beta\right)\delta\xi'\right]_0^L - \left[\left(EI_y\xi'' + M\beta\right)'\delta\xi'\right]_0^L \\
&+ \left[\left(EC_w\beta''\right)\delta\beta'\right]_0^L - \left[\left(\left(EC_w\beta''\right)' - GJ\beta'\right)\delta\beta\right]_0^L = 0
\end{aligned} \tag{1.9}$$

In Equation (1.9), the first two functions are the equilibrium conditions for lateral torsional buckling of a beam, the rest of functions give the boundary conditions, four at each support.

Since the beam is simply supported and under constant bending moment, the displacement and rotation are shown in the following equations:

$$\xi(0) = \xi''(0) = \xi(\mathrm{L}) = \xi''(\mathrm{L}) = 0 \tag{1.10}$$

$$\beta(0) = \beta''(0) = \beta(\mathrm{L}) = \beta''(\mathrm{L}) = 0 \tag{1.11}$$

Substituting Equation (1.10) and (1.11) into the equations of equilibrium conditions and boundary conditions, the classical solution is presented as follows:

$$M_u = \frac{\pi}{L}\sqrt{EI_yGJ + \left(\frac{\pi E}{L}\right)^2 I_yC_w} \tag{1.12}$$

The second method is assuming $\xi = A\sin\left(\pi z/L\right)$ and $\beta = B\sin\left(\pi z/L\right)$ due to the lateral displacement and twisting angle are equal to zero at each supports ($z = 0, L$). Substituting these two values into Equation (1.8), the expression can be written as follow:

$$\pi_p = \frac{1}{2}\int_0^L EI_y \left[A\sin\left(\frac{\pi z}{L}\right)'' \right]^2 dz + \frac{1}{2}\int_0^L EC_w \left[B\sin\left(\frac{\pi z}{L}\right)'' \right]^2 dz$$
$$+\frac{1}{2}\int_0^L GJ \left[B\sin\left(\frac{\pi z}{L}\right)' \right]^2 dz + \int_0^L M \left[B\sin\left(\frac{\pi z}{L}\right) \right] \left[A\sin\left(\frac{\pi z}{L}\right) \right]'' \mathrm{dz} \quad (1.13)$$

Formulating the derivative of energy expression π with the respect to A and B equal to zero ($(\partial\pi)/(\partial A) = 0$ and $(\partial\pi)/(\partial B) = 0$), the following matrix form is obtained:

$$\begin{bmatrix} a_{11} & a_{12} \\ a_{21} & a_{22} \end{bmatrix} \begin{Bmatrix} A \\ B \end{Bmatrix} = \begin{Bmatrix} 0 \\ 0 \end{Bmatrix} \quad (1.14)$$

The critical moment can be obtained by setting the determinant of the above system to zero ($\begin{bmatrix} a_{11} & a_{12} \\ a_{21} & a_{22} \end{bmatrix} = 0$), the same classical solution of critical moment (Equation 1.12) would be obtained.

The resistance provided by warping of non-rectangular sections has a significant contribution to the capacity for members such as wide flange beams in steel design, however, the effect is very small in rectangular beam, and is typically ignored. The warping deformation of a rectangular cross-section is shown in Figure 1.5.

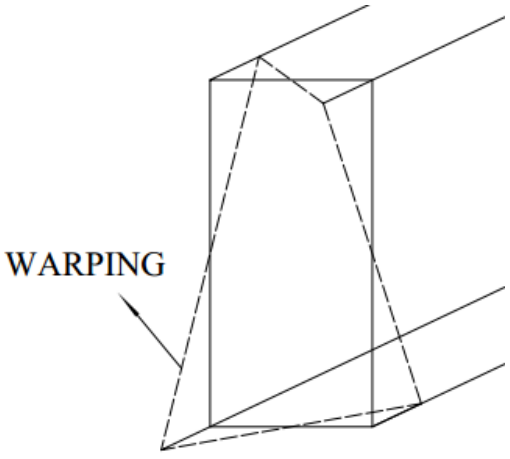

Figure 1.5 Warping of cross-section in lateral torsional buckling

In order to simplify the equation, the resistance from warping constant can be ignored when the beam is rectangular (AFPA, 2003), and the simplified equation of lateral torsional buckling

for simply-supported beam under a constant moment is therefore given by:

$$M_u = \frac{\pi}{L_u}\sqrt{EI_y GJ} \tag{1.15}$$

To generalize the lateral torsional buckling solutions to include beams with different boundary conditions and loading pattern, two methods can be used to modify the equation: the first is effective length approach and the other one is equivalent moment factor approach. The two methods will be described next.

1.1.3 Effective Length Approach

This method adjusts the reference basic case of a beam with constant moment by substituting the unbraced length by the effective length as shown in Equation (1.16). This method has been adopted by the Canadian and the US timber design standards (AFPA, 2003).

$$M_{cr} = \frac{\pi}{L_e}\sqrt{EI_y GJ} \tag{1.16}$$

Where L_e is the effective length, as shown in Table 1.1, reproduced from the CSA Standard (CSA, 2009).

Table 1.1 Effective length for the bending members (CSA, 2009):

	Intermediate support	
	Yes	No
Beams		
Any loading	1.92a	1.92l_u
Uniformly distributed load	1.92a	1.92l_u
Concentrated load at centre	1.11a	1.61l_u
Concentrated load at 1/3 points	1.68a	
Concentrated load at 1/4 points	1.54a	
Concentrated load at 1/5 points	1.68a	
Concentrated load at 1/6 points	1.73a	
Concentrated load at 1/7 points	1.78a	
Concentrated load at 1/8 points	1.84a	
Cantilevers		
Any loading		1.92l_u
Uniformly distributed load		1.23l_u
Concentrated load at free end		1.69l_u

Note: l_u is unsupported length and a is the maximum purlin space

1.1.4 Equivalent Moment Factor Approach

The American Institute of Steel Construction (AISC) adopted the equivalent moment factor approach in 1961. This method adjusts the reference basic case (simply-supported under a constant moment) by multiplying the equation with a modification factor C_b (AFPA, 2003), as provided in Equation (1.17)

$$M_{cr} = C_b M_u \tag{1.17}$$

Where C_b is the equivalent moment factor.

The energy method can provide the critical moment solution for many load options and the equivalent moment factor can be calculated by comparing the solution of the other load options with Equation (1.12). To show how this method can be used, a concentrated load applied at the mid-span of a simply supported beam is used as an example. Equation (1.13) can be written as:

$$\begin{aligned}\pi_p = {} & \frac{1}{2}\int_0^L EI_y \left[A\sin\left(\frac{\pi z}{L}\right)\right]''^2 dz + \frac{1}{2}\int_0^L EC_w \left[B\sin\left(\frac{\pi z}{L}\right)''\right]^2 dz \\ & + \frac{1}{2}\int_0^L GJ\left[B\sin\left(\frac{\pi z}{L}\right)\right]'^2 dz + 2\int_0^{\frac{L}{2}} \frac{Pz}{2} B\sin\left(\frac{\pi z}{L}\right)\left[A\sin\left(\frac{\pi z}{L}\right)\right]'' \mathrm{dz}\end{aligned} \tag{1.18}$$

Enforcing the stationary conditions $(\partial\pi)/(\partial A) = 0$ and $(\partial\pi)/(\partial B) = 0$, the following equation is obtained:

$$\left(\left[K_g\right] + P\left[K_G\right]\right)\begin{Bmatrix} A \\ B \end{Bmatrix} = \begin{Bmatrix} 0 \\ 0 \end{Bmatrix} \tag{1.19}$$

Where

$$\left[K_g\right] = \begin{bmatrix} EI_y\left(\frac{\pi}{L}\right)^4 \int_0^L \sin^2\left(\frac{\pi z}{L}\right) dz & 0 \\ 0 & EC_w\left(\frac{\pi}{L}\right)^4 \int_0^L \sin^2\left(\frac{\pi z}{L}\right) dz + GJ\left(\frac{\pi}{L}\right)^2 \int_0^L \cos^2\left(\frac{\pi z}{L}\right) dz \end{bmatrix}$$

$$[K_G]=\begin{bmatrix} 0 & -\left(\frac{\pi}{L}\right)^2\int_0^{\frac{L}{2}} z\sin^2\left(\frac{\pi z}{L}\right)dz \\ -\left(\frac{\pi}{L}\right)^2\int_0^{\frac{L}{2}} z\sin^2\left(\frac{\pi z}{L}\right)dz & 0 \end{bmatrix}$$

The critical force can be obtained by setting the determinant of the above system to zero, as shown in following equation:

$$\left|\left[K_g\right]+P\left[K_G\right]\right|=0 \tag{1.20}$$

Solving the Equation (1.20) and substituting P into the maximum moment solution ($M_{\max}=PL/4$), the critical moment solution is shown in Equation (1.21):

$$M_{cr}=1.423\frac{\pi}{L}\sqrt{EI_yGJ+\left(\frac{\pi E}{L}\right)^2 I_yC_w} \tag{1.21}$$

The ratio of the critical moment for a concentrated load at mid-span to the critical moment of constant moment yields the critical moment factor:

$$C_b=\frac{M_{cr}}{M_u}=1.423 \tag{1.22}$$

The development of the moment modification factor C_b is described in more details in Chapter 2.

1.2. Research Objective

The goal of this study is to investigate, experimentally and analytically, the behavior of timber members prone to lateral torsional buckling failure. More specifically, the study's objectives are:

- Investigate the modulus of elasticity and shear modulus of solid sawn and glue-laminated members
- Investigate the behavior of solid sawn lumber in the elastic region through full-scale tests
- Develop a linear material model to predict the behaviour of solid sawn and glue-laminated

bending members

- Investigate the effect of mechanical properties such as modulus of elasticity and shear modulus on critical moment
- Investigate the effect of load eccentricity, support location and dimension on critical moment

1.3. Research Methodology

The approach taken to meet the objectives of the study relies on both experimental and numerical analysis of the flexural members including investigation at the material level as well as full-scale tests to establish the behaviour under well-known loading and boundary conditions. Material tests including the determination of the weak direction modulus of elasticity (E_y) and the shear modulus (G_T) about the transverse direction, weak direction modulus of elasticity and shear modulus about transverse direction were conducted to obtain inputs to the finite element analysis (FEA) model. The same solid lumber beam elements were then tested in full scale and the critical moment was compared with that obtained from the FEA model. Once verified, the FEA model was used to investigate the effects of load configurations, load locations and support locations on lateral torsional buckling.

1.4. Structure of the Thesis

Chapter 1 includes the problem definition, research goals, and research strategy.

Chapter 2 surveys the literature for information on wood members under the effect of bending moment, and describes research studies conducted on lateral torsional buckling.

Chapter 3 describes the sensitivity analysis performed in order to determine the influence of various parameters on the lateral torsional buckling of beam elements.

Chapter 4 describes the experimental setup and loading configurations.

Chapter 5 presents the test results and provides comparison between test data and results obtained from the classical solution.

Chapter 6 describes the finite element modeling and validates the model using the experimental

test results.

Chapter 7 contains a parametric study to investigate the influence of load configuration, load location, support conditions and effect of change in dimensions on the critical moment capacity.

Chapter 8 provides conclusions obtained from the experimental and FEA model studies in each chapter and provides recommendations of future research.

1.5. Notation for Chapter 1

a	the maximum purlin space
C_b	the equivalent moment factor
C_w	the warping constant
d	beam depth (mm)
E	modulus of elasticity (MPa)
E_L	modulus of elasticity along the longitudinal direction (MPa)
E_R	modulus of elasticity along the radial direction (MPa)
E_T	modulus of elasticity along the tangential direction (MPa)
G	shear modulus (MPa)
G_{LR}	shear modulus about longitudinal and radial direction (MPa)
G_{LT}	shear modulus about longitudinal and tangential direction (MPa)
G_{RT}	shear modulus about radial and tangential direction (MPa)
I_y	moment of initial in weak axis (mm^4)
J	Saint Venant torsion constant (mm^4)
L	the span of beam between two supports (mm)
L_e	the effective length of beam (mm)
L_u	the unbraced length of beam (mm)
M_u	the critical moment of simply supported beam under constant moment

M_{cr}	critical moment of beam
P	magnitude of concentrated load applied on the mid-span of beam
U	internal strain energy
V	load potential energy gain
β	rotation about longitudinal direction
γ_{LR}	engineering shear strain about longitudinal and radial direction
γ_{LT}	engineering shear strain about longitudinal and tangential direction
γ_{RT}	engineering shear strain about radial and tangential direction
ε_{LL}	strain along longitudinal direction
ε_{RR}	strain along radial direction
ε_{TT}	strain along tangential direction
ν	Poisson's ratio
ν_{LR}	Poisson's ratios about longitudinal and radial direction
ν_{LT}	Poisson's ratios about longitudinal and tangential direction
ν_{RL}	Poisson's ratios about radial and longitudinal direction
ν_{RT}	Poisson's ratios about radial and tangential direction
ν_{TL}	Poisson's ratios about tangential and longitudinal direction
ν_{TR}	Poisson's ratios about tangential and radial direction
ξ	centroidal displacement along lateral direction
π_p	total potential energy
σ_{LL}	stress along longitudinal direction
σ_{RR}	stress along radial direction
σ_{TT}	stress along tangential direction
τ_{LR}	stress about longitudinal and radial direction

τ_{LT} stress about longitudinal and tangential direction

τ_{RT} stress about radial and tangential direction

1.6. References

[1] Canadian Standard Association. (2009, May). CSA Standard O86-09 Engineering design in wood, Mississauga, Ontario, Canada.

[2] Isopescu, D., Stanila, O., and Asatanei, I. (2012). Analysis of Wood Bending Properties on Standardized Samples and Structural Size Beams Tests, Buletinul Insititutului PolitehnicDIN Din Iasi, Publicat de Universitatea Tehnică „Gheorghe Asachi" din Iaşi

[3] Forest Products Laboratory. (2010). Wood Handbook-Wood as an Engineering Material, Madison, D.C., USA.

[4] Simulia. (2011). ABAQUS analysis user's manual (Version 6.11), Dassault Systemes.

[5] Shepard, K and Gromicko, N. (2009). Master Roof Inspections: Wood Shakes and Shingles, Part 1, http://www.nachi.org/wood-shakes-shingles-part1-133.htm.

[6] Trahair, N. S. (1993). Flexural-Torsional Buckling of Structures. CRC Press Inc. Florida, USA.

[7] American Forest and Paper Association. (2003). Technical Report 14: Deisigning for lateral-torsional stability in wood members. Washington, D.C.

CHAPTER 2

Literature Review

2.1 Design Methods for Lateral Torsional Buckling of Beams

2.1.1 Development of Classical LTB Solution

The first solution of lateral torsional buckling of thin rectangular sections was obtained by Prandtl and Michell in 1899 (Timoshenko, 1961). The reference case consisted of a prismatic beam under constant end moments, and where the ends are prevented from rotation about longitudinal direction (Hooley and Madsen, 1964). Three equations can be provided for estimating the bending moment about the strong axis, bending moment about the weak axis and out-of-plane bending (Galambos and Surovek, 2008). Based on these equations, a closed-form expression for the reference case was derived (AFPA, 2003) and given by:

$$M_u = \frac{\pi}{L_u}\sqrt{EI_y JG} \tag{2.1}$$

Equation (2.1) shows an approximation to the general lateral torsional buckling equation, where an assumption is made that the beam under consideration is deep, with a much larger value of moment of initial in major axis, I_x than the weak axis, I_y. Federhofer and Dinnik argued that the solution obtained in Equation (2.1) was conservative for less slender beams (Timoshenko, 1961). In order to enable the solution to predict the capacity of less slender beams, a modification was suggested to Equation (2.1), as shown in Equation (2.2) (AFPA, 2005):

$$M_u = \frac{\pi}{L_u}\sqrt{\frac{EI_y JG}{r}} \tag{2.2}$$

Where r is given by $r = 1 - I_y / I_x$

The reference case, with uniform moment is either adjusted by the effective length or the equivalent moment approach to account for loading and support conditions other than those

assumed in the classical solution (Equation 2.1). The development of these approaches is described next.

2.1.2 The Development of the Equivalent Moment Factor

The first expression for the equivalent moment factor, C_b, was adopted by the American Institute of Steel Construction in 1961, and was expressed as shown in Equation (2.3) (AISC, 1999). This equation only applies in cases where the bending moment diagram between the two lateral bracing points is a straight line and M_1 / M_2 is negative (Figure 2.1).

$$C_b = 1.75 + 1.05\frac{M_1}{M_2} + 0.3\left(\frac{M_1}{M_2}\right)^2 \leq 2.3 \tag{2.3}$$

Where M_1 and M_2 are the minimum and maximum moments, respectively.

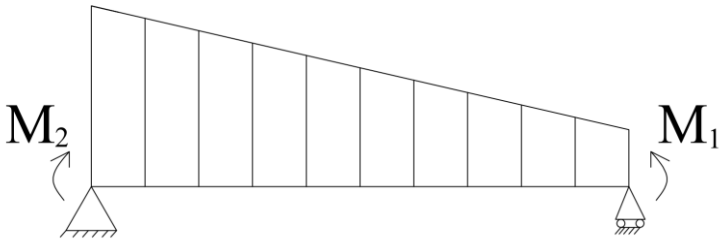

Figure 2.1 Moment diagram of $M_1 / M_2 < 0$

Another equation, applicable where the bending moment diagram is linear and where $M_1 / M_2 > 0$, is shown in Figure (2.2). The solution is shown in Equation (2.4) and it offered a better match to predict C_b than Equation (2.3) (AISC, 1999).

$$C_b = \frac{1}{0.6 - 0.4\frac{M_1}{M_2}} \leq 2.5 \tag{2.4}$$

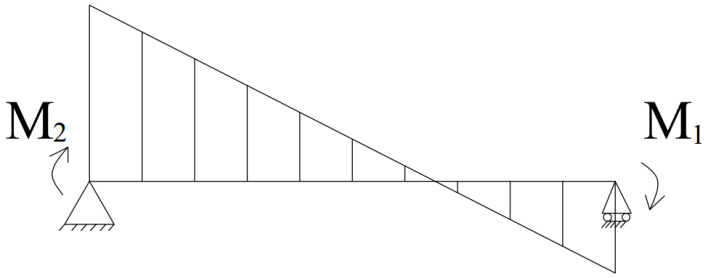

Figure 2.2 Moment diagram of $M_1 / M_2 > 0$

In order to make the equation applicable to cases with non-linear moment diagrams, an empirical solution of C_b was proposed by Kirby and Nethercot in 1979, as provided in Equation (2.5) (Kirby and Nethercot, 1979).

$$C_b = \frac{12|M_{\max}|}{3|M_{\max}| + 4|M_A| + 3|M_B| + 2|M_C|} \tag{2.5}$$

Where $M_{\max}$ is the maximum moment along the span between two lateral bracing points, M_A is the value of the moment in one quarter point between two lateral bracings, M_B is the value of moment in two quarter point between two lateral bracing and M_C is the value of moment in three quarter point between two lateral bracing. The definition of the parameters is also shown in Figure 2.3.

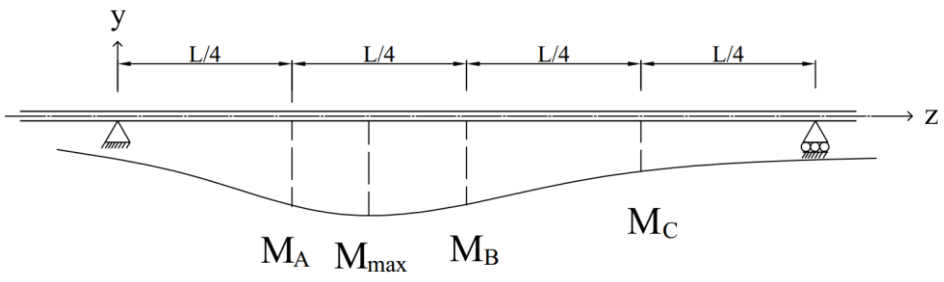

(a)

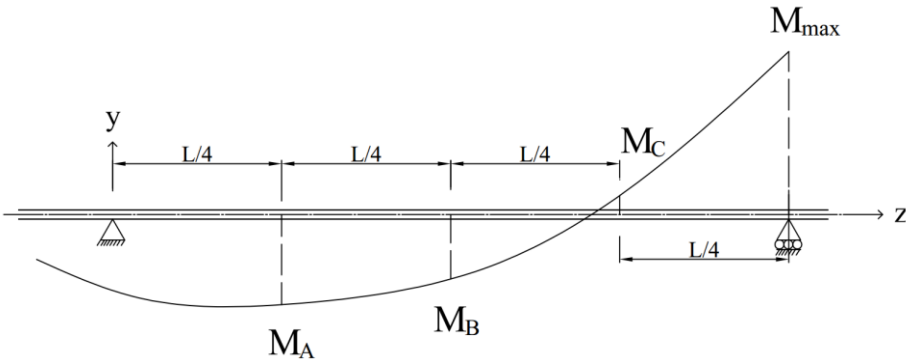

(b)

Figure 2.3 The various shape moment diagram between two lateral bracing
(a) The beam bent in single curvature, (b) the beam bent in reversed curvature

In 1999, Load and Resistance Factor Design (LRFD) for presented the modified version of the equation by Kirby and Nethercot (1979), as shown in Equation (2.6). This equation provided a more accurate result in relation to linear and non-linear bending moment diagrams and is applicable for various shapes of moment diagram (AISC, 1999).

$$C_b = \frac{12.5|M_{\max}|}{2.5|M_{\max}| + 3|M_A| + 4|M_B| + 3|M_C|} \tag{2.6}$$

2.1.3 Development of Effective Length Approach on Timber Beams

The effective length approach was adopted in the 1977 in the National Design Specification (NDS) for Wood Construction (AFPA, 2005). The load configurations and boundary conditions included simply supported beams with uniformly distributed load, a concentrated load at mid-span and constant moment, cantilever beam with uniformly distributed load, concentrated load at the free end, and conservative solutions for the other load configurations and boundary

conditions. The range of load configurations was subsequently extended in the NDS. The solution of simply supported rectangular beam using the effective length approach was formulated as shown in the Equation (2.7) (AFPA, 2005). Similar provisions were adopted in the Canadian timber design standard (CSA, 2009):

$$M_{cr} = \frac{2.40EI_y}{L_e} \tag{2.7}$$

Where the effective length L_e varies with different load configurations

2.1.4 Effect of the Location of Load

The applied load needs to be considered in relation to the neutral axis and three load location scenarios can be considered: load at centroid, top compression fiber and bottom tension fiber. These situations are illustrated in Figure 2.4. All the equations for the critical moment shown previously in this chapter are given for load applied at the centroid. The load applied below or above the centroid would result in an increase or decrease of the lateral torsional buckling resistance, respectively. When the load applied at the bottom of the cross-section, a torsional moment is introduced due to the horizontal distance between the locations of the load to the centroid. In this case, the load would enhance the stability of beam, resulting in an increase in the critical moment resistance or buckling load. Similarly, load exerted at the top of the cross-section would destabilize the member.

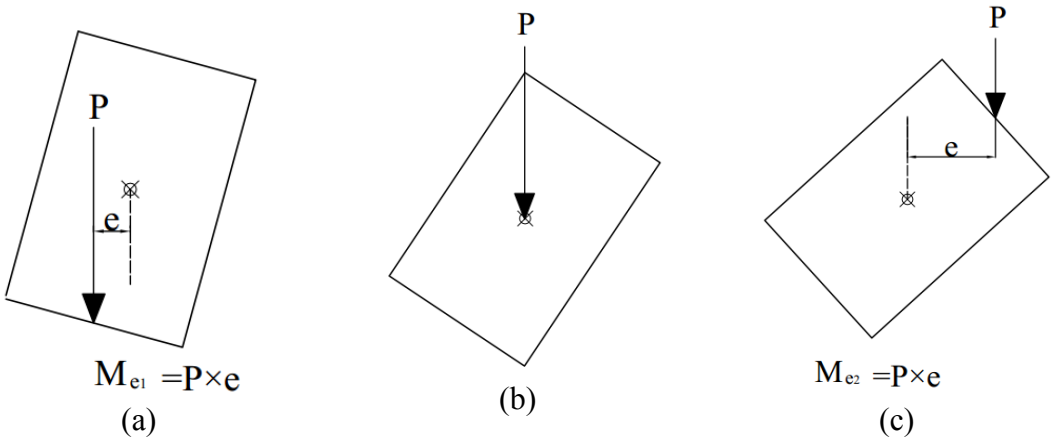

Figure 2.4 The location of load

(a) Bottom face loading induces a stabilization moment M_{e1} , (b) Shear center loading, and (c) Top face loading induces a destabilization moment M_{e2}

There are two methods to adjust the equation of critical moment for the position of load, which are the effective length approach and the load eccentricity factor method. The effective length approach obtains the critical moment by substituting the effective lengths to the solution based on different load positions, and the load eccentricity factor method adjusts the critical moment by multiplying the load eccentricity factor C_e with the critical moment obtained for load applied at the centroid. The solution for C_e is shown in Equations (2.8) and (2.9) (AFPA, 2003):

$$C_e = \sqrt{\eta^2 + 1} - \eta \tag{2.8}$$

$$\eta = \frac{Kd}{2L_u}\sqrt{\frac{EI_y}{GJ}} \tag{2.9}$$

Where K is a constant based on loading and boundary conditions as shown in Table 2.1, d is the depth of cross section. Negative values of η means the load is applied below the centroid and positive values mean the loads applied above the centroid (AFPA, 2003).

Table 2.1 The value of equivalent moment factor C_b and K for different load options and locations (AFPA, 2003):

Loading condition	Laterally Braced at point of loading	Laterally Unbraced at point of loading	
	C_b	C_b	K
Single Span beams			
Concentrated load at centre	1.67	1.35	1.72
Concentrated load at 1/3 points	1.00	1.14	1.63
Concentrated load at 1/4 points	1.11	1.14	1.45
Concentrated load at 1/5 points	1.00	1.14	1.51
Concentrated load at 1/6 points	1.05	1.14	1.45
Concentrated load at 1/7 points	1.00	1.13	1.47
Concentrated load at 1/8 points	1.03	1.13	1.44
Eight or more equal conc. Loads at equal spacings	1.00	1.13	1.46
Uniformly distributed load	1.00	1.13	1.44
Equal end moments (opposite rotation)	1.00		
Equal end moments (same rotation)	2.3		
Cantilever beams			
Concentrated load at end	1.67	1.28	1.00
Uniformly distributed load	1.00	2.05	0.9

2.1.5 Continuous Rectangular Beams in Lateral Torsional Buckling

Timber beams that are continuous over multiple supports and used to support floor or roof loads are typically laterally restraint by means of sheathed joist members or decking boards. However, due to the continuity in the beam, the compression zone could possibly be located at the bottom side of the beam, where it is laterally unbraced, which may result in lateral buckling of the beam.

The interior supports can be divided to two types: one where lateral bracing is provided to prevent lateral displacement and rotation, such as full-height blocking or sheathing on both sides of the beam, and the other type, which only provides vertical support to the beam but without any lateral bracing (Bradford and Douglas, 2006).

The equivalent moment factor approach can be applied to continuous beams and the solution is identical to that presented in Equation (2.6). $M_{\max}$, M_A, M_B and M_C are moment values at selected points along the length of the beam (Flint, 2012). For a two-span continuous beam, for example, if the interior bearing point is unbraced, $M_{\max}$, M_A, M_B and M_C are calculated based on the full length of the beam, $2L$, as shown in Figure 2.5 (a). If the interior bearing point is laterally braced, $M_{\max}$, M_A, M_B and M_C are calculated based on the L, as shown in Figure 2.5 (b).

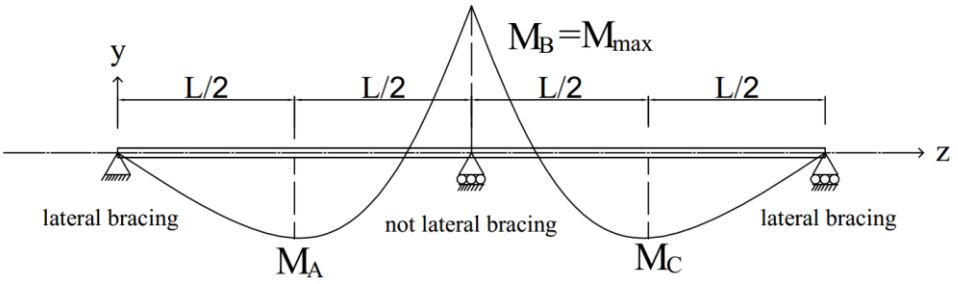

(a)

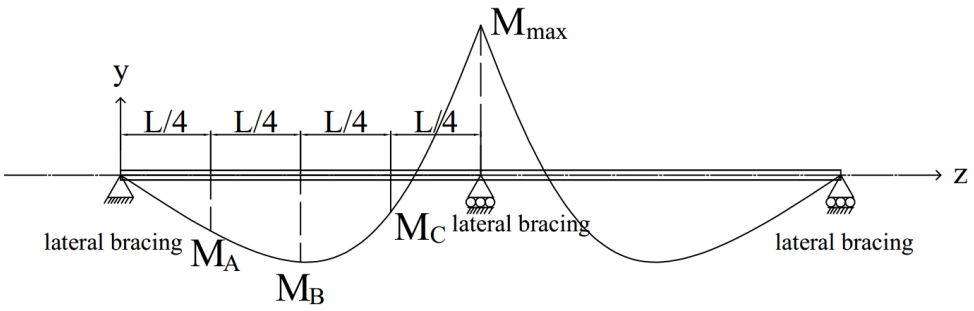

(b)

Figure 2.5 The various shape of moment in continuous beam

(a) the interior support is not laterally braced, (b) the interior supports is laterally braced

2.1.6 Lateral Torsional Buckling for Cantilever of Rectangular Section

For cantilevered beams which are unbraced at both ends, the equation of equivalent moment factor in Equation (2.6) is not appropriate (Bradford and Douglas, 2006). Martinelli (2012) provided functions for the critical moment resistance for a cantilever beam subjected to uniform bending moment and uniformly distributed load, as shown in Equation 2.10 and 2.11, respectively.

$$M_{cr} = \frac{\pi}{2L}\sqrt{GJEI_y} \tag{2.10}$$

$$M_{cr} = \frac{6.25}{L}\sqrt{GJEI_y} = \frac{2.05\pi}{L}\sqrt{GJEI_y} \tag{2.11}$$

Comparing the obtained value with that derived from the direct solution of the equivalent moment factor C_b of cantilever beam with uniform distributed load ($C_b = 2.06$) provided in

(AFPA, 2003), it can be seen that the values are nearly identical.

2.2 Lateral Torsional Buckling Tests Related to Wood Members

2.2.1 Hooley and Madsen (1964)

Hooley and Madsen (1964) carried out 33 glued-laminated beam tests in bending without lateral bracing along the span. Twenty-seven of those beams were tested in the elastic range. The objective of the study was to present simple code provisions in a rational way. The study examined the validity of the existing theory of lateral torsional buckling. The beams were simply supported or cantilevered, subjected to a concentrated load. The test data were compared with those based on the theory in the elastic range with reasonable agreement. The study confirmed that the capacity of a rectangular beam in lateral torsional buckling is governed by the ratio of $L_e d / b^2$. Based on the ratio, the concept of long, intermediate and short beams was defined and proposed to the cotemporary timber design code. A simple formula was derived for glulam beams and compared with the test results. The comparison yielded a safety factor ranging between 2.5 in the "short beam" region and 3 in the "long beam" region.

2.2.2 Hindman et al. (2005a)

Hindman et al. (2005a) performed lateral torsional buckling tests on 12 rectangular cantilever beams of machine stress rated lumber and structural composite lumber. The beams were fixed at one end and a concentrated load was applied at the free end. This study aimed at investigating the difference in the elastic constants ratios and torsional rigidity between solid wood and structural composite lumber. The experimental buckling load for a cantilevered beam was compared with that predicted based on the load resistance factor (LRFD) equation for wood design. The material was tested at three different lengths. It was found that the LRFD equation was non conservative for Laminated Veneer Lumber (LVL) but was suitable for solid sawn and Parallel Strand Lumber (PSL). The study also found that the incorporation of the measured torsional rigidity term did not significantly improve the critical buckling load prediction. Assuming that the specimens were isotropic produced more agreeable critical load predictions than the use of measured torsional rigidity values.

2.2.3 Hindman et al. (2005b)

Hindman and his collaborators (2005b) compared the measured and predicted critical buckling loads from 60 I-joists, where the flanges consisted of structural composite lumber of either Laminated Veneer Lumber (LVL) or Laminated Strand Lumber (LSL). Plywood or oriented strand board (OSB) were used for constructing the I-joist web. An unbraced cantilever beam test method was used and the experimental critical loads were compared with those obtained from the LRFD design equations and the elastic beam buckling theory. The study found that the LRFD equation and the elastic beam buckling prediction yielded values that were on average, respectively, 77% and 28% less than the measured critical buckling loads.

2.2.4 Burow et al. (2006)

Burow and his collaborators (2006) performed lateral torsional buckling tests on 22 cantilevered and simply supported composite wood I-joists. The study investigated the critical buckling loads of the composite wood I-joists utilizing cantilevered and simply supported configurations as well as the measurement of the torsional rigidity and flat bending stiffness values for the composite wood I-joists. The study also compared the lateral stability predictions generated using the Nethercot LRFD equation (Nethercot, 1983), Euler LRFD model (Timoshenko, 1961) and Equivalent moment factor model (AFPA, 2003). The results found that Nethercot LRFD equation was overly conservative for nearly the entire range of beam slenderness ratios tested. The Euler LRFD and equivalent moment factor models were found to be the best predictors of the critical buckling moments over the 13.8 and 42.4 range of beam slenderness ratios tested. The overall percent difference between the observed and predicted wood I-joist critical moment values for the Euler LRFD and equivalent moment factor models were -14.1 and 5.7% respectively.

2.2.5 Suryoatmono and Tjondro (2008)

Suryoatmono and Tjondro (2008) performed lateral torsional buckling tests for three rectangular beams of Bangkirai, Meranti and Albasia wood species under simply supported end conditions and with a concentrated load applied at mid-span. The experimental critical loads were compared with classical lateral torsional buckling solution and finite element model. The models were investigated assuming isotropic and orthotropic material properties. The classical solution was found to be able to predict the capacity of isotropic finite element model well, but

much higher than orthotropic finite element models. In their comparison with the orthotropic FEA model with the experimental test, results were observed to agree well for the Albasia material. The Bangkirai model underestimated the critical load while the Meranti model overestimated the critical load.

2.2.6 Hindman (2008)

Hindman (2008) performed lateral torsional buckling tests on three simply supported I-joist members under concentrated load at mid-span. The goals of this study were to determine the critical buckling load and measure the response of I-joists subjected to the load from a worker walking on the unbraced I-joists. To achieve the first goal, a static bending test was performed where three methods were used to determine buckling loads. A novel loading jig was developed to measure the lateral buckling due to vertical loads. The results of the testing were analyzed in an attempt to precisely determine the lateral buckling. Lateral buckling tests of unbraced beams were conducted and the measured loading was observed to include a significant dynamic load component to cause the lateral torsional buckling.

2.2.7 Bamberg (2009)

Bamberg (2009) studied the behavior of wood I-joists loaded by human test subjects. The goal of the study was to analyze the relationship between lateral acceleration, displacement and twist and the brace configuration and stiffness. The study found that the braced configuration did not exhibit lateral acceleration, while having a lateral displacement and twist. The research also concluded that an increase in brace stiffness reduced the lateral displacement and twist response.

2.3 Notation for Chapter 2

C_b the equivalent moment factor

C_e load eccentricity factor

C_w the warping constant

d beam depth (mm)

e distance between load position and shear center

E modulus of elasticity (MPa)

G	shear modulus (MPa)
I_x	moment of initial in strong axis (mm^4)
I_y	moment of initial in weak axis (mm^4)
J	Saint Venant torsion constant (mm^4)
K	Constant based on loading and boundary conditions
L	the span of beam between two supports (mm)
L_e	the effective length of beam (mm)
L_u	the unbraced length of beam (mm)
M_1	minimum end moment
M_2	maximum end moment
M_A	value of moment in one quarter point between two lateral bracing
M_B	value of moment in two quarter point between two lateral bracing
M_C	value of moment in three quarter point between two lateral bracing
M_{cr}	critical moment of beam
M_{e1}	stabilization moment
M_{e2}	destabilization moment
$M_{\max}$	maximum moment along the span between two lateral bracing points
M_u	the critical moment of simply supported beam under constant moment
P	Applied load at mid-span
r	$=1-I_y/I_x$

2.4 References

[1] Timoshenko, S. (1961). Theory of Elastic Stability. Second Edition. McGraw-Hill Book Co.

[2] Hooley, R. F. and Madsen, B. (1964). Lateral Buckling of Glued Laminated Beams, Journal

of Structural Engineering Division, ASCE, Vol. 90, No. ST3, pp. 201-303.

[3] Galambos, T. V. and Surovek, A.E. (2008). Structural Stability of Steel: Concepts and Applications for Structural Engineers. John Wiley & Sons, Inc., Hoboken, New Jersey.

[4] American Forest and Paper Association. (2003). Technical Report 14: Designing for lateral-torsional stability in wood members. Washington, D.C.

[5] American Forest and Paper Association. (2005). DES 140: Designing for Lateral-Torsional Stability in Wood Members. Washington, D.C.

[6] American Institute of Steel Construction, Inc. (1999). Load and Resistance Factor Design Specification for Structural Steel Buildings, AISC Manual of Steel Construction, Second Edition

[7] Kirby, P. A. and Nethercot, D. A. (1979). Design for Structural Stability. Constrado Monographs, Granada Publishing, Suffolk, UK.

[8] Canadian Standards Association. (2009). CSA standards O86-09, Engineering design in wood, Mississauga, Ontario, Canada.

[9] Bradford K. & Douglas, P.E. (2006). Design for Lateral-Torsional Stability in Wood Members. American Forest & Paper Association, Washington, DC, USA.

[10] Filler, J. (2012). Calculating the Beam Stability Factor for a Continuous Timber Beam. http://voices.yahoo.com/calculating-beam-stability-factor-continuous-11676794.html?cat=15

[11] Martinelli, E. (2012). Stability of Structures. Department of Civil Engineering, University of Salerno, Italy, http://www.enzomartinelli.eu/MaterialeDidattico/stabilita/week04.pdf

[12] Hindman D. P., Harvey, H. B. and Janowiak, J. J. (2005a). Measurement and Prediction of Lateral Torsional Buckling Loads of Composite Wood Materials: Rectangular Section. Forest Products Journal, Vol. 55, No. 9, pp 42-47.

[13] Hindman D. P., Harvey, H. B. and Janowiak, J. J. (2005b). Measurement and Prediction of Lateral Torsional Buckling Loads of Composite Wood Materials: I-joist sections. Forest Products Journal, Vol. 55, No. 10, pp 43-48.

[14] Burow, J. R., Manbeck, H. B. and Janowiak, J. J. (2006). Lateral Stability of Composite Wood I-joists under Concentrated-load Bending. American Society of Agricultural and Biological Engineers, Vol. 49, pp 1867-1880.

[15] Nethercot, D. A. (1983). Elastic Lateral Buckling of Beams, in Beams and Beam Columns: Stability in Strength.R. Narayanan, ed. Barking, Essex, U.K.: Applied Science Publishers

[16] Suryoatmono B. and Tjondro A. (2008). Lateral-torsional Buckling of Orthotropic Rectangular Section beams. Department of Civil Engineering, Parahyangan Catholic University, Bandung, Indonesia.

[17] Hindman D.P. (2008). Lateral Buckling of I-joist. Department of Wood Science and Forest Products, Virginia Tech Blacksburg, VA, USA

[18] Bamberg, C. R. (2009). Lateral Movement of Unbraced Wood Composite I-joists Exposed to Dynamic Walking Loads. M.A.Sc thesis, Virginia Polytechnic Institute and State University, Blacksburg, Virginia, USA.

Chapter 3

Sensitivity Analysis

3.1 General

This chapter aims at conducting a sensitivity analysis of the mechanical properties on the critical moment capacity of a wooden beam of typical dimensions. According to CSA Standard O86-09 (CSA, 2009), the capacity of the beam is dictated by lateral torsional buckling due to lateral stability factor which is equal or less than 1.

Consider a simply supported beam with 80×600 mm cross-section and 5000 mm span (Glued laminated timber). Beam material properties are Pine lodgepole (Table 3.1). The beam is assumed to be subjected to a uniform moment. The lateral torsional buckling capacity of the beam based on a 3D FEA model will be compared to that based on the classical solution. This will be followed by a sensitivity analysis on a study on the effect of the constitutive properties on the lateral torsional buckling resistance of the beam.

Table 3.1 Mechanical properties of Pine lodgepole glue-laminated beam (CSA, 2009) (FPL, 2010)

Parameter	Value
Modulus of elasticity in the longitudinal direction E_L (MPa)	10300
Modulus of elasticity in the tangential direction E_T (MPa)	700
Modulus of elasticity in the radial direction E_R (MPa)	700
Shear modulus about longitudinal and radial direction G_{LR} (MPa)	474
Shear modulus about longitudinal and tangential direction G_{LT} (MPa)	474
Shear modulus about radial and tangential direction G_{RT} (MPa)	51.5
Poisson's ratios along longitudinal and radial direction ν_{LR}	0.347
Poisson's ratios along longitudinal and tangential direction ν_{LT}	0.347
Poisson's ratios along radial and tangential direction ν_{RT}	0.469

3.2 Model Description

3.2.1 Introduction

As discussed in the Introduction and Literature review sections, wood is an anisotropic material but can generally be considered as an orthotropic material. On a cube taken from a wooden beam which includes three faces: the L face is perpendicular to the longitudinal direction, the R face is perpendicular to the radial direction and the T face is perpendicular to the tangential direction, as shown in Figure 3.1.

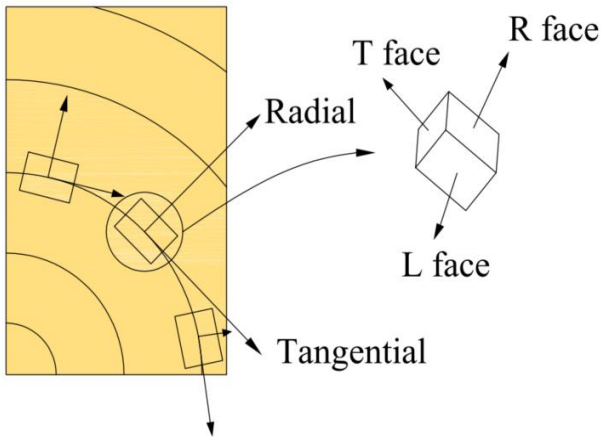

Figure 3.1 The Radial and tangential faces of a cube wooden beam

These three faces correspond to the modulus of elasticity (E_L , E_T and E_R) along the longitudinal, tangential and radial direction, respectively. On each face, there are two Poisson's ratios (v_{LT} and v_{LR}) and two shear moduli (G_{LT} and G_{LR}) about the longitudinal-tangential direction and longitudinal-radial direction, respectively, and one Poisson's ratio (v_{RT}) and one shear modulus (G_{RT}) about radial and tangential direction. However, the difference between the properties in the radial and tangential direction can be considered insignificant. Therefore, $E_T = E_R$, $v_{LT} = v_{LR}$ and $G_{LT} = G_{LR}$. In order to determine the effect of constitutive parameters on the lateral torsional buckling capacity of a beam, a 3D finite element eigenvalue buckling analysis is conducted, the three principle axes of the model are shown in Figure 3.2. The effect of various material properties on the critical moment was systematically investigated by varying the magnitude of constitutive parameters.

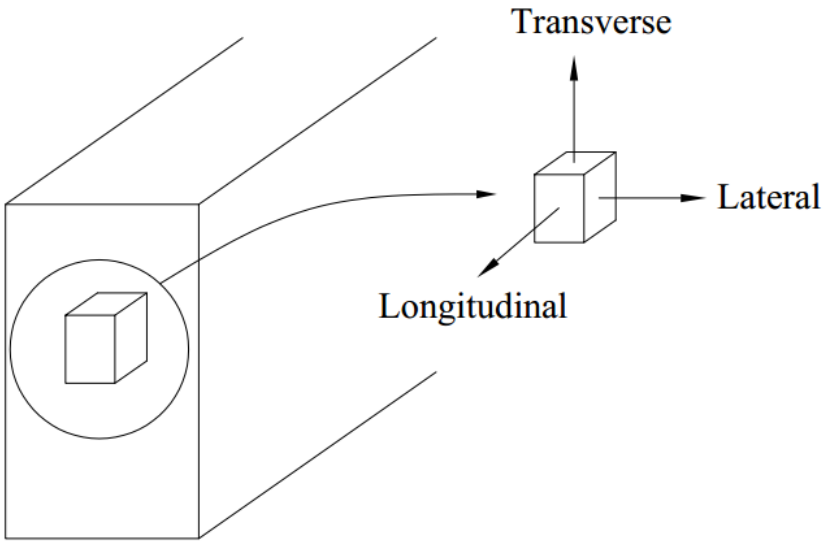

Figure 3.2 The three principal axes

3.2.2 The Element Type and Mesh of Model

The C3D8 eight-noded brick element from the ABAQUS library of elements was used to model the beam (Figure 3.3). The C3D8 element has 8 nodes at the corners and 24 degrees of freedom (three translations at each node) (Simulia, 2011).

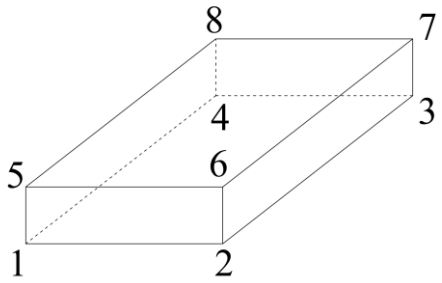

Figure 3.3 C3D8 Element

The finite element model was developed to investigate the lateral torsional buckling capacity of Pine lodgepole Glued-laminated beams, the beams cross-sections were 80 mm in width, by 600 mm in depth and 5000 mm in span. The dimensions were selected specifically to ensure that elastic lateral torsional buckling takes place prior to material failure and are thus the beam capacity and are independent of the strength properties of beam material. In order to ensure the accuracy of the model, the aspect ratio for each element should be as close as possible to unity.

Also, for computational efficiency, the element dimension in the longitudinal direction can be twice its width or depth. A mesh sensitivity analysis was conducted by increasing the mesh until no significant change was observed in the critical load. The critical load remained stable when there were 8 elements taken along the section width $n_1 = 8$, 60 elements along the section depth $n_2 = 60$ and 250 elements along the span $n_3 = 250$, as shown in Figure 3.4. Therefore, the element dimensions were 10 mm ×10 mm × 20 mm in length (Figure 3.4).

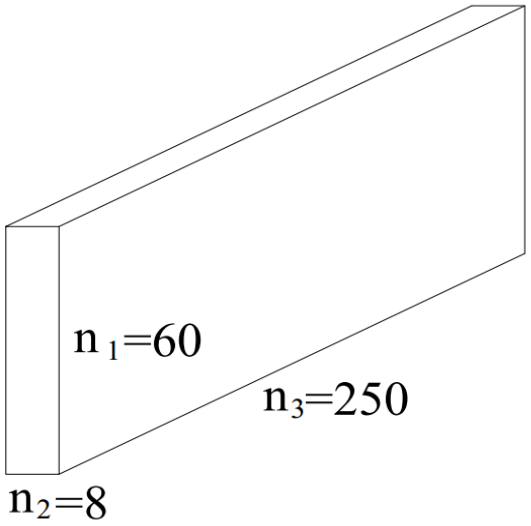

Figure 3.4 Mesh of model

3.2.3 Eigenvalue Analysis

Eigenvalue buckling analysis is a linear perturbation procedure to estimate the critical loads by solving the system of equation, as shown in Equation (3.1):

$$\left(\left[K_0\right] + \lambda_i \left[K_G\right]\right)\left\{v_i\right\} = 0 \tag{3.1}$$

where $\left[K_0\right]$ is the elastic stiffness matrix with respect to the base state, $\left[K_G\right]$ is the geometric matrix, λ_i represent the eigenvalues, corresponding to the buckling mode shapes $\left\{v_i^M\right\}$. For n degrees of freedom, Equation (3.1) has up to n Eigen pairs λ_i, $\left\{v_i\right\}$. The lowest positive eigenvalue among all Eigen value provides the critical loads.

3.2.4 Mechanical Material Properties

The mechanical material properties were taken as those for Pine lodgepole glue-laminated

beam. The mean properties as reported in the CSA O86-09 (CSA, 2009) and Wood handbook (FPL, 2010) are provided in Table 3.1, assuming the properties in the radial direction are identical to those in tangential direction. These will be taken for adopted for the FEA model of reference case.

3.2.5 Boundary Conditions

The beam is assumed to be simply supported at both ends relative to the strong axis bending, weak axis bending, and twist. This includes two types of constraints:

a) Those related to displacements within the plane of the cross-section, a set of restraints are enforced on the horizontal (AB and A'B') and vertical lines (CD and C'D') passing through the centroid (Figure. 3.5). Degrees of freedom along the transverse direction were restrained at AB and A'B', degree of freedom along the lateral direction was restrained at CD and C'D'.

b) Those related to longitudinal displacement on the centroid of cross-section. At one end of beam (Figure 3.5), degree of freedom along the longitudinal, transverse, lateral direction were restrained on centroid of the cross-section, at the other end, only the degree of freedom along the tangential and radial directions were restrained on the centroid of cross-section. The above explanation simulates the simply supports of the beam, at both ends, the lateral and transverse displacements were restrained but free to rotate about strong and weak axis, at one end, the displacement along the longitudinal direction was restrained but the other end is free to move along the longitudinal direction.

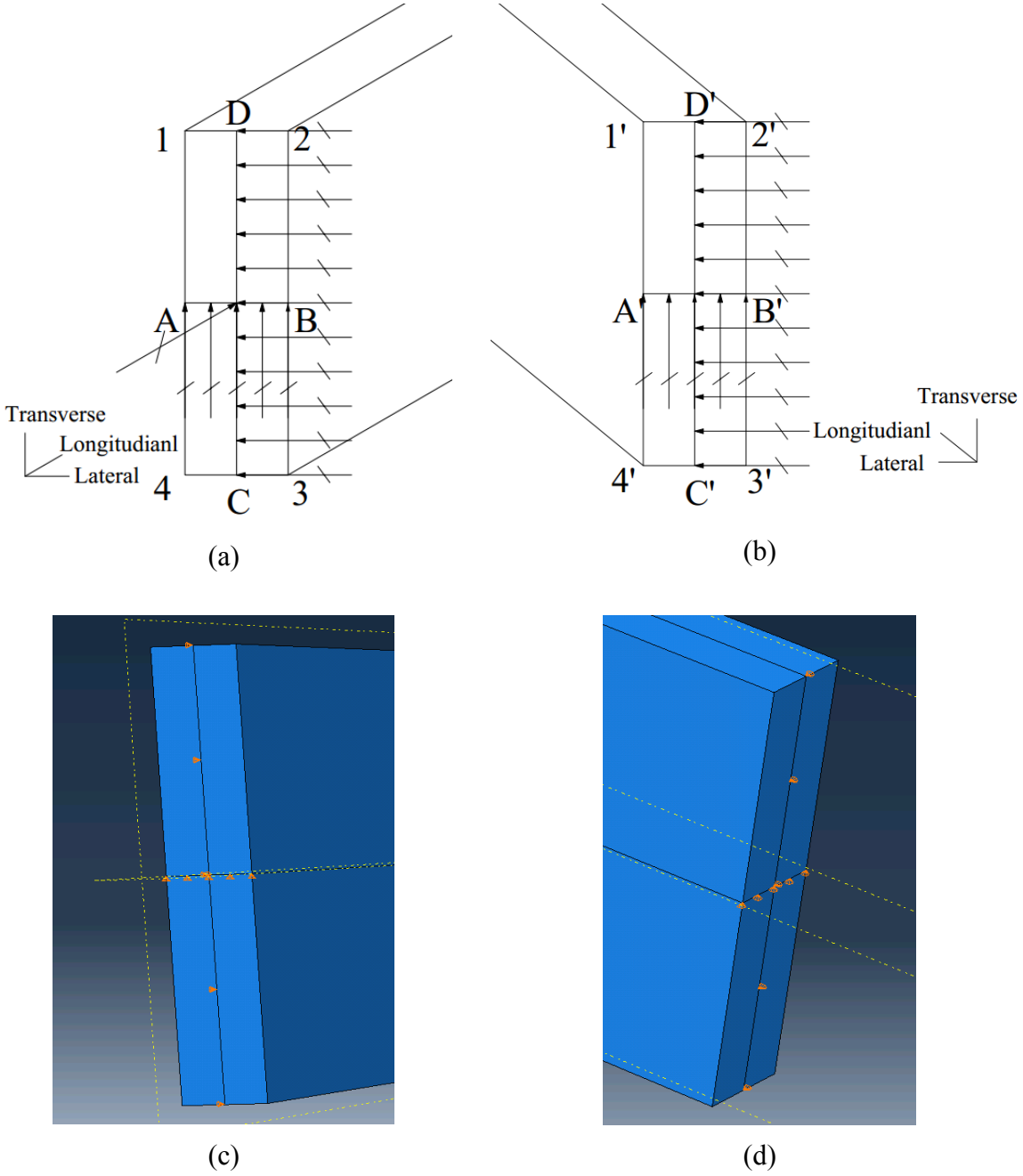

Figure 3.5 Boundary conditions (all crossed arrows denote restrained degrees of freedoms that are restrained)

(a) sketch of left end, (b) sketch of right end, (c) left end in ABAQUS model, and (d) right end in ABAQUS model

3.2.6 Constraints Related to the Longitudinal Degrees of Freedom

In line with the longitudinal displacement w for a generic point (x, y) at both beam ends

($l_e = 0$ and l) is given by

$$w(l_e, y, \mathrm{x}) = \varsigma(l_e) - \xi'(l_e)\,x - \eta'(l_e)\,y - \beta'(l_e)\,xy \tag{3.2}$$

$\varsigma(l_e)$ is the displacement of the centre of the cross-section along the longitudinal direction, $\xi(l_e)$ is the displacement along x axis (along the lateral direction), $\eta(l_e)$ is the displacement along y axis (along the tangential direction), $\beta(l_e)$ is the rotation about the longitudinal direction.

Applying Equation (3.2) at all 4 corner points with coordinates $(x_i, y_i)\, i = 1,2,3,4$, the longitudinal displacements of corners of end cross-section are given by

$$\begin{Bmatrix} w_1 \\ w_2 \\ w_3 \\ w_4 \end{Bmatrix} = \begin{bmatrix} 1 & x_1 & y_1 & x_1y_1 \\ 1 & x_2 & y_2 & x_2y_2 \\ 1 & x_3 & y_3 & x_3y_3 \\ 1 & x_4 & y_4 & x_4y_4 \end{bmatrix} \times \begin{Bmatrix} \varsigma(l_e) \\ \xi'(l_e) \\ \eta'(l_e) \\ \beta'(l_e) \end{Bmatrix} \tag{3.3}$$

Solving Equation (3.3), for vector $\langle \varsigma(l_e) \quad \xi'(l_e) \quad \eta'(l_e) \quad \beta'(l_e) \rangle^T$, results in

$$\begin{Bmatrix} \varsigma(l_e) \\ \xi'(l_e) \\ \eta'(l_e) \\ \beta'(l_e) \end{Bmatrix} = \begin{bmatrix} 1 & x_1 & y_1 & x_1y_1 \\ 1 & x_2 & y_2 & x_2y_2 \\ 1 & x_3 & y_3 & x_3y_3 \\ 1 & x_4 & y_4 & x_4y_4 \end{bmatrix}^{-1} \times \begin{Bmatrix} w_1 \\ w_2 \\ w_3 \\ w_4 \end{Bmatrix} \tag{3.4}$$

From Equation (3.4) into (3.2), gives

$$w(l_e, x, y) - \langle 1 \quad x \quad y \quad xy \rangle^T \begin{bmatrix} 1 & x_1 & y_1 & x_1y_1 \\ 1 & x_2 & y_2 & x_2y_2 \\ 1 & x_3 & y_3 & x_3y_3 \\ 1 & x_4 & y_4 & x_4y_4 \end{bmatrix}^{-1} \begin{Bmatrix} w_1 \\ w_2 \\ w_3 \\ w_4 \end{Bmatrix} = 0 \tag{3.5}$$

Equation (3.5) provides the longitudinal displacement w at any generic point (l_e, x, y) on end l_e in terms of the longitudinal displacements of corner points. The above constraint is then enforced in the ABAQUS model on all nodal points of the end cross-sections using the

Equation feature of ABAQUS. The procedure is shown in Figure 3.6 for node (x,y) = (20,30). Equation (3.5) provides the constraint $w(l_e, x, y) - 0.4125w_1 - 0.1375w_2 - 0.1125w_3 - 0.3375w_4 = 0$. The first coefficient corresponds to the node at which the constraint is enforced and the rest of the coefficients are those of the four corner points.

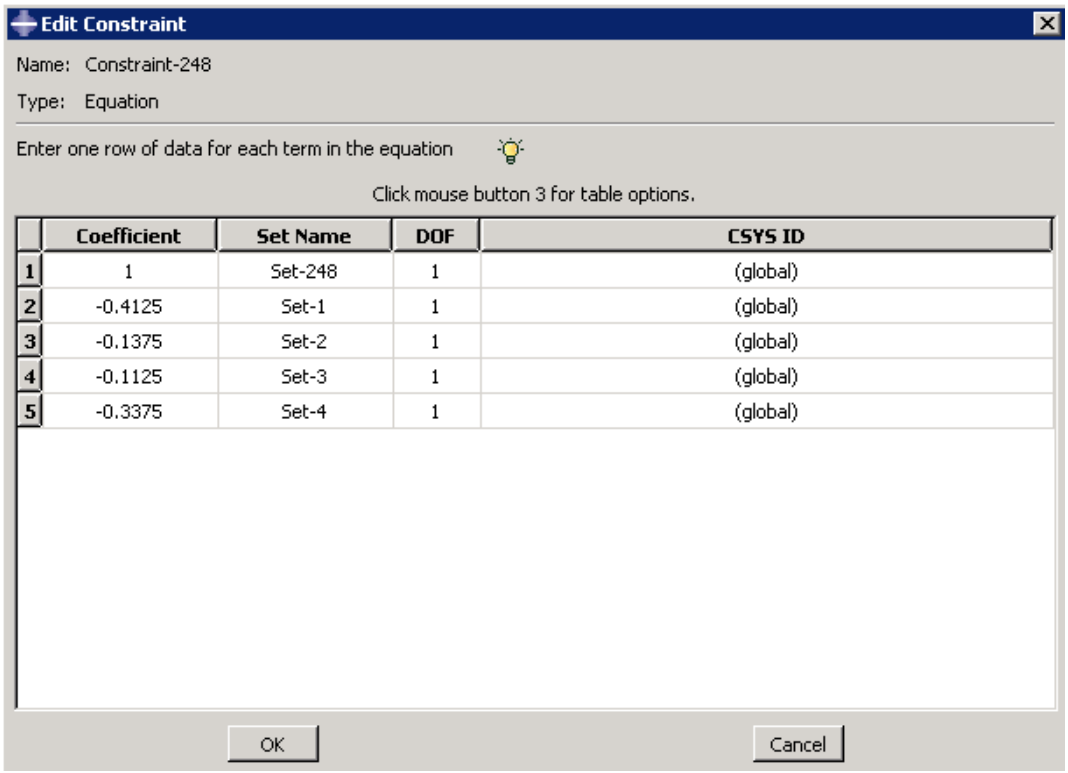

Figure 3.6 Edit equation constraint of node (x,y) =(20,30) (Simulia, 2011)

3.2.7 Load Application

The beam is subjected to equal end moments. This is achieved by applying four concentrated longitudinal forces P applied at the corners of the end cross-sections along the longitudinal direction, as shown in Figure 3.7. It is evident that the applied forces have zero longitudinal resultant, weak axis moments, and bi-moments. The resultant strong axis moment is equal to $4p \times (d/2) = 2pd$.

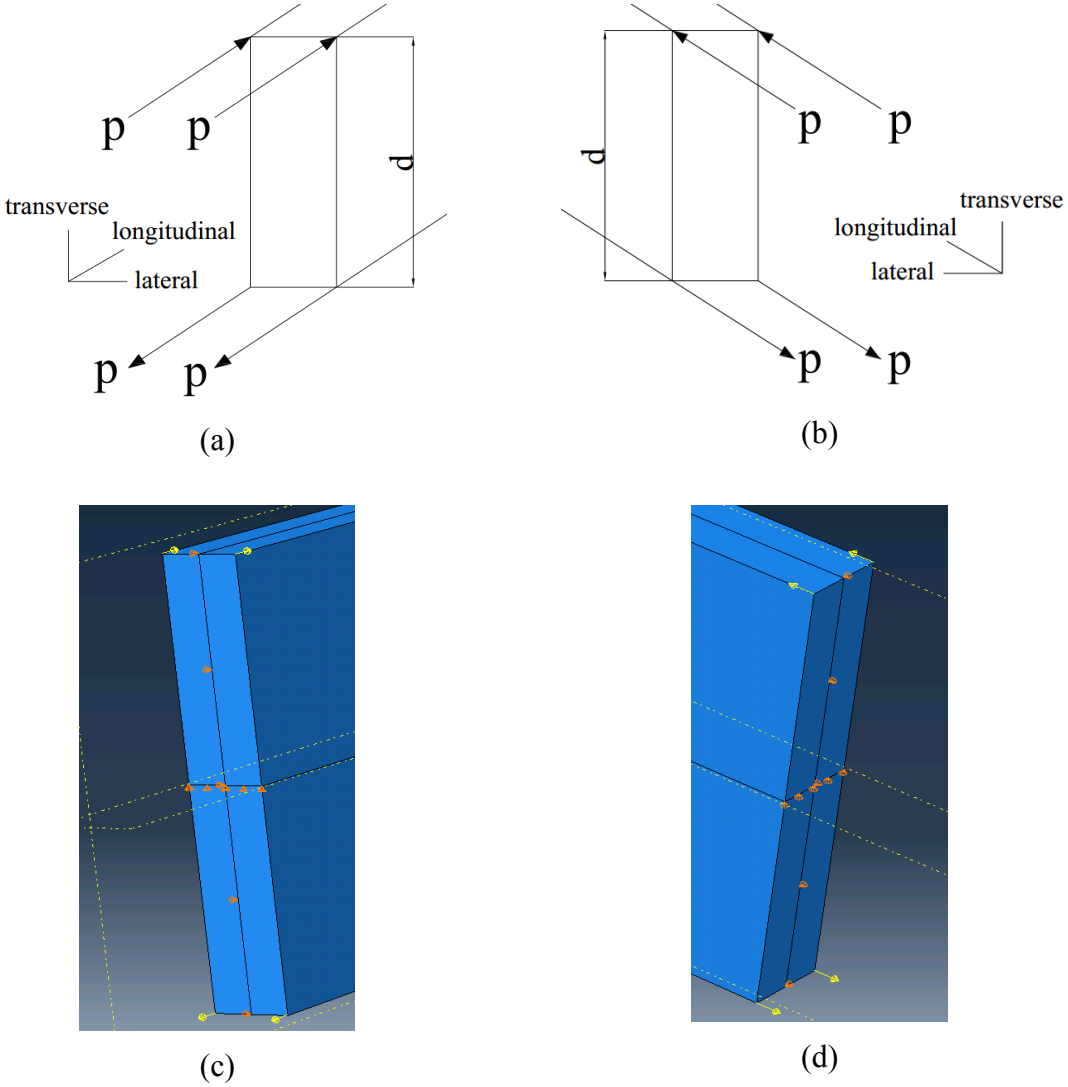

Figure 3.7 Load Application in the FEA model

(a) at the left end of the beam, (b) at the right end of the beam,

(c) at the left end in model, (d) at the right end in model

3.3 Comparison with Classical LTB Solution

The critical moment M_u for a simply supported beam subject to uniform bending as given by the classical solution is

$$M_u = \frac{\pi}{L_u}\sqrt{E_L I_y G_T J + \left(\frac{\pi E_L}{L_u}\right)^2 I_y C_w} \tag{3.6}$$

on which L_u is the unbraced length of beam, E_L is modulus of elasticity along the longitudinal

direction. Since the shear modulus about longitudinal and tangential direction G_{LT} is assumed to have the same magnitude as the shear modulus about longitudinal and radial direction G_{LR}, shear modulus about transverse direction G_T is used to replace the value of G_{LT} and G_{LR}. J is Saint Venant Torsion constant, I_y is moment of inertia in weak axis and C_w is warping constant.

For a rectangular section of width b and depth d, the weak axis moment of inertia is $I_y = db^3/12$. The Saint Venant Torsional constant is $J = kdb^3$, where k is a constant depending on the aspect ratio d/b. For a cross-section aspect ratio of $d/b = 600/80 = 7.5$ and given that $k_{(d/b=6)} = 0.299$ and $k_{(d/b=10)} = 0.312$ (Ugural & Fenster, 1975), through linear interpolation, one obtains $k_{(d/b=10)} = 0.312$. The warping constant C_w for a rectangular section is given by

$$C_w = \int (xy)^2 dA = \int_{-\frac{b}{2}}^{\frac{b}{2}} \int_{-\frac{d}{2}}^{\frac{d}{2}} x^2 y^2 dxdy = \frac{b^3 d^3}{144} \tag{3.7}$$

In summary, the section properties are $I_y = 2.56 \times 10^7 mm^4$, $C_w = 7.68 \times 10^{11} mm^6$, $J = 9.34 \times 10^7 mm^6$. When applying Equation (3.6) to an orthotropic material, the modulus of elasticity in the longitudinal direction $E_L = 10,300\ MPa$ and the shear modulus about transverse is taken as $G_T = 474\ MPa$.

For the 5 m span considered, the critical moment as obtained by Equation (3.6) is 70.2 kNm while that predicted by FEA is 67.9 kNm. This corresponds to a ratio of FEA to classical solution of 0.967. Figure 3.8 shows the buckled configuration for a beam subjected to uniform moment as predicted by the FEA model.

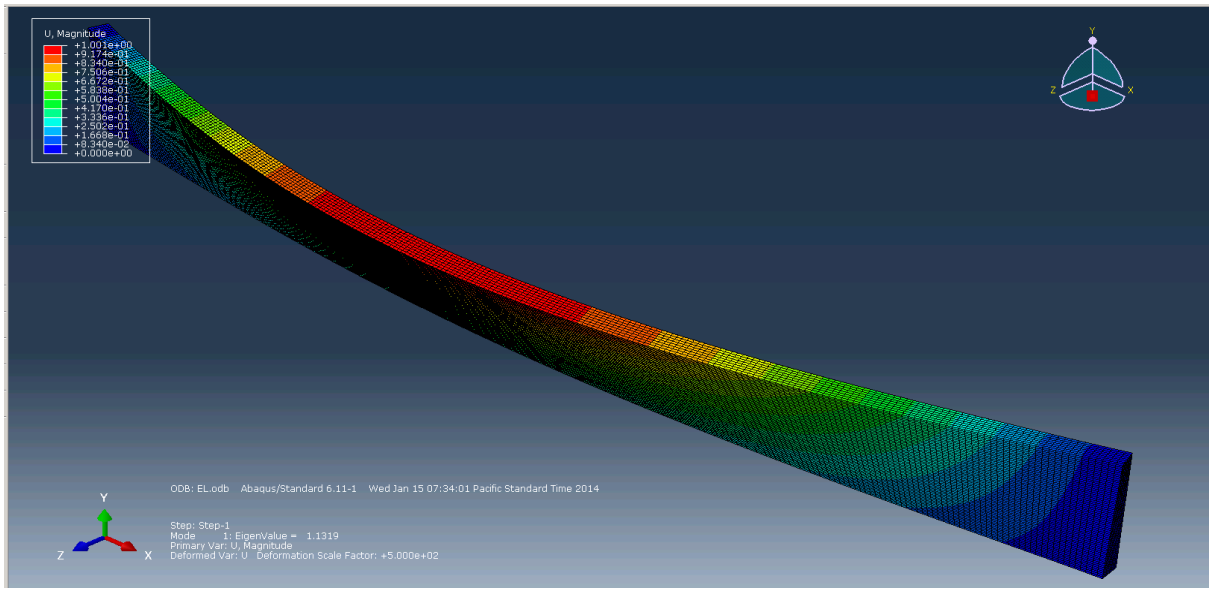

Figure 3.8 ABAQUS model of lateral torsional buckling

3.4 Sensitivity Analysis

In addition to the reference case investigated under Section 3.2 for which $E_{L-ref} = 10300\ MPa$, $E_{t-ref} = 700\ MPa$, $G_{T-ref} = 474\ MPa$, $v_{T-ref} = 0.347$, $G_{RT-ref} = 51.5\ MPa$ and $v_{RT-ref} = 0.469$. 12 sensitivity runs were conducted. In each of the runs, five of the six constitutive constants were kept unchanged and the value of the remaining constitutive constant was changed, once by a factor of 1.5 and another time by a factor of 0.5. The ratio of the resulting critical moment to the reference critical moment is then provided. The resulting critical moments and ratio between the resulting critical moments and that based on the reference case are shown in Table 3.2:

Table 3.2 Effect of Constitutive parameters on critical moments as predicted by FEA

Case	$\frac{E_L}{E_{L-ref}}$	$\frac{G_T}{G_{T-ref}}$	$\frac{E_t}{E_{t-ref}}$	$\frac{\nu_T}{\nu_{T-ref}}$	$\frac{\nu_{RT}}{\nu_{RT-ref}}$	$\frac{G_{RT}}{G_{RT-ref}}$	M_{cr} (MPa)	$\frac{M_{cr}}{M_{cr-ref}}$
Reference case	1	1	1	1	1	1	67.9	1.00
1	1.5	1	1	1	1	1	84.4	1.24
2	0.5	1	1	1	1	1	47.3	0.697
3	1	1.5	1	1	1	1	81.6	1.20
4	1	0.5	1	1	1	1	49.9	0.735
5	1	1	1.5	1	1	1	68.0	1.00
6	1	1	0.5	1	1	1	67.8	1.00
7	1	1	1	1.5	1	1	67.9	1.00
8	1	1	1	0.5	1	1	67.9	1.00
9	1	1	1	1	1.5	1	67.9	1.00
10	1	1	1	1	0.5	1	67.9	1.00
11	1	1	1	1	1	1.5	68.3	1.01
12	1	1	1	1	1	0.5	67.1	0.988

Note: Since the difference between the properties in the radial and tangential direction can be considered insignificant and assumed to be the same value in analysis, the modulus of elasticity about transverse (E_t) $(E_R = E_T = E_t)$ and the Poisson's ratio about transverse (ν_T) are used to replace the corresponding properties in the radial and tangential direction.

Figures 3.9 shows the normalized critical moment versus the normalized longitudinal Young Modulus as predicted by FEA and that based on the classical solution. Also, Figure 3.10 shows the normalized critical normalized critical moment versus the normalized longitudinal shear modulus as predicted by FEA and that based the classical solution.

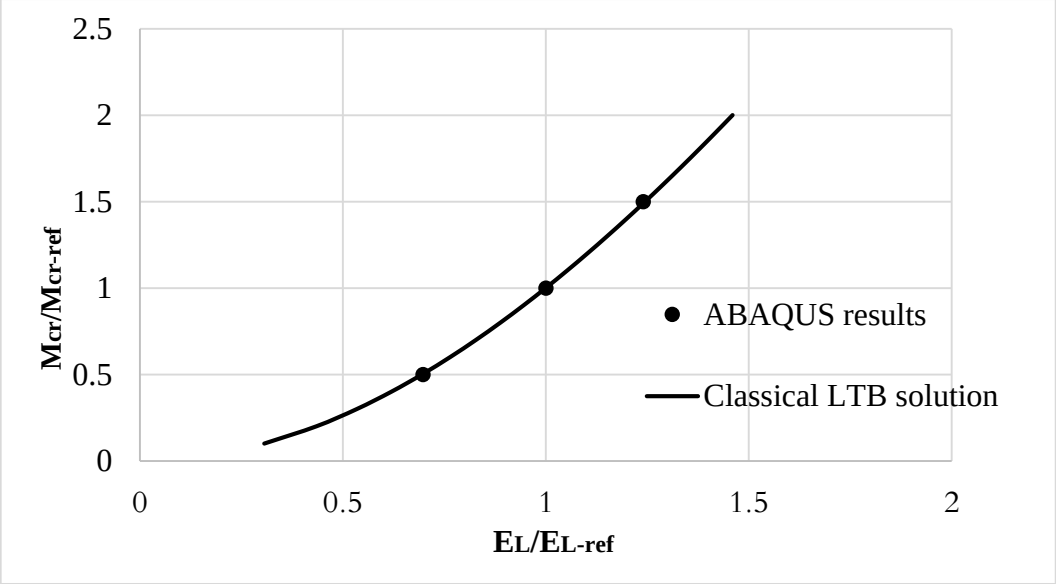

Figure 3.9 The comparison of $M_{cr}/M_{cr\text{-}ref}$ with $E_L/E_{L\text{-}ref}$

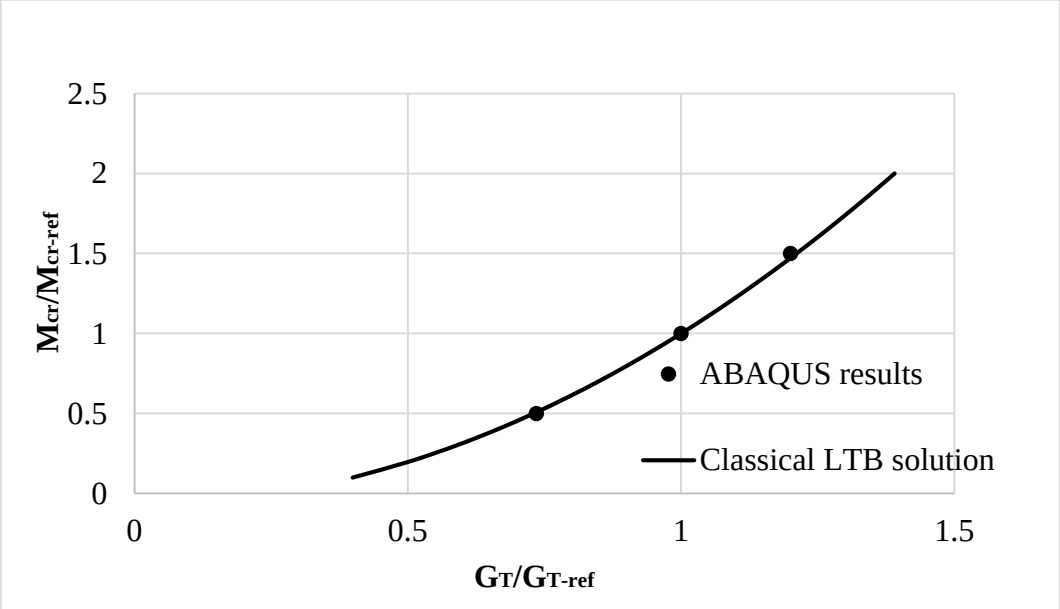

Figure 3.10 The comparison of $M_{cr}/M_{cr\text{-}ref}$ with $G_T/G_{T\text{-}ref}$

The sensitivity results (Table 3.2) show that the critical moments are significantly affected by the modulus of elasticity (E_L) in the longitudinal direction, and the transverse shear modulus (G_T). Thus, an accurate determination of these constants is needed. This will be the scope of Chapter 4 and 5. In contrast, the effect of the modulus of elasticity (E_t), Poisson's ratios (ν_T), (ν_{RT}) and shear modulus (G_{RT}) have a negligible effect on critical moment. An accurate determination of these material constants is not needed.

3.5 Notation for Chapter 3

b	beam width (mm)
C_w	the warping constant (mm^6)
d	beam depth (mm)
E_L	modulus of elasticity in the longitudinal direction (MPa)
E_T	modulus of elasticity in the tangential direction (MPa)
E_t	modulus of elasticity about transverse (MPa)
E_R	modulus of elasticity in the radial direction (MPa)
G_{LT}	shear modulus about longitudinal and tangential direction (MPa)
G_{LR}	shear modulus about longitudinal and radial direction (MPa)
G_T	shear modulus about transverse (MPa)
I_y	moment of initial in weak axis (mm^4)
J	Saint Venant torsion constant (mm^4)
k	constant depending on the aspect ratio d / b
K_0	elastic stiffness matrix with respect to the base state
K_G	geometric matrix
p	concentrated load applied on the corner of cross-section
w	longitudinal displacement
$\beta(l_e)$	rotation about longitudinal direction
$\varsigma(l_e)$	displacement of centre of cross-section along the longitudinal direction
$\eta(l_e)$	displacement along transverse axis
λ_i	eigenvalues
v_i^M	buckling mode shapes

ν_{LR} Poisson's ratios about longitudinal and radial direction

ν_{LT} Poisson's ratios about longitudinal and tangential direction

ν_{RT} Poisson's ratios about radial and tangential direction

ν_{T} Poisson's ratios about transverse

$\xi(l_e)$ displacement along lateral axis

3.6 References

[1] Canadian Standards Association. (2009). CSA standards O86-09, Engineering design in wood, Mississauga, Ontario, Canada.

[2] Forest Products Labratory. (2010): Wood Handbook-Wood as an Engineering Material. Madison, USA.

[3] Simulia. (2011), ABAQUS analysis user's manual (Version 6.11), Dassault Systemes.

[4] Uqural, A.C. and Fenster, S.K. (1975). Advanced Strength and Applied Elasticity, American Elsevier Pub Co, New York, USA.

Chapter 4

Experimental Program

4.1 Introduction

As discussed in the Sensitivity analysis section (Chapter 3), the lateral torsional buckling is only dependent on the weak direction modulus of elasticity along the longitudinal direction (E_L) and shear modulus about the transverse direction (G_T). All other parameters in lateral torsional buckling analysis are determined by the geometry of beam. As wood can be considered an orthotropic material, E_L and G_T values are direction dependent. The modulus of elasticity is that achieved from the lateral bending stiffness, which introduces strain parallel to the grains. The value of G_T is more complex to estimate because it depends on how the piece of wood is cut, as seen in Figure 1.2 in the Introduction section (Chapter 1) and how the wood element is installed.

Therefore, depending on the orientation of the cut, the value of G_T would be that of G_{LR} or G_{LT}. The value of G_T will, in reality, likely be a combination of the two values, and is best determined experimentally. Values in the literature (FPL, 2010) of G_{LR} and G_{LT} do not have high variability but they could introduce a significant error into the calculations. The effect of such difference was investigated in Chapter 3.

The testing program involved the two generic materials used in the CSA O86 standard (CSA, 2009), namely lumber and glue-laminated timber. The provisions in the design code are provided in the glulam design clause but they are also applicable to lumber. To the author's knowledge, few reported testing has ever been done on lumber products to validate the general theory for lateral torsional buckling. Therefore, this study's emphasis for the full scale tests was on lumber joists.

Due to its dimensional stability and precise manufacturing, the variation in dimension of glue-laminated timber members is usually found to be very small. However, this consistency cannot

always be found in lumber materials. The average measured dimension and variability of the lumber joists are presented in Table 4.1 and compared to the standard sizes assumed in the design code.

Table 4.1 Dimension of SPF specimens

2inch×8inch×14feet			
Dimension	Width	Height	Length
Average value (mm)	38	181	4276
COV	1.31×10^{-2}	5.54×10^{-3}	8.27×10^{-4}
Standard size (mm)	38	184	4267
Average value/Standard size	1.00	0.981	1.00
2inch×10inch×12feet			
Dimension	Width	Height	Length
Average value (mm)	38	234	3672
COV	9.27×10^{-3}	6.03×10^{-3}	3.76×10^{-4}
Standard size (mm)	38	235	3658
Average value/Standard size	1.00	0.996	1.00
2inch×12inch×10feet			
Dimension	Width	Height	Length
Average value (mm)	39	284	3051
COV	1.39×10^{-2}	8.24×10^{-3}	1.16×10^{-3}
Standard size (mm)	38	286	3048
Average value/Standard size	1.03	0.993	1.00
2inch×12inch×12feet			
Dimension	Width	Height	Length
Average value (mm)	38	285	3684
COV	2.44×10^{-2}	7.21×10^{-3}	1.10×10^{-3}
Standard size (mm)	38	286	3658
Average value/Standard size	1.00	0.997	1.01
2inch×12inch×14feet			
Dimension	Width	Height	Length
Average value (mm)	38	284	4291
COV	9.27×10^{-3}	7.48×10^{-3}	1.09×10^{-3}
Standard size (mm)	38	286	4267
Average value/Standard size	1.00	0.993	1.01

4.2 Torsional Test to Determine the Shear Modulus

Tests to determine the shear modulus were conducted in accordance with the ASTM D198 (2009) standard. Ten (10) glulam and thirty-eight (38) lumber specimens were tested. All glulam timber beams consisted of 20f-E bending grade and had the dimensions of 80 mm in width and 228 mm depth. Each member consisted of a single lamination in width and was connected by finger joints in length, as shown in Figure 4.1.

(a) (b)

Figure 4.1 The glued laminated timber for torsional testing
(a) Laminations of glulam beam and (b) Finger joint of lamination

All the lumber joists were Spruce-Pine-Fir (SPF), No.1/No.2 grade. The geometries included 2×8 inch nominal dimension with 14 feet in length, 2×10 inch with 12 feet length, 2×12 inch with 10, 12, and 14 feet lengths. The specimens were conditioned to a moisture content of 12% on average. The maximum moisture content measured was 16.1%.

4.2.1 Torsion Test Set-up

The glulam test specimens were clamped symmetrically about the longitudinal axis by two steel clamps at each end. The load was applied by a hydraulic jack on the top of the wide flange steel bracket. The magnitude of the applied load was measured using a load cell located between the jack and the steel bracket. The load application points and the support were made from beveled wood cross section in order to allow for free rotation about the longitudinal axis

of the specimens. The distance between the contact points of bearing and the center of the cross-section was 400 mm and the distance between the two clamps was 2000 mm. Due to the symmetry in the setup, the specimens received a uniform coupled torsional moment at each end. Based on the requirement of ASTM 198 (2009), the total length of specimen (and distance between clamps) should be at least eight times greater than the larger cross-sectional dimension. Figure 4.2 and 4.3 show a schematic and laboratory test set-up, respectively, of the glulam torsion tests.

The only differences between the glulam and lumber torsional test were that for lumber the brackets were made out of wood, to reduce the weight on the test specimens and the distance between the clamps was 2600 mm. Figure 4.4 presents the laboratory test set-up for the SPF joists.

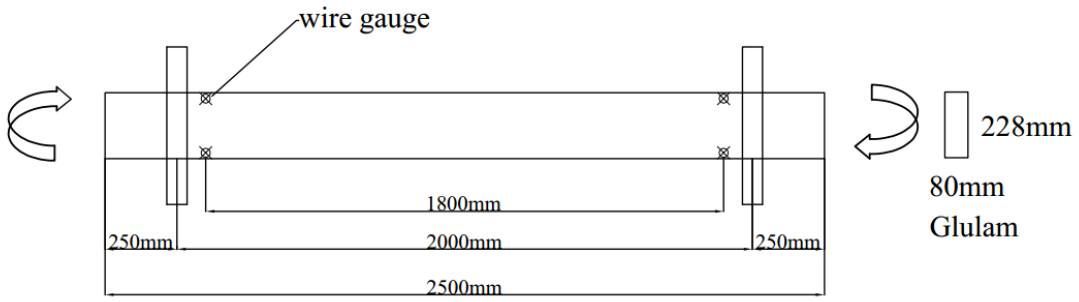

(a)

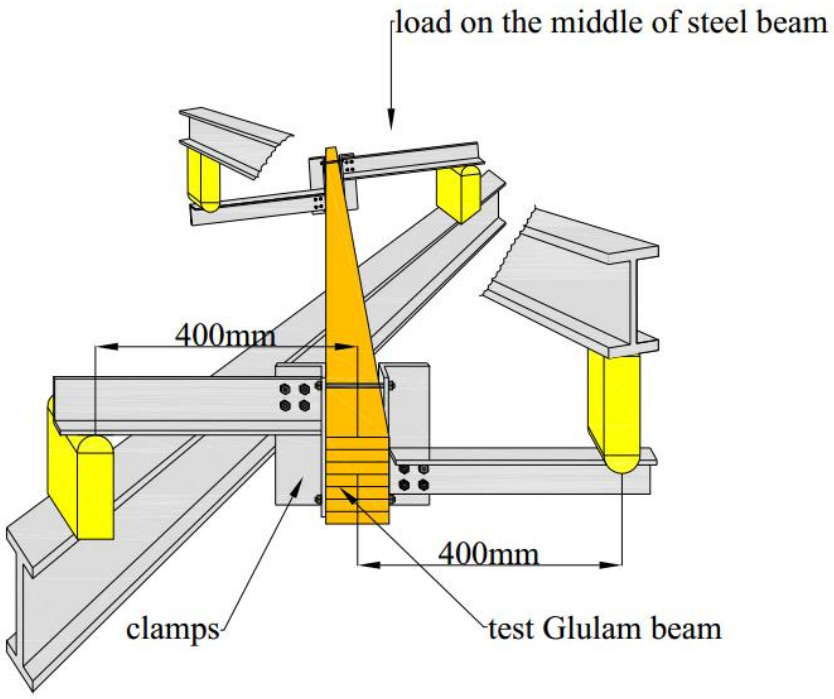

(b)

Figure 4.2 Schematic of torsion test set-up for glulam

(a) Two dimensional view of the torsion test set-up, (b) Three dimensional view of torsion test setup

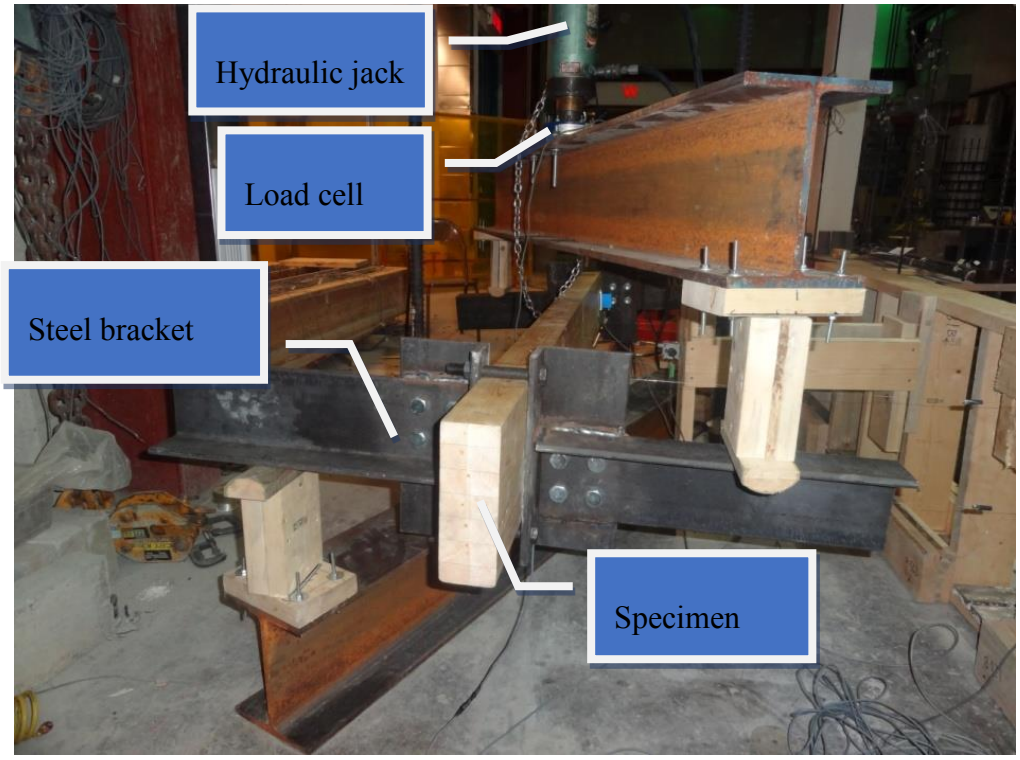

Figure 4.3 Laboratory torsion test of glulam

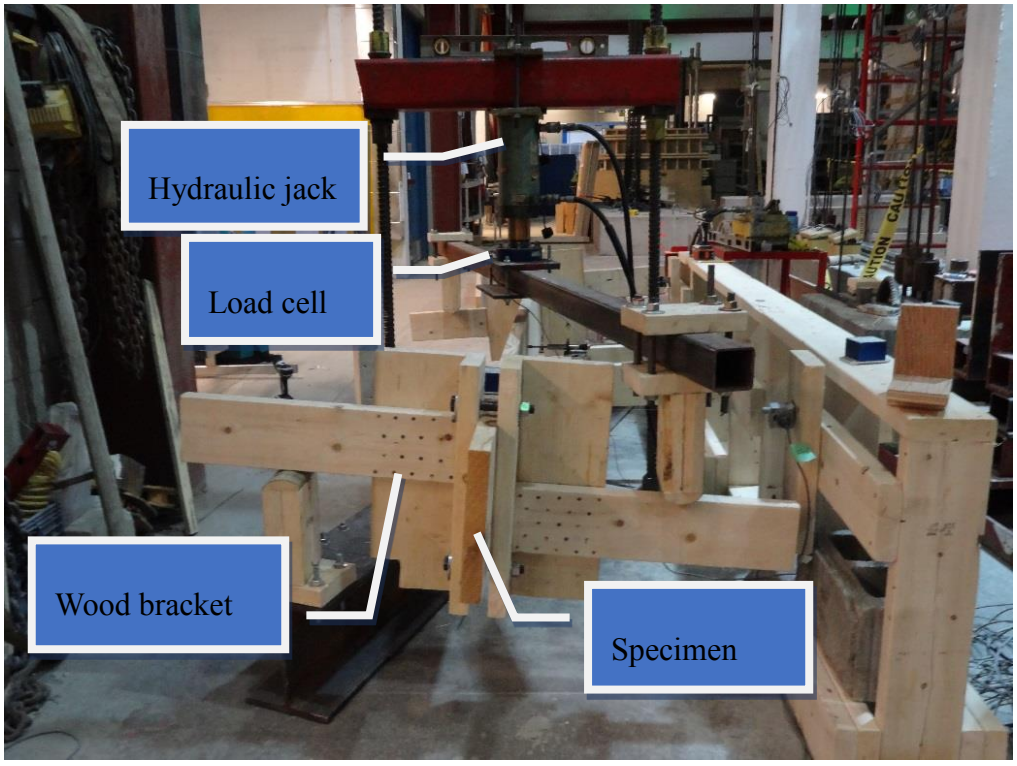

Figure 4.4 Laboratory torsion test of SPF

4.2.2 Determining the Angle of Twist

To obtain the angle of twist, the displacements at the top and bottom of the beam at each end near the clamps were measured using wire gauges with a 600 mm stroke. A knee-wall constructed near the test setup was used as a reference point for the displacement measurements. Figure 4.5 shows the connection between wire gauge and the test specimen. Inclinometers were also used to measure the angle of twist. They were installed on the top of the test specimens as close as possible to the clamps, as shown in Figure 4.6.

(a) (b)

Figure 4.5 The connection between wire gauge to Glulam beam
(a) Wire gauge connect to the glulam, and (b) End of wire gauge were fixed on the frame

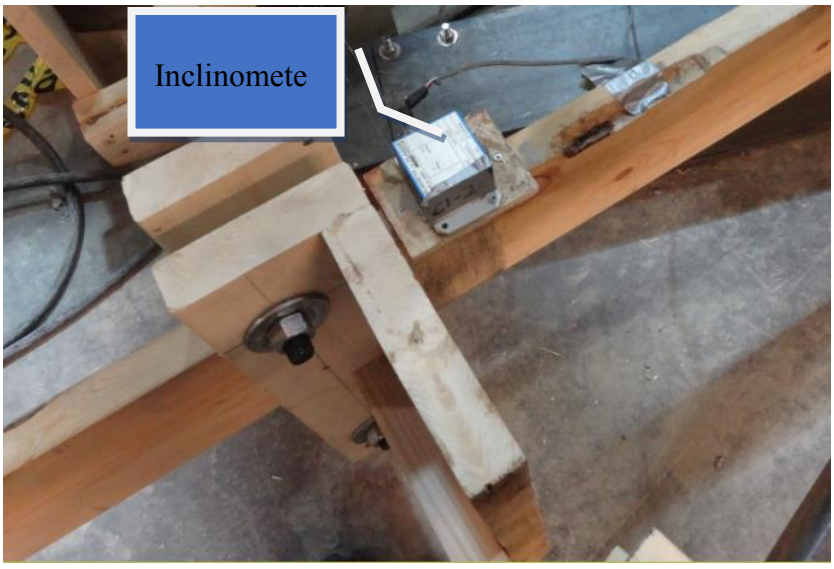

Figure 4.6 The installation of inclinometer in SPF

4.3 Bending Test Set-up

Seventeen (17) glulam and thirty-six (36) lumber specimens were tested in the weak-direction bending in accordance with the ASTM D198 standard (ASTM, 2009) to obtain their modulus of elasticity (E_L). The load application points were located at the third point of the clear span. No bracing of the beams was required as out of plane buckling could not occur. Since the direction of lateral torsional buckling in a beam is random, the E_L was measured on both sides of the specimens and the average values were used in calculating the critical value in the capacity calculation. The applied load was measured using a load cell which was located between the hydraulic jack and load transfer device. The mid-span deflection was measured using a wire gauge with the lab strong floor as reference. The set-up for bending test is shown in Figures 4.7 and 4.8.

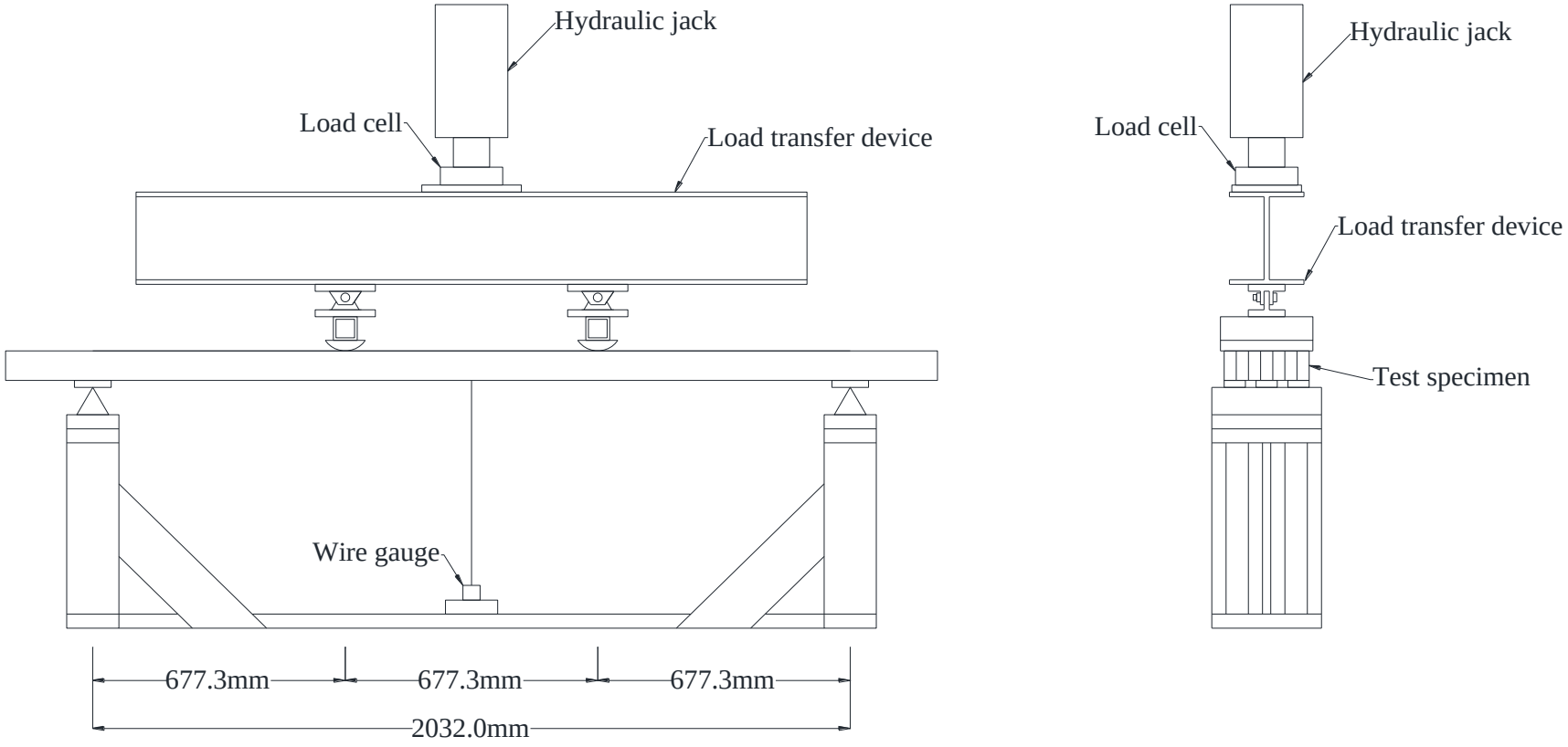

(a) (b)

Figure 4.7 Schematic drawing of the weak axis bending test set-up

(a) Profile, and (b) Side

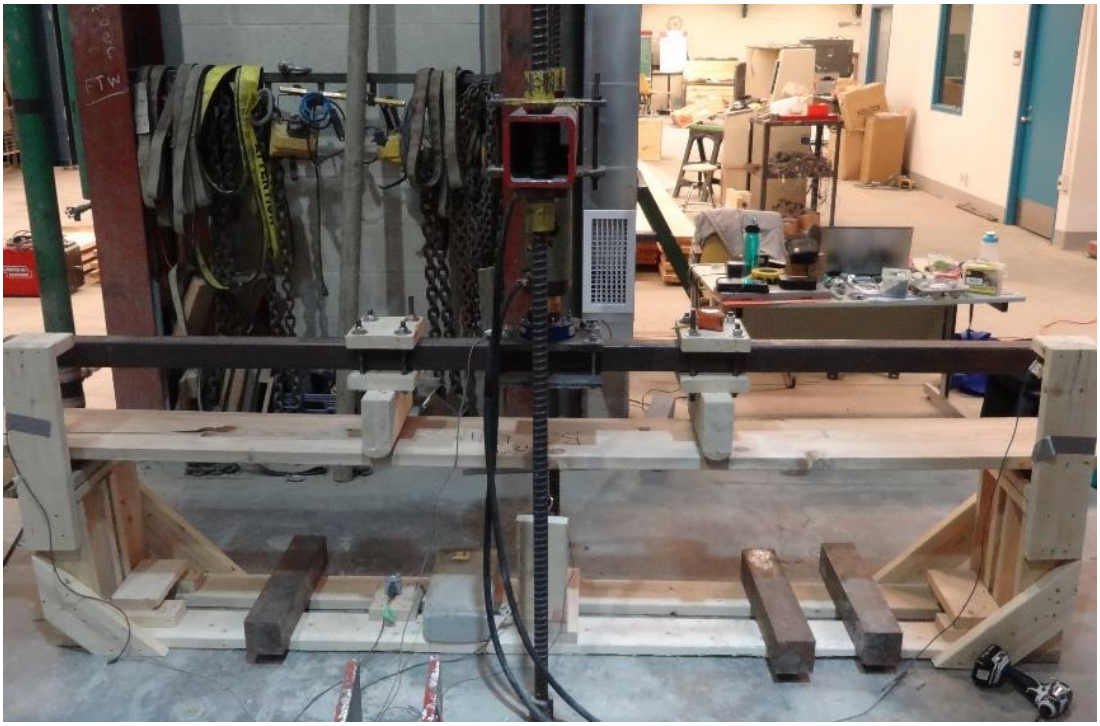

Figure 4.8 The set-up of weak axis bending for SPF

4.4 Full-scale Lateral Torsional Buckling Test Set-up

As mentioned earlier, the focus of the full scale lateral torsional buckling experimental testing was on lumber due to the lack of data in this area. The main objective was to demonstrate the validity of classical lateral torsional solution for orthotropic wood material. Eighteen test samples with aspect ratios that would yield failure in the elastic region, according to Canadian timber design code provisions (CSA, 2009), were selected for the full scale lateral torsional buckling tests. The slenderness ratios C_B were calculated to 29.4, 30.7, and 36.6 for specimens 2"×8"×14', 2"×10"×12', and 2"×12"×14', respectively (Table 4.2). C_K , in Table 4.2, is equal to $\sqrt{(0.97EK_{SE}K_T)/(C_B^2F_bK_X)}$, and it constitutes the point beyond ($C_B > C_K$) which the element is in elastic region, where F_b is specified strength in bending, K_{SE} is the service condition factor of modulus of elasticity, K_T is treatment factor, K_X is curvature factor, and the value of K_{SE}, K_T and K_X are equal to 1.

Table 4.2 Slenderness of the tested specimens

Beam sectional dimension (inch)	Clear span(mm)	Specimen amount	Slenderness ratio	C_K
2×8	4200	5	29.4	27.9
2×10	3600	6	30.7	27.9
2×12	4200	7	36.6	27.9

4.4.1 Boundary Conditions

A very important aspect of the full scale lateral torsional buckling test setup is the boundary support conditions. The boundary conditions assumed in the classical solution to the lateral torsional buckling problem are the end cross-sections are free to rotate about the strong and weak axis but restrained to move along the tangential and lateral direction. The boundary supports chosen in the experimental program attempted to mimic as much as possible these assumptions. The supports were constructed using two steel rods which were welded to the bottom plate and fastened with one piece of HSS steel on top to prevent rotation of the specimen about the longitudinal direction and buckling laterally at each end. The end supports were made to rotate about the weak axis of end cross-section. A hole with 3/4" in diameter was drilled into the wood support and a steel shaft with same diameter was welded underneath the end support. A thrust bearing was placed between the steel rod and hole of wood support, as shown in Figure 4.9. Since the steel rod and hole had the same diameter, the support is free to rotate but braced from buckling laterally.

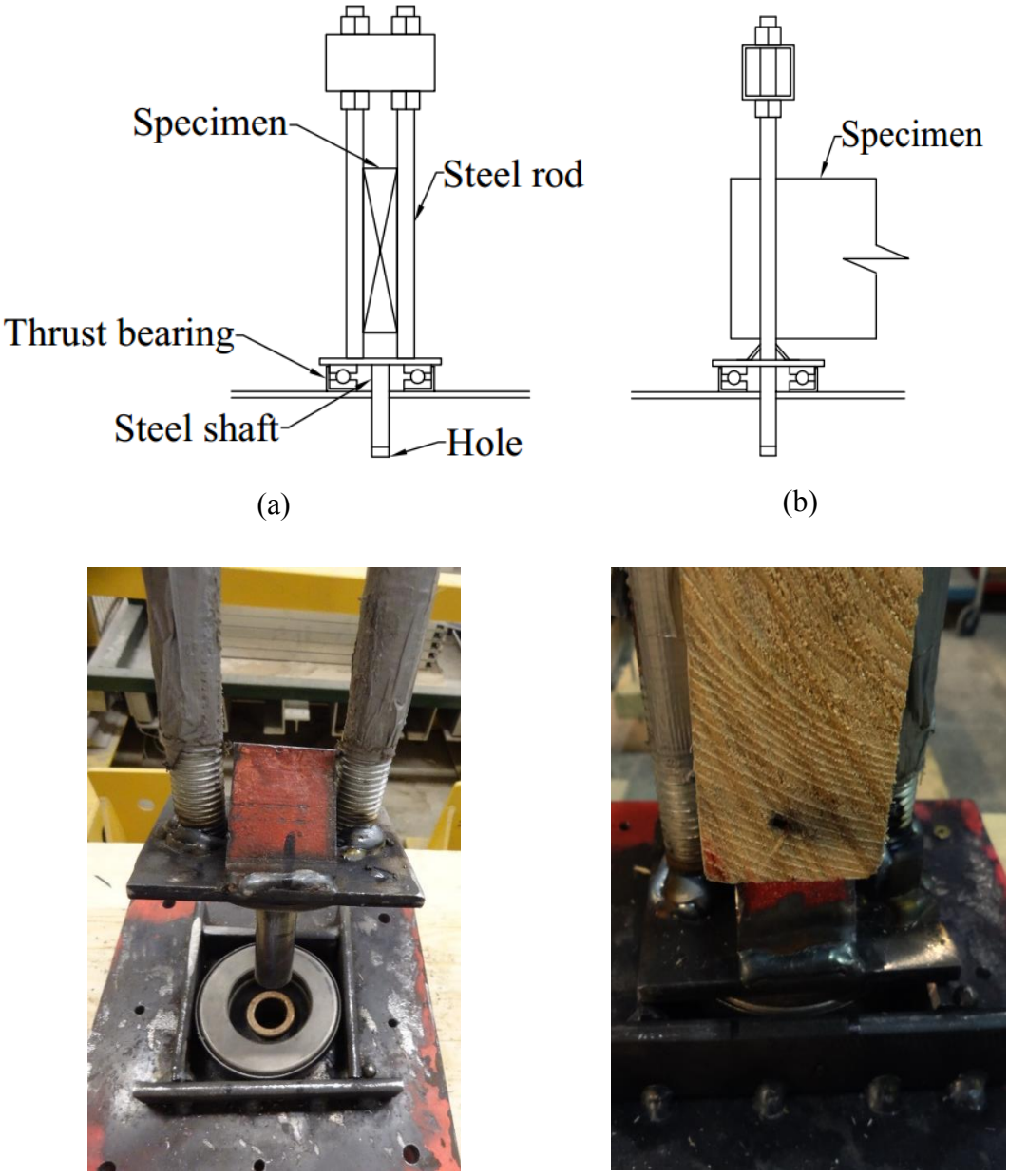

Figure 4.9 Rotatable end support of LTB set-up

(a) Profile, (b) side, (c) rotatable end support, and (d) rotation in test

4.4.2 Load Application Mechanism

It is important that the load application mechanism does not provide any lateral restrain to the beam, because such restraint would affect the results of the critical load. For this reason, the applied load consisted of weights that were suspended from the top of the test specimens at mid-span. The specimens would therefore be able to move laterally

without any additional restraints. As shown in Figure 4.10, the loading frame consisted of three parts: A steel HSS load transfer beam, a wood base to support the weight and a steel rod that allows rotation of the frame when the beam starts deflecting laterally

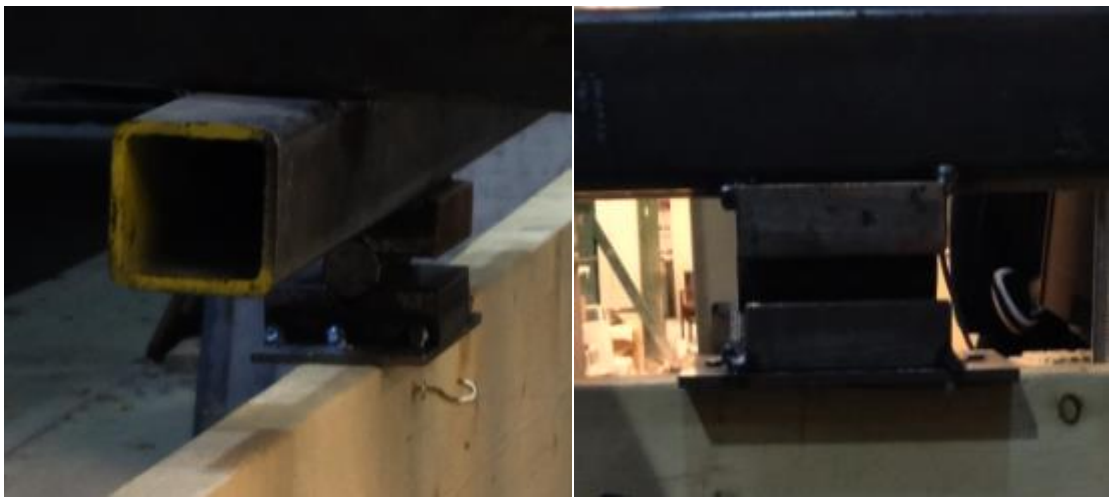

(a) (b)

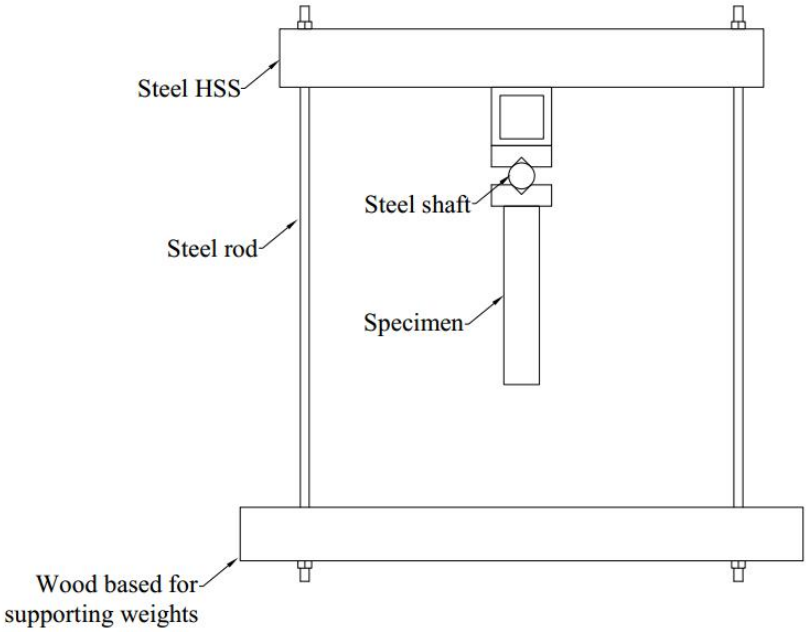

(c)

Figure 4.10 Connection between load frame and specimen
(a) Profile, (b) Side, and (c) Load application frame

4.4.3 Instrumentation

The angle of twist and lateral deflection at mid-span were measured by two wire gauges,

the lateral displacement of middle height was the average value of two wire gauges (located at the top and bottom of mid-span), the twist was calculated by the difference of top and bottom lateral displacement of mid-span, and the vertical deflection of middle span was measured using a wire gauge, which was located on the mid-height at mid-span. A schematic drawing and a picture of the set-up are presented in Figure 4.11 and 4.12.

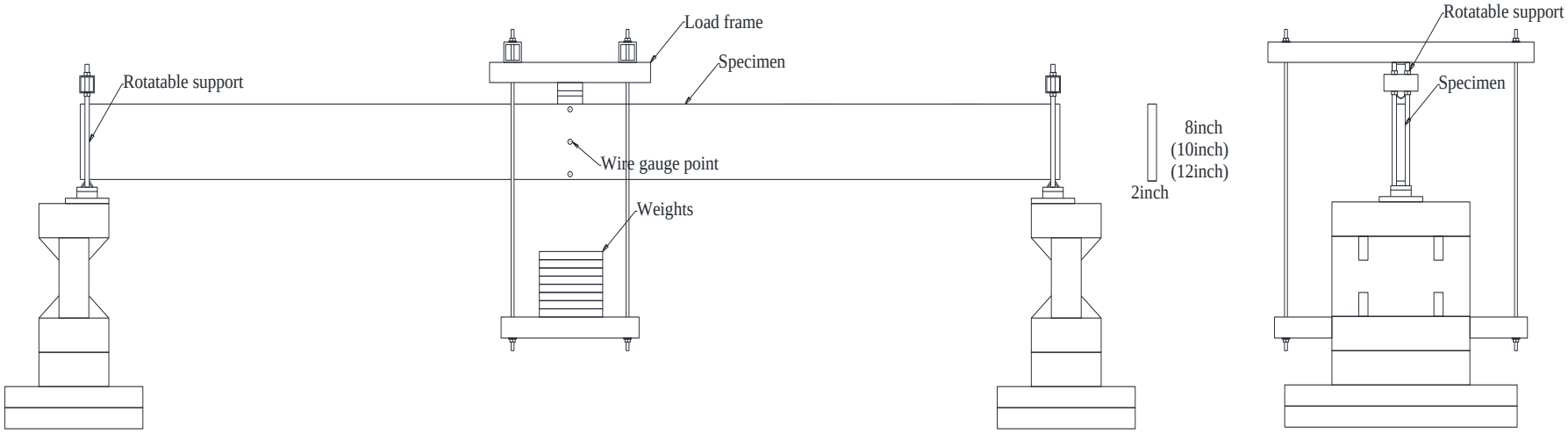

(a) (b)

Figure 4.11 Schematic Lateral torsional buckling set-up

(a) Profile, and (b) side

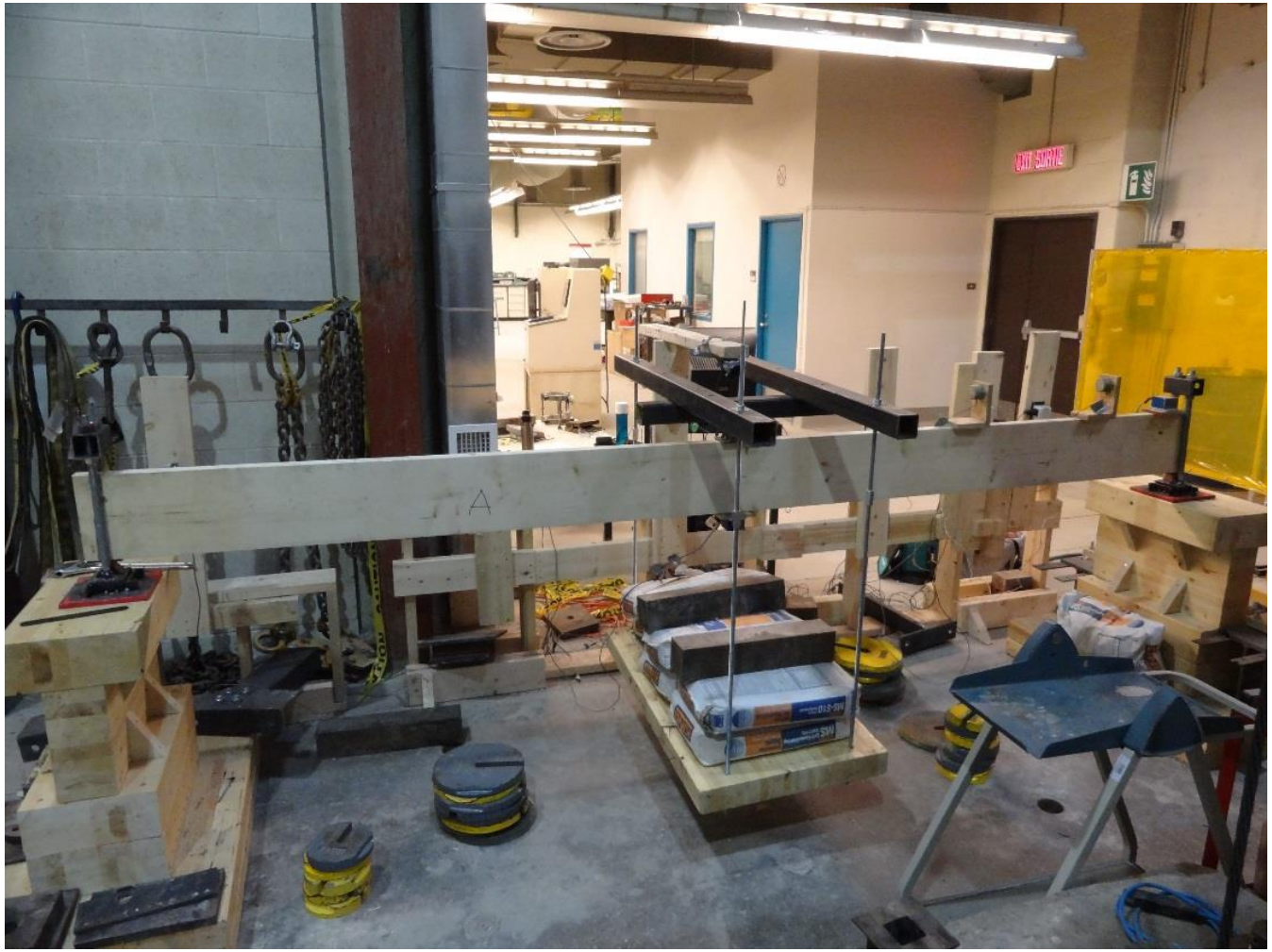

Figure 4.12 The set-up of lateral torsional buckling test

4.5 Notation for Chapter 4

C_B	slenderness ratios
E	modulus of elasticity (MPa)
E_L	modulus of elasticity in the longitudinal direction (MPa)
F_b	specified strength in bending (MPa)
G_{LR}	shear modulus about longitudinal and radial direction (MPa)
G_{LT}	shear modulus about longitudinal and tangential direction (MPa)
G_T	shear modulus about transverse (MPa)
K_{SE}	service condition factor of modulus of elasticity
K_T	treatment factor
K_X	curvature factor

4.6 References

[1] Forest Products Labratory. (2010). Wood Handbook-Wood as an Engineering Material. Madison, USA.

[2] Canadian Standards Association. (2009). CSA standards O86-09, Engineering design in wood, Mississauga, Ontario, Canada.

[3] ASTM Standard D198. (2009). Standard Test Method of Static Tests of Lumber in Structural Sizes. Philadelphia, Pa.

Chapter 5

Experimental Results

5.1 General

The experimental results from the torsion, bending and full-scale lateral torsional buckling tests are presented in this chapter. The chapter also presents the failure characteristics observed in the torsional and lateral torsional buckling tests.

5.2 Torsional Test Results

5.2.1 Calculation Method

A torsional test setup was constructed and tests were conducted in accordance with the ASTM D198 (2009) standard. The value of the shear modulus G_T for each test specimen was calculated using Equation (5.1) (Hibbeler, 2011):

$$\theta = \frac{TL_i}{JG_T} \tag{5.1}$$

Where T is the applied torque force, L_i is the distance between inclinometers, G_T is the shear modulus about the transverse direction, θ is the angle of twist， J is the Saint Venant Torsional constant.

5.2.2 Torsional Test to Failure

There are very few studies that have looked at wood failure in torsion both in terms of failure capacity and failure modes. Torsion is expected to be very low in wood and is therefore typically ignored and load causing torsional stresses are usually avoided in structural design and detailing.

In order to estimate a level of stress required to obtain the torque force and angle of twist relationships while still remaining in the linear elastic region, destructive tests were conducted on both glulam beams and lumber joists to determine the failure load and failure modes.

As shown in Figure 5.1, torsional shear stressed cause fracture to occur along the fibers and multiple such cracks were observed on the side face of the beam. The load-angle of twist curves were almost linear until failure, as seen in Figure 5.2. This trend is consistent with those found in the literature (Yang, 2012, Khokhar, 2012).

(a)

(b)

Figure 5.1 Failure of torsion test

(a) Failure of Glulam beam in torsion, and (b) Failure of SPF beam in torsion

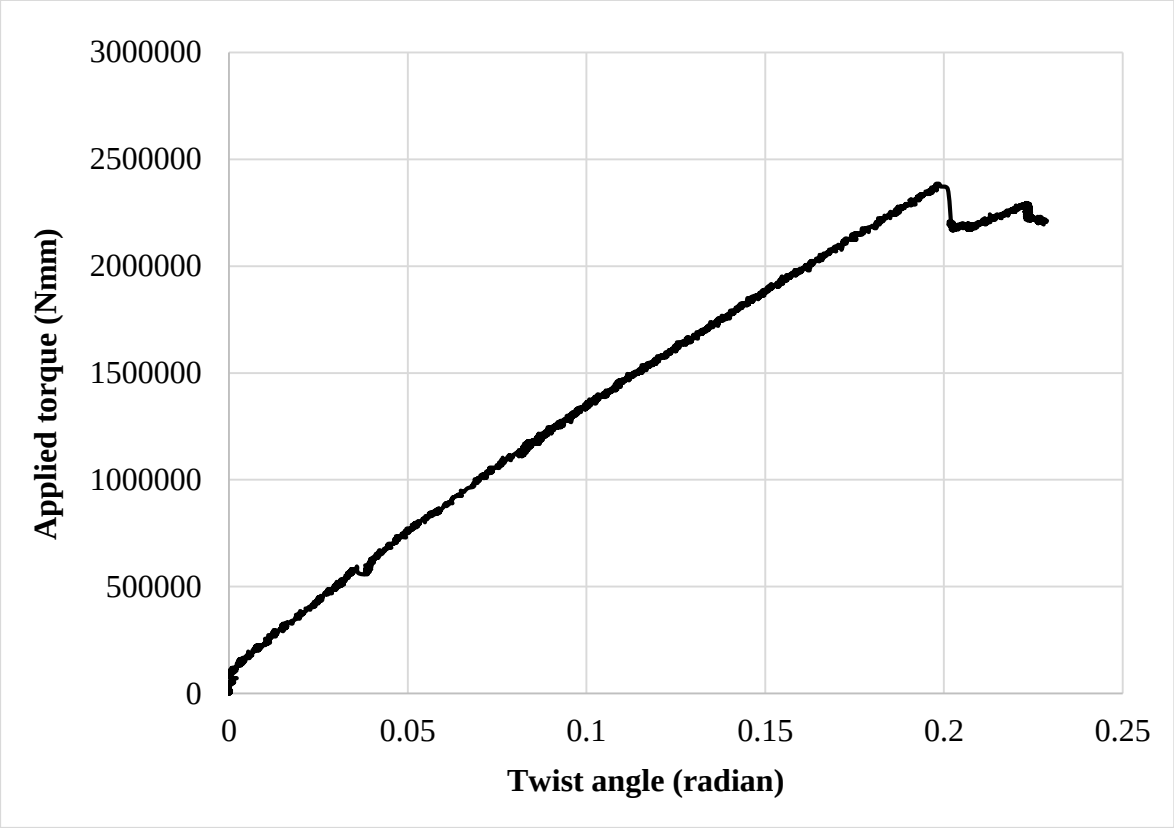

Figure 5.2 Force-twisting angle plot until failure of Glulam beam

Based on the test results, it was deemed appropriate to load the test specimens up to approximately 40% of the ultimate load, to ensure that the specimens were within the linear-elastic region and that no damage was incurred by the specimens during the loading.

5.2.3 Shear Modulus for Glulam Beams

The average G_T value for ten glulam beams tested was 672 MPa with a COV 0.06. The test results are shown in Table 5.1 and illustrated graphically in Figure 5.3. Such low variability in the test results is expected for engineered wood products such as glulam beams. Figure 5.4 shows a typical torque-angle of twist relationship for glulam.

Table 5.1 Experimental results for G_T of Glulam beams

Test specimen	G_T (MPa)
1	708
2	631
3	689
4	657
5	635
6	657
7	744
8	620
9	724
10	659
Average value (MPa)	672
COV	0.06

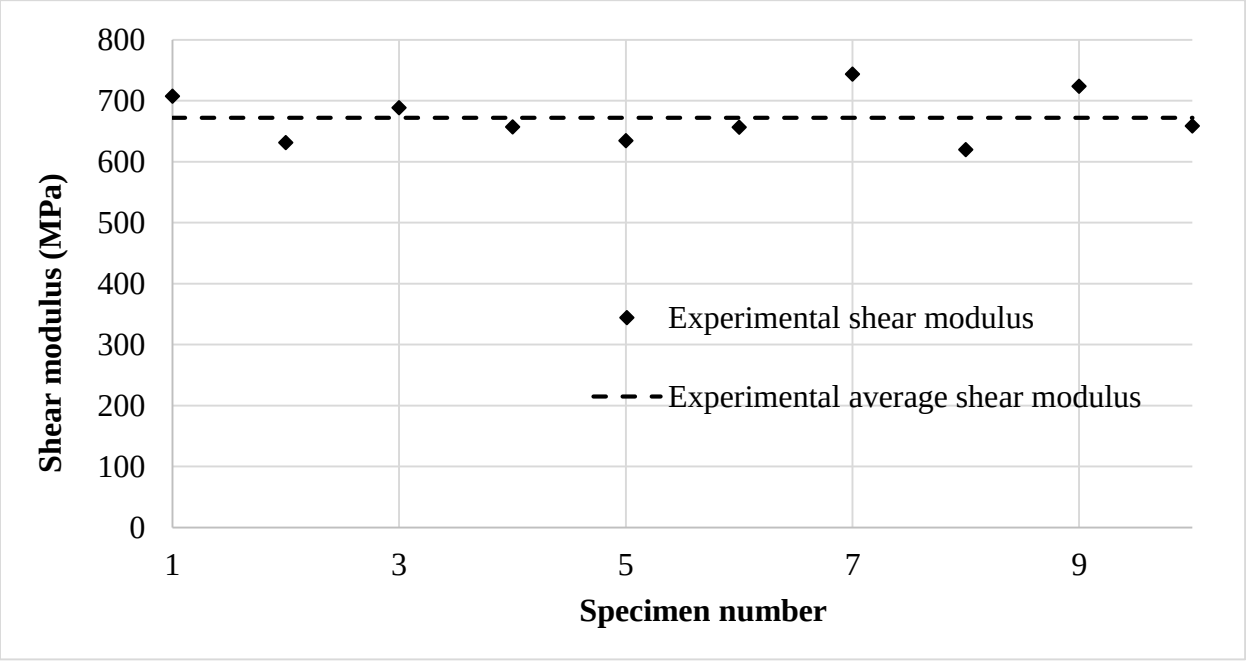

Figure 5.3 Experimental shear modulus for Glulam beams

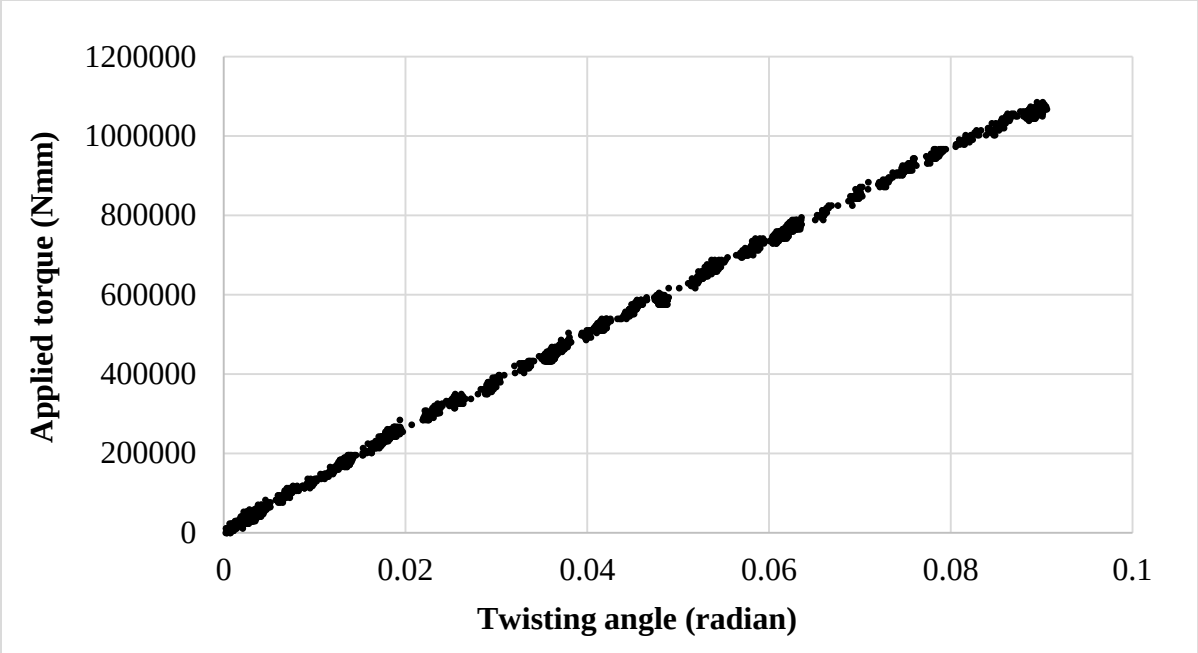

Figure 5.4 Typical torque-twisting angle plot for Glulam specimen

5.2.4 Shear Modulus for Lumber

The G_T values obtained from the torsional test for the SPF elements are summarized in Table 5.2. The average G_T of all the specimens tested was 550 MPa, which is slightly lower than that obtained for glulam. This is expected as the grade of glulam, especially of the outer laminates, is higher than that of the lumber joists. The COV varied between 0.11 and 0.22, which is also expected given the variability expected from visually graded lumber joists. This variability is illustrated graphically in Figure 5.5. The force-twisting angle relationship for the lumber joists was also linear-elastic, similar to what was observed for glulam.

Table 5.2 The experimental shear modulus value of SPF beams

Sectional dimension	Beam number	k	J ($\times 10^6$ mm)	G_T (MPa)
2”×8”×14’	1	0.289	2.886	501
	2	0.289	2.870	614
	3	0.288	2.845	558
	4	0.289	2.870	548
	5	0.288	2.845	705
	6	0.287	3.064	540
	7	0.289	2.870	808
	Average value			610
	COV			0.18
2”×10”×12’	1	0.299	3.839	542
	2	0.299	3.806	535
	3	0.300	3.868	569
	4	0.299	3.839	710
	5	0.299	3.790	606
	6	0.300	3.868	550
	7	0.299	4.150	632
	8	0.299	3.839	515
	Average value			583
	COV			0.11

Table 5.2: The experimental shear modulus value of SPF beams

Sectional dimension	Beam number	k	J ($\times 10^6$ mm)	G_T (MPa)
2”×12”×10’	1	0.303	5.140	447
	2	0.304	4.754	470
	3	0.303	5.105	482
	4	0.304	4.771	536
	5	0.303	5.140	457
	6	0.303	5.033	650
	7	0.304	4.704	414
	Average value			494
	COV			0.16
2”×12”×12’	1	0.304	4.771	462
	2	0.304	4.687	465
	3	0.304	5.193	391
	4	0.303	5.140	593
	5	0.304	4.754	656
	6	0.304	4.737	675
	7	0.304	4.737	457
	8	0.305	4.041	690
	Average value			549
	COV			0.22

Table 5.2: The experimental shear modulus value of SPF beams

Sectional dimension	Beam number	k	J ($\times 10^6$ mm)	G_T (MPa)
2”×12”×14’	1	0.304	4.737	451
	2	0.304	4.754	521
	3	0.303	5.140	479
	4	0.304	4.754	515
	5	0.304	4.687	442
	6	0.304	4.737	720
	7	0.304	4.754	537
	8	0.303	4.655	471
	Average value			517
	COV			0.172

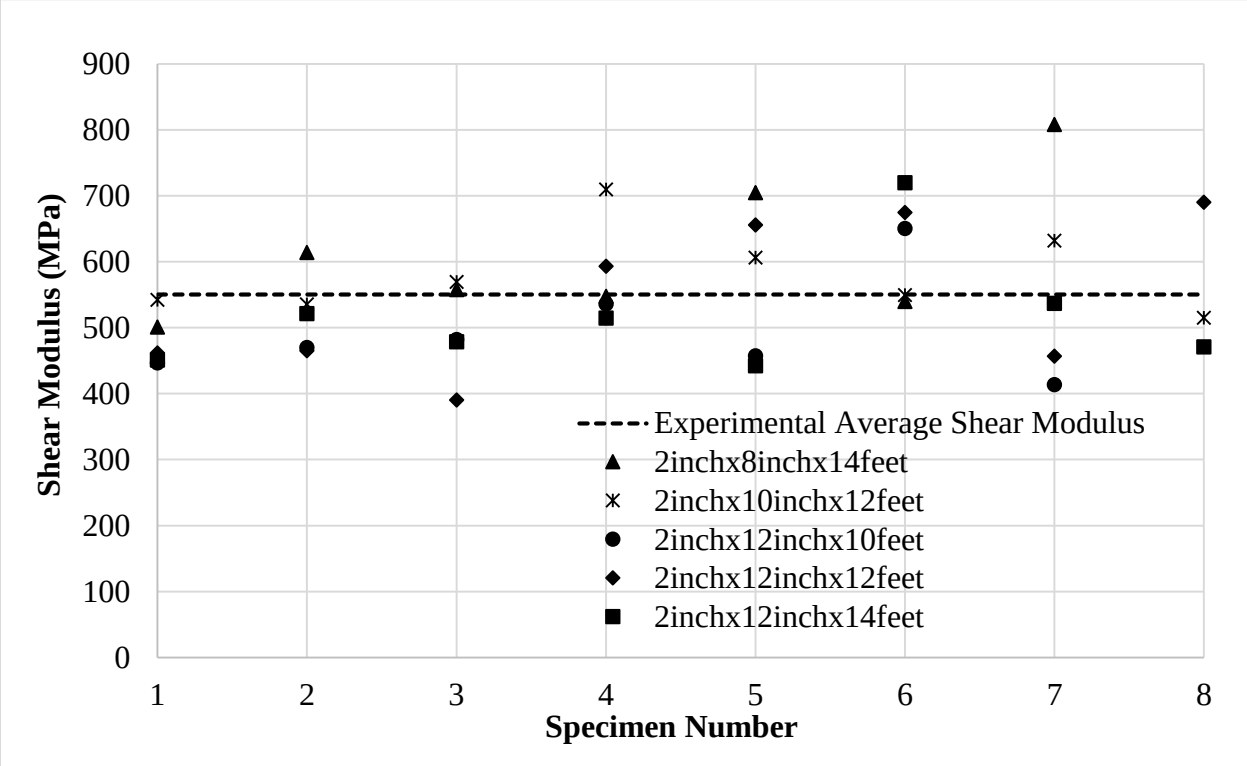

Figure 5.5 Experimental shear modulus for SPF beams

5.3 Bending Test Results

5.3.1 Determining the Modulus of Elasticity of Glulam Beams about the Weak Axis

The same glulam beams that were tested non-destructively in torsion and the other seven glulam specimens with same grade and dimensions were subjected to four-point bending loading to determine their weak axis modulus of elasticity along the longitudinal direction E_L. The end conditions were pinned and no lateral bracing was deemed necessary due to the low depth to width aspect ratios of the beams. As mentioned in Chapter 3, due to the uncertainty in the direction of the buckling, E_L of both faces were determined. Table 5.3 summarizes the test results for each side and the average E_L calculated. The average E_L of all specimens was 8503 MPa with COV of 0.07. The experimental results of the 17 Glulam beams are also presented in Figure 5.6.

Table 5.3 The E_L values of Glulam beams about weak axis

Beam number	surface	E_L values of individual side (MPa)	E_L values of specimen (MPa)
1	1-a	9613	9826
	1-b	10039	
2	2-a	8055	8031
	2-b	8007	
3	3-a	9364	9395
	3-b	9427	
4	4-a	8302	8158
	4-b	8014	
5	5-a	8324	8130
	5-b	7936	
6	6-a	7513	7373
	6-b	7232	

Table 5.3 The E_L values of Glulam beams about weak axis

Beam number	surface	E_L values of individual side (MPa)	E_L values of specimen (MPa)
7	7-a	8963	8901
	7-b	8839	
8	8-a	8475	8721
	8-b	8968	
9	9-a	8042	8065
	9-b	8087	
10	10-a	8374	8261
	10-b	8147	
11	11-a	8449	8572
	11-b	8694	
12	12-a	8545	8292
	12-b	8039	
13	13-a	8226	8458
	13-b	8691	
14	14-a	8511	8669
	14-b	8828	
15	15-a	8740	8711
	15-b	8682	
16	16-a	8711	8732
	16-b	8754	
17	17-a	8397	8251
	17-b	8106	
Average of all Glulam beams (MPa)			8503
COV			0.07

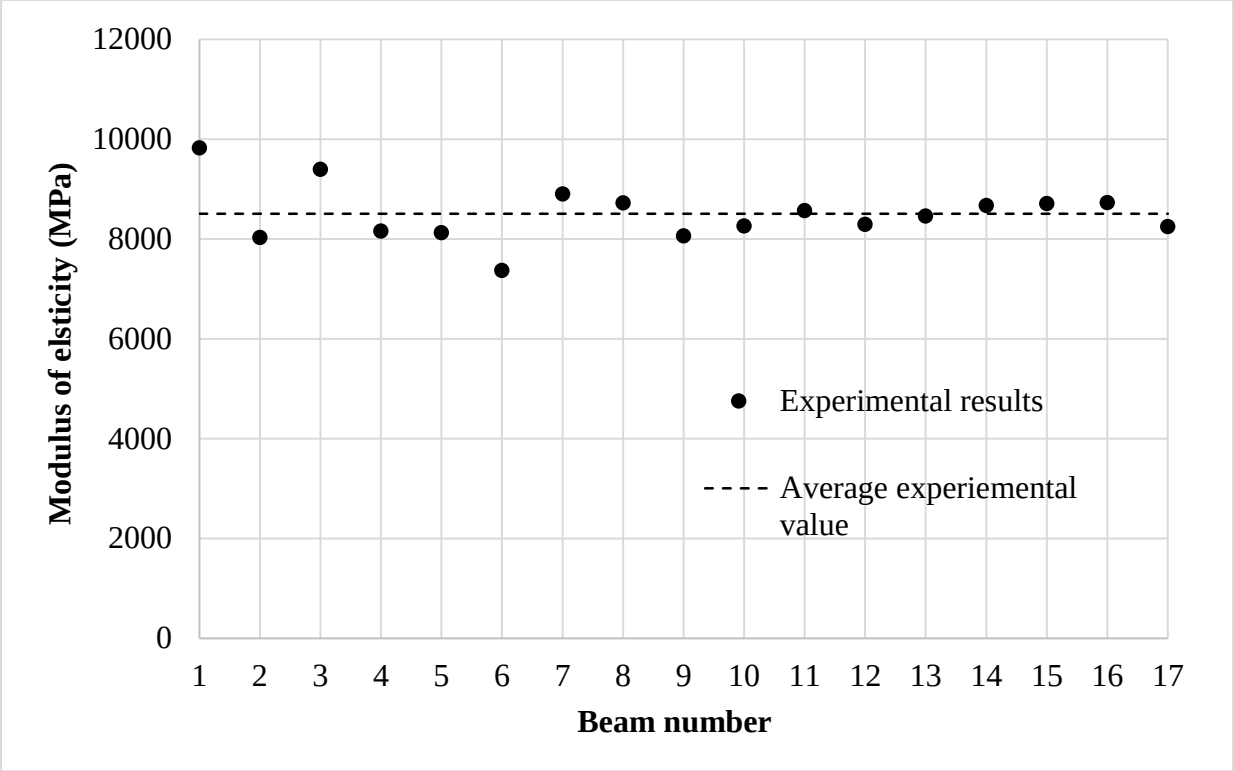

Figure 5.6 Experimental results for weak axis bending of Glulam specimens

5.3.2 Determining the Modulus of Elasticity of Lumber Joists about the Weak Axis

The results from the non-destructive weak-axis bending tests on the lumber joists are summarized in Table 5.4. The average E_L was found to be 8136 MPa for all specimens. The variability in the results was significantly higher than those found in glulam with COV values varying between 0.14 and 0.27. The obtained E_L was also based on the force-displacement plot in linear deformation, similar to what was observed for glulam.

Table 5.4 The experimental results of weak axis bending tests for SPF specimens

Sectional dimension	Beam number	Surface	E_L values of individual side (MPa)	E_L values of specimen (MPa)
2”×8”×14’	1	1-a	10333	10434
		1-b	10535	
	2	2-a	8966	9022
		2-b	9077	
	3	3-a	11163	11185
		3-b	11207	
	4	4-a	10269	10111
		4-b	9952	
	5	5-a	7226	7382
		5-b	7537	
	6	6-a	10000	9947
		6-b	9894	
	Average value of SPF beam (MPa)			9680
	COV			0.14
2”×10”×12’	1	1-a	11418	11217
		1-b	11015	
	2	2-a	9274	9745
		2-b	10215	
	3	3-a	5575	5563
		3-b	5550	
	4	4-a	9693	9279
		4-b	8864	
	5	5-a	12196	12339
		5-b	12482	
	6	6-a	6337	7619
		6-b	8902	

Table 5.4 The experimental results of weak axis bending tests for SPF specimens

Sectional dimension	Beam number	Surface	E_L values of individual side (MPa)	E_L values of specimen (MPa)
2”×10”×12’	7	7-a	8416	8092
		7-b	7768	
	8	8-a	9025	9009
		8-b	8992	
	Average value of SPF beam (MPa)			9108
	COV			0.23
2”×12”×10’	1	1-a	7395	7057
		1-b	6719	
	2	2-a	8264	8227
		2-b	8189	
	3	3-a	9086	9103
		3-b	9120	
	4	4-a	10415	10339
		4-b	10264	
	5	5-a	5855	6165
		5-b	6474	
	6	6-a	6242	6151
		6-b	6059	
	7	7-a	7906	7706
		7-b	7505	
	Average value of SPF beam (MPa)			7821
	COV			0.21
2”×12”×12’	1	1-a	9166	9061
		1-b	8956	
	2	2-a	8495	8459
		2-b	8423	

Table 5.4 The experimental results of weak axis bending tests for SPF specimens

Sectional dimension	Beam number	Surface	E_L values of individual side (MPa)	E_L values of specimen (MPa)
2”×12”×12’	3	3-a	6794	6932
		3-b	7070	
	4	4-a	3854	3776
		4-b	3697	
	5	5-a	7274	7728
		5-b	8182	
	6	6-a	9262	9305
		6-b	9347	
	7	7-a	6211	6070
		7-b	5929	
	Average value of SPF beam (MPA)			7333
	COV			0.265
2”×12”×14’	1	1-a	5976	6668
		1-b	7359	
	2	2-a	6725	7171
		2-b	7617	
	3	3-a	6340	6469
		3-b	6598	
	4	4-a	5654	5960
		4-b	6265	
	5	5-a	7987	7880
		5-b	7774	
	6	6-a	5722	5491
		6-b	5261	
	7	7-a	6544	6364
		7-b	6183	

Table 5.4 The experimental results of weak axis bending tests for SPF specimens

Sectional dimension	Beam number	Surface	E_L values of individual side (MPa)	E_L values of specimen (MPa)
2”×12”×14’	8	8-a	9959	9876
		8-b	9792	
	Average value of SPF beam (MPA)			6985
	COV			0.197

5.4 Results from the Full-scale Lateral Torsional Buckling Tests

Figures 5.7, 5.8 and 5.9 show typical force-lateral displacement, force-vertical displacement and force-twist angle plots of the specimens at mid-span. It can be seen that when the applied load approached to the critical load, a slight increase in load created very large deformations.

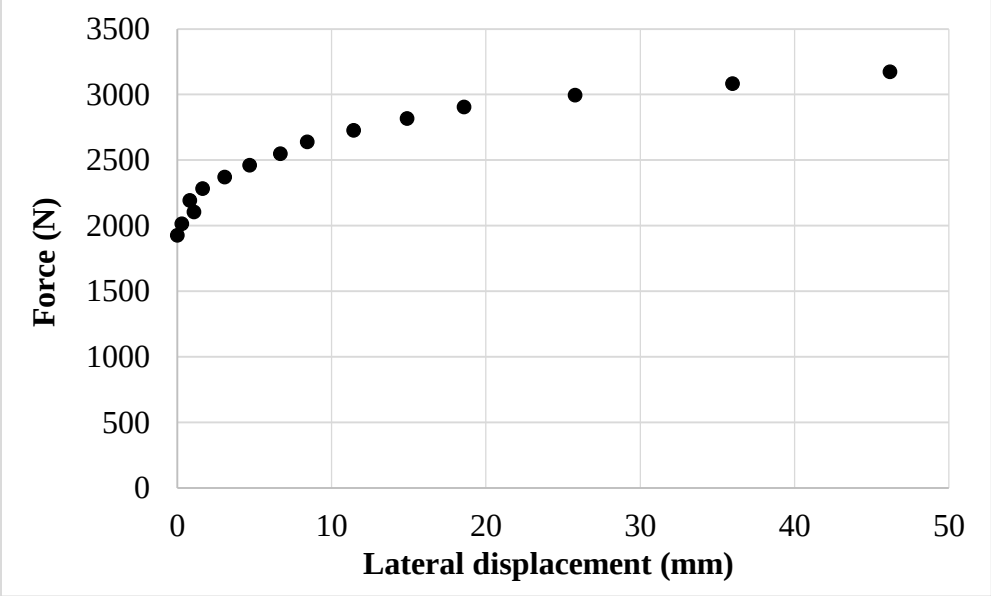

Figure 5.7 Typical force-lateral displacement of LTB tests

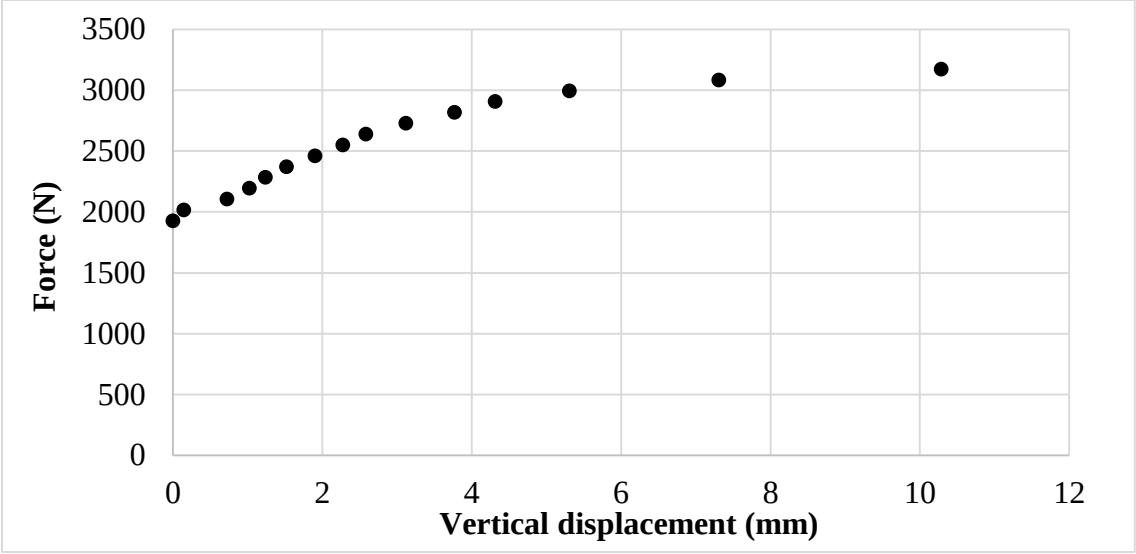

Figure 5.8 Typical force-vertical displacement of LTB tests

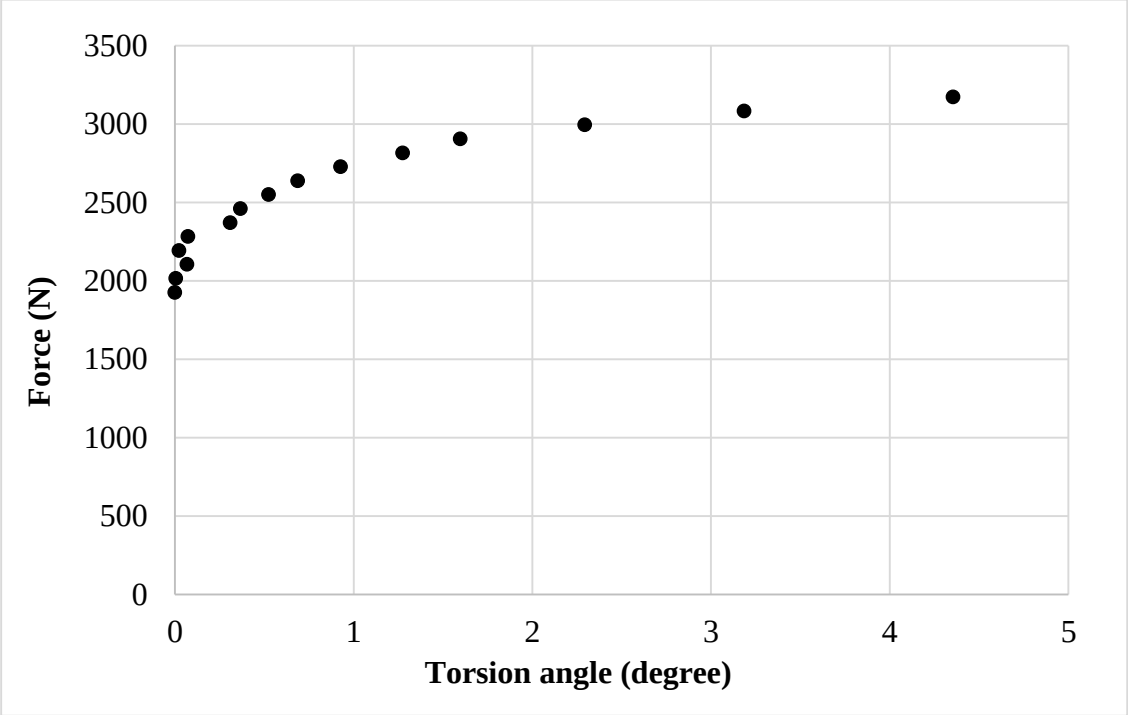

Figure 5.9 Typical force-twist angle of LTB tests

Table 5.5 provided the experimental results and the values obtained from the classical solution for lateral torsional buckling. Since the load was applied on the top of cross-section, the load eccentricity factors were included in the classical solution.

Table 5.5 The experimental results of LTB test

Sectional dimension	Beam number	E_L of weak axis (MPa)	G_T about transverse (MPa)	LTB capacity (N)	Classical solution (N)	Classical solution/ test
2”×8”×14’	1	10434	501	3344	3125	0.935
	2	9022	614	3719	3243	0.872
	3	11185	558	3576	3379	0.945
	4	10111	548	3620	3216	0.889
	6	9947	540	3620	3393	0.937
	Average experimental value			3576	3271	0.915
	COV			0.04	0.03	0.03
2”×10”×12’	1	11217	542	4598	5779	1.26
	2	9745	535	5672	5348	0.943
	3	5563	569	3441	4350	1.26
	5	12339	606	6300	6342	1.01
	6	7619	550	4868	4927	1.01
	7	8092	632	4779	5873	1.23
	8	9009	515	4512	5095	1.13
	Average experimental value			4881	5388	1.12
	COV			0.19	0.12	0.12
2”×12”×14’	1	6668	451	3163	3708	1.17
	2	7171	521	3280	4161	1.27
	3	6469	479	3680	4106	1.12
	4	5960	515	3870	3803	0.98
	5	7880	442	3190	3915	1.23
	6	5491	720	4525	4378	0.97
	Average experimental value			3618	4012	1.13
	COV			0.15	0.06	0.11

The capacities obtained from the experimental results for 2”×8”×14’ appear to be slightly higher than those obtained from the classical solution. The opposite is observed for the results obtained from the 2”×10”×12’ and 2”×12”×14’. One plausible reason for this might be that the joists with the deeper cross-section were observed to have more imperfection (eg. bow, crook and twist), which may have affected the capacity. In general, it can be concluded from Figure 5.10 that the calculated values using the classical solution compare well with those obtained from the experimental study.

To avoid destroying the measuring equipment (wire gauges), they were removed immediately before reaching the ultimate capacity of the joist members. The load did, however, continue to be applied until complete failure was observed.

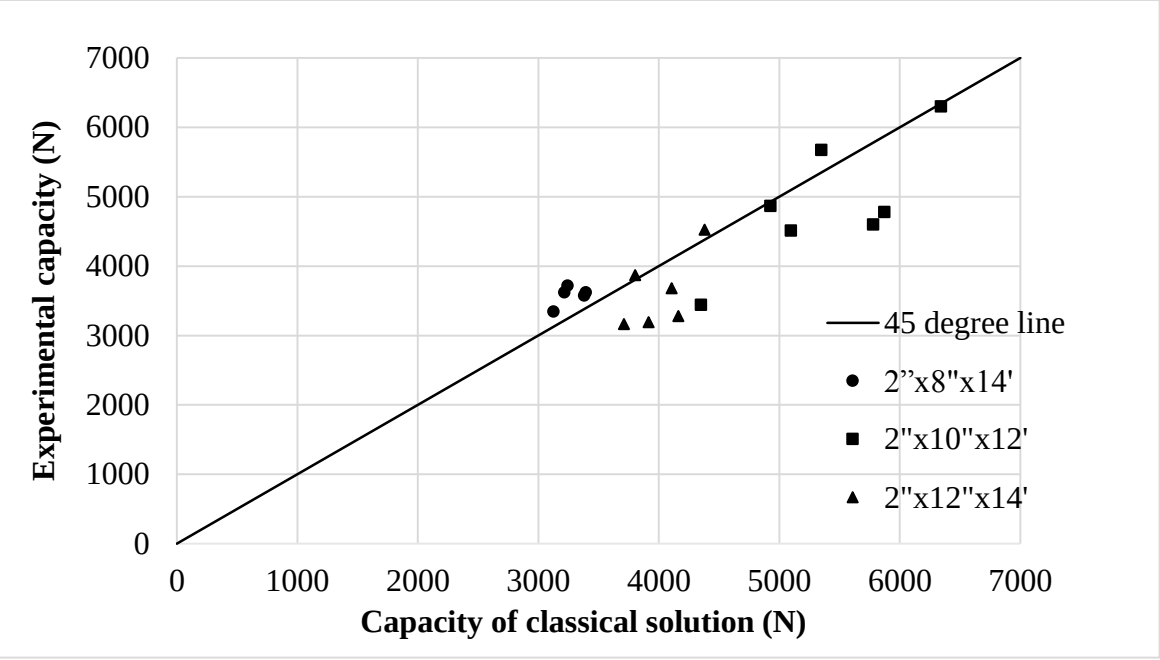

Figure 5.10 Comparison with classical solution and experimental tests

5.5 Deformation and Typical Failure Modes

5.5.1 Deformed Shape

The theoretically anticipated deformed shape for an ideal joist or beam which is perfectly straight such as the ones considered in this study would initially be represented by a deflection in the in-

plane direction, until reaching a critical moment, after which the bending member would start to deform laterally (Galambos & Surovek, 2008). However, due to initial imperfection in the real wood member (e.g. crook and bow), the joist was observed to deflect in the out-of-plane direction before the critical moment was reached. This is illustrated schematically in Figure 5.11, and was also observed in the experimental results as shown in Figures 5.7, 5.8 and 5.9. Therefore, in addition to the geometry and mechanical properties, the critical load and failure of the real beam is also influenced by the imperfection and non-linear deformation (Ahnlén, 2013).

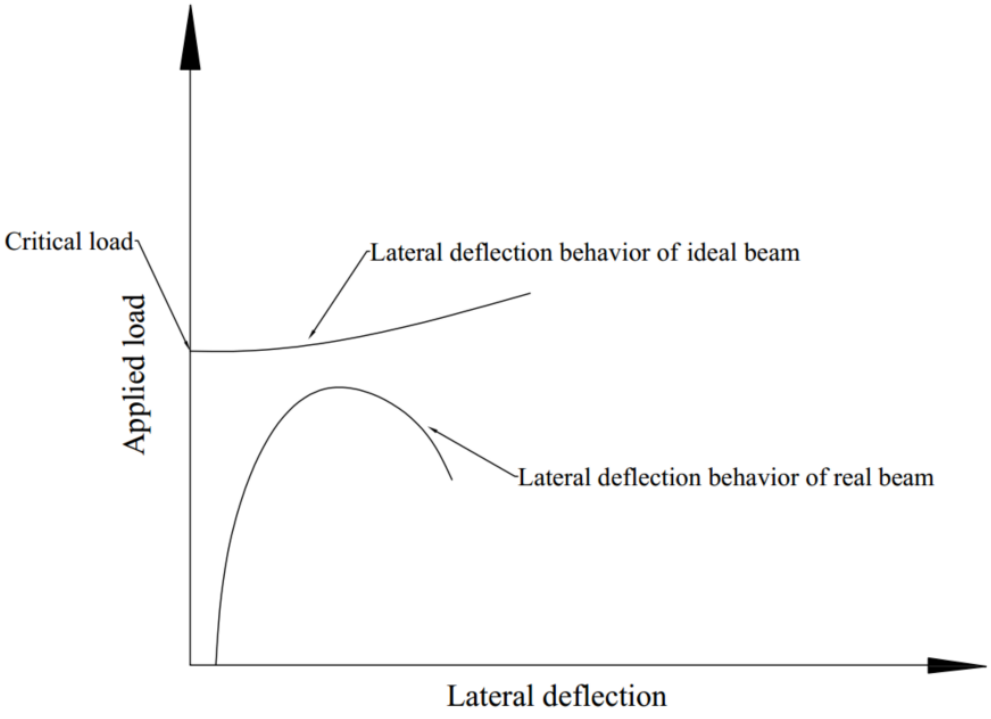

Figure 5.11 The lateral deflection of ideal beam and real beam

Figure 5.12 shows a typical deformed shape during a full scale lateral torsional buckling test. As it can be seen in Figures 5.12 (b) and (c), there is significant out-of-plane deformation and twist in the beam, which decreased gradually towards the end supports.

(a)

(b)

(c)

Figure 5.12 Typical LTB deformation in the test

(a) initial stage of LTB test, (b) final stage of LTB test, and (c) typical top view of LTB deformation in the test

5.5.2 Typical Failure Modes

Three distinct failure modes were observed under the full scale lateral torsional buckling tests. In some of the cases, the beam failed due to large lateral displacement, one side face was fully in tension and the opposite side in compression as shown in Figure 5.13.

Figure 5.13 Failure mode with outside lateral surface under tension

Another observed failure mode was when the top face of the beam was experiencing compressive stresses and the bottom face tensile stresses. The failure resembles that usually obtained under static bending tests about the major axis of the cross section with lateral bracing, as shown in Figure 5.14 (a). Figure 5.14 (b) shows the compressive failure of the beam. The failure typically occurred near or at the beam mid-span.

(a)

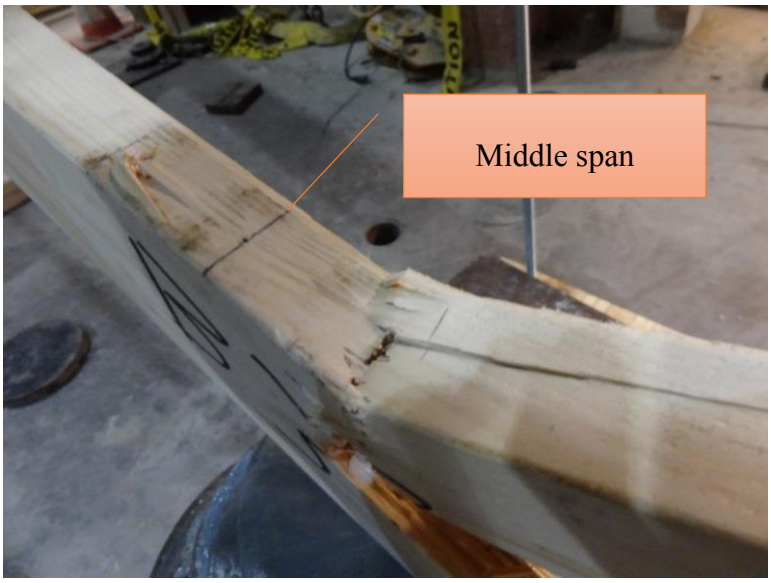

(b)

Figure 5.14 Failure mode with top face under compression and bottom face under tension (a) Profile, and (b) top view

The third observed failure mode is longitudinal shear as shown in Figure 5.15. The torsional shear crack was usually located around the mid-height of the beam and extend along the longitudinal direction from middle span to the end of beam.

Figure 5.15 Failure mode by shear stress

5.6 Notation for Chapter 5

b	beam width (mm)
d	beam depth (mm)
E_L	modulus of elasticity along the longitudinal direction (MPa)
G_T	shear modulus about transverse (MPa)
J	Saint Venant Torsional constant (mm^4)
k	constant depending on the aspect ratio d / b
L_i	distance between inclinometers (mm)
T	applied torque force (Nmm)
θ	angle of twist (degree)

5.7 References

[1] ASTM Standard D198. (2009). Standard Test Method of Static Tests of Lumber in Structural Sizes. Philadelphia, Pa.

[2] Hibbeler R.C., (2011). Mechnics of Materials, Eighth Edition, Pearson Prentice Hall, USA.

[3] Yang, Z. (2012). Torsional Shear Strength and Size Effect in Structural Composite Lumber. M.A.Sc Thesis, Department of Environmental Conservation, University of Massachusetts Amherst, Amherst, Massachusetts. USA.

[4] Khokhar, A., and Zhang, H. (2012). The use of torsion test method to evaluate the shear properties of timber joists. In World Conference on Timber Engineering, Auckland.

[5] Galambos T. V. and Surovek. A. E. (2008). Structural Stability of Steel: Concepts and Applications for Structural Engineers, John Wiley & Sons, Inc. Hoboken, New Jersey. USA.

[6] Ahnlén, M and Westlund, J. (2013). Lateral Torsional Buckling of I-beams. M.A.Sc Thesis, Department of Civil and Environmental Engineering, Chalmers University of Technology, Göteborg, Sweden.

Chapter 6

Comparison between FEA Model and Experimental Results

6.1 Model Description

6.1.1 Introduction

The objective of this chapter is to compare the FEA model with the results obtained from the experiment. As discussed in Experimental study (Chapter 4) and in Experimental results (Chapter 5), the modulus of elasticity in the longitudinal direction (E_L) and shear modulus about the transverse direction (G_T) were obtained from the experiments. Based on the mechanical properties and dimensions of each specimen, finite element models were developed to investigate the lateral torsional buckling capacity. A comparison was made between experimental programs and numerical analyses to verify the accuracy of linear elastic Eigen value finite element analysis.

6.1.2 Mesh Details

Similar to sensitivity analysis in Chapter 3, the C3D8 eight-noded brick element beams from the ABAQUS library of elements was used to model the entire beam (Simulia, 2011). The models have the same dimensions as those of the experimental program. The nominal dimensions of the specimens were 2"×8"×14' (38mm×184mm×4267mm), 2"×10"×12' (38mm×235mm×3658mm), and 2"×12"×14' (38mm×286mm×4267mm). However, as discussed in the experimental study section (Chapter 4), the actual dimensions varied slightly from the nominal dimensions. In order to predict the accurate capacity of each specimen, the models were developed based on the actual sizes. In all cases, the clear spans were $4200\,mm$ and $3600\,mm$. The dimensions of each model are shown in column 1, 2, 3 and 4 of Table 6.1.

In order to unify the mesh, all beams in the same nominal size were modelled with identical mesh, i.e., the number of elements along the width, height and length were kept constant for 2"x8"x14', 2"×10"×12' and 2"×12"×14' specimens. Similar to the sensitivity analysis, to ensure the best results, the value of width and height for each element were chosen to be close while the length of the element was taken as approximately twice the width. The mesh is fully defined by four parameters m_1, m_2, m_3 and m_4 as shown in Figure 6.1. Typical element dimensions were nearly 3.8 mm in width and height and about 7.6 mm in length. The mesh parameters for each specimen modelled are presented in Column 5, 6, 7 and 8 Table 6.1.

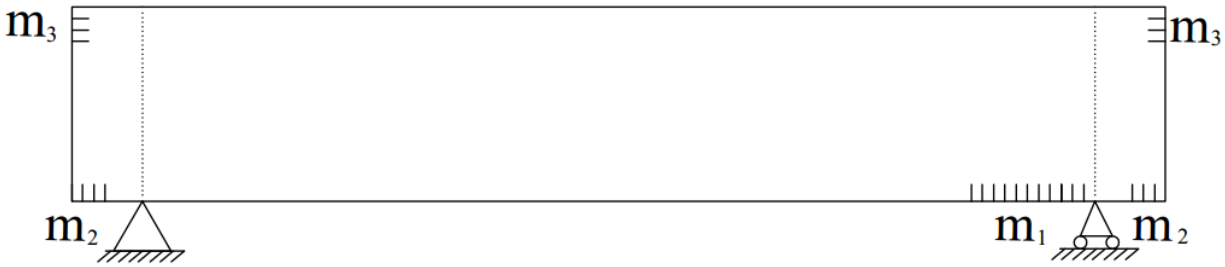

(a)

(b)

Figure 6.1 Parameters defining the FEA mesh
(a) front view, (b) top view

Note: m_1 is the number of elements along the clear span, m_2 is the number of elements along the extra part of clear span

6.1.3 Mechanical Properties of Material

The objective of the FEA models is to compare the critical load of experimental results with the finite element analyses results. Each numerical model was defined with mechanical properties identical to those of the corresponding experimental specimen. As proved in the sensitivity analysis (Chapter 3), only the modulus of elasticity in the longitudinal direction (E_L) and the shear modulus about the transverse direction (G_T) affect the lateral torsional buckling capacity of a beam. The values of E_L and G_T have been obtained through testing in experiments and the results have been provided in the experimental results section (Chapter 5). The rest of the mechanical properties for all the models are consistent with the model in the sensitivity analysis. The values of these parameters are provided in table 6.1.

Table 6.1 Comparison of experimental results with FEA model results

	1	2	3	4	5	6	7	8	9	10	11	12	13
size	clear span (mm)	width (mm)	depth (mm)	span (mm)	m_1	m_2	m_3	m_4	E_L (MPa)	G_T (MPA)	M_{cr}(kNm) (experiments)	M_{cr}(kNm) (FEA)	(12) /(11)
2"×8" ×14'	4200	38	182	4273	552	5	48	10	10434	501	3.51	3.21	0.914
	4200	38*	181*	4276*	552	5	48	10	9022	614	3.90	3.33	0.853
	4200	38	180	4276*	552	5	48	10	11185	558	3.75	3.47	0.924
	4200	38*	181*	4276*	552	5	48	10	10111	548	3.80	3.31	0.871
	4200	39	180	4278	552	5	48	10	9947	540	3.80	3.49	0.918
	Average value										3.75	3.36	0.90
	COV										0.0391	0.0348	0.0358
2"×10" ×12'	3600	38	234	3673	472	5	62	10	11217	542	4.14	5.05	1.22
	3600	38	232	3672	472	5	62	10	9745	535	5.10	4.68	0.917
	3600	38	235	3673	472	5	62	10	5563	569	3.10	3.80	1.23
	3600	38	231	3671	472	5	62	10	12339	606	5.67	5.52	0.974
	3600	38	235	3672*	472	5	62	10	7619	550	4.38	4.30	0.981
	3600	39	234	3672	472	5	62	10	8092	632	4.30	5.13	1.19
	3600	38	234	3669	472	5	62	10	9009	515	4.06	4.46	1.10
	Average value										4.39	4.71	1.09
	COV										0.186	0.123	0.119
2"×12" ×14'	4200	38	284	4293	552	6	74	10	6668	451	3.32	3.77	1.14
	4200	38	285	4294	552	6	74	10	7171	521	3.44	4.24	1.23
	4200	39	286	4296	552	6	74	10	6469	479	3.86	4.18	1.08
	4200	38	285	4291	552	6	74	10	5960	515	4.06	3.85	0.95
	4200	38	281	4295	552	6	74	10	7880	442	3.35	3.99	1.19
	4200	38	284	4286	552	6	74	10	5491	720	4.76	4.42	0.93
	Average value										3.80	4.08	1.08
	COV										0.147	0.061	0.117

*Dimensions were not measured but estimated from nominal dimensions

The remaining mechanical properties are $E_T = 700MPa$, $E_R = 700MPa$, $G_{RT} = 51.5MPa$, $\nu_{LR} = 0.347$, $\nu_{LT} = 0.347$, $\nu_{RT} = 0.469$.

6.1.4 Boundary Conditions

In the classical lateral torsional buckling solution, the boundary conditions are simply supported and located on the center of the end cross-section. However, the FEA models are intended to predict the capacity of the specimens tested. Hence, the boundary conditions should be representative, as much as possible, of those of the experimental setup. In the experiments, the supports were located at the underside of the section at the end of the clear span and restrained at the edge of the cross-section. The lateral displacement was restrained by two steel rods and vertical displacement was supported by a steel angle (Figure 6.2 a-b). The end boundary conditions in the models emulate in an approximate manner of the boundary conditions in the test (Figure 6.2 c-f). This includes two types of constraints:

a) Those related to displacements within the plane of the cross-section. A set of restraints are enforced on the horizontal line (DC and D'C') located at the underside of the section and vertical lines (AD, BC, A'D', and B'C') located at the lateral sides of the section at the end of the clear span. The degrees of freedom along vertical direction were restrained along DC and D'C. Also, the degrees of freedom along the lateral direction were restrained along AD, BC, A'D' and B'C'.

b) Those related to the longitudinal displacements at the location of the support. At one end (Point E), the displacement along the longitudinal direction was restrained but at the other end, Point E' was free to move longitudinally. In the experiment, the two supports were identical, there was a steel plate between the specimen and the steel angle support, the tension fiber of specimen were able to extend along the longitudinal direction under applied load since there was not any longitudinal brace in the setup.

(a)

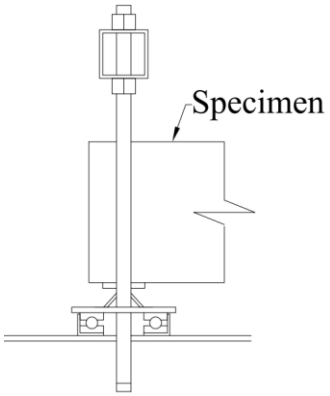

(b)

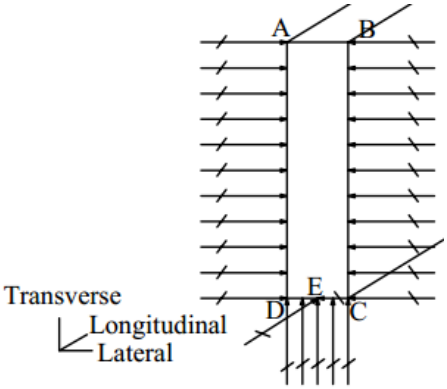

(c)

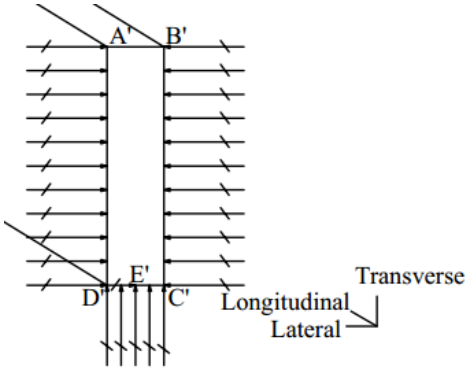

(d)

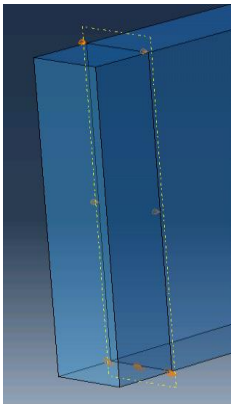

(e)

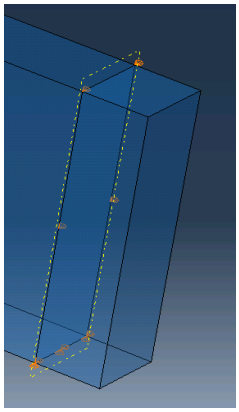

(f)

Figure 6.2 Boundary conditions (crossed arrows denote restrained DOFs)
(a) Experimental End Detail, (b) Elevation of Experimental end detail, (c) DOFs Restrained at left end, (d) DOFs Restrained at right end, (e) Left end in ABAQUS model, and (f) Right end in ABAQUS model

6.1.5 Modelling of Load Application

In the experiments, the beams were subjected to a mid-span load applied at the top face of the beam (Figures 6.3 a, b). The load was applied on the small area and remained vertical when the beam buckled laterally. In order to avoid stress concentration at the load point and try to model the load as close as possible to the setup, the concentrated load was constituted of forty-nine concentrated loads on forty-nine nodes which are on a small area at the center of the clear span, and the magnitude of the individual concentrated load decreased progressively from the center to the edge of the small area, as shown in Figure 6.3 c and d.

(a)

(b)

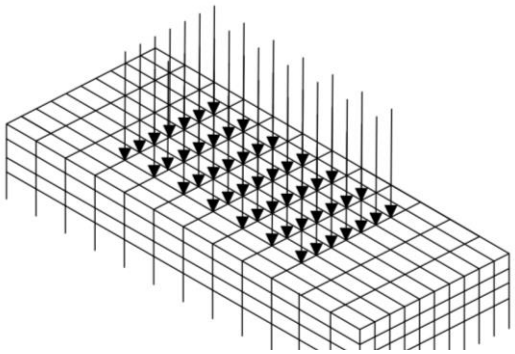

(c)

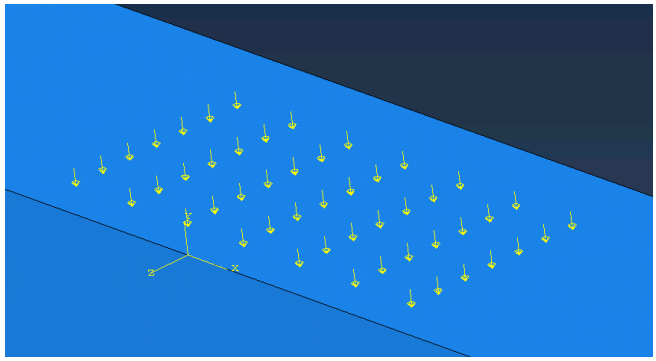

(d)

Figure 6.3 Load Application Detail

(b) Experimental Details and (c) and (d) Corresponding FEA model Detail

6.2 Results of FEA model and comparison

By running each FEA model with linear Eigen-value analysis and obtaining the critical load which is applied at the center of the beams, a comparison was established between experimental programs and the numerical analysis. As shown in column 11 and 12 of Table 6.1 and Figure 6.4. It can be seen that the results of the numerical model are close to the experimental results. The obtained results from FEA model and experimental work are found in the vicinity of $M_{FEA}=M_{test}$ line and the average ratio of the models with experiments is 1.03 and coefficient of variation (COV) of all ratios is 0.132, the average ratio of 2"×8"×14', 2"×10"×12' and 2"×12"×14' beams are 0.9, 1.09 and 1.08 respectively. A large portion of ratios are within the range of 0.9 to 1.1, the lowest value observed is 0.853 and the highest value is found to be 1.23. The COV of ratios are 0.0358, 0.119 and 0.117 for the three standard sizes beam respectively, since the 2"×8"×14' specimens have better conditions (less defects and imperfections) and stable values of modulus of elasticity and shear modulus due to the smaller dimensions than 2"×10"×12' and 2"×12"×14' beams. The COV of ratios of standard size 2"×8"×14' is much smaller than the other dimensions specimens. In Hooley and Madsen's lateral torsional buckling test of glue-laminated timbers, the ratio of critical stress of the test with critical stress of lateral torsional buckling theory falls under the limits of 0.81 to 1.19, and the average value of ratios and COV of ratios are 0.994 and 0.104 respectively (Hooley and Madsen, 1964). The variation range of ratios are similar as that shown in Table 6.1, however, the COV of all ratios shown in Table 6.1 is higher than Hooley and Madsen's tests, one possible reason is glue-laminated timber has less imperfections to affect critical moment except mechanical properties than sawn lumber. In general, the values shown in Table 6.1 are found to be similar to the of the results of Hooley and Madsen's test. Based on the results and comparison, the models are able to capture the beams behaviour. Figure 6.4 provides the plot of experimental and FEA model results. The typical buckling shape of experiments and FEA model of each standard size subjected to concentrated load at the center are shown in Figure 6.5, 6.6 and 6.7.

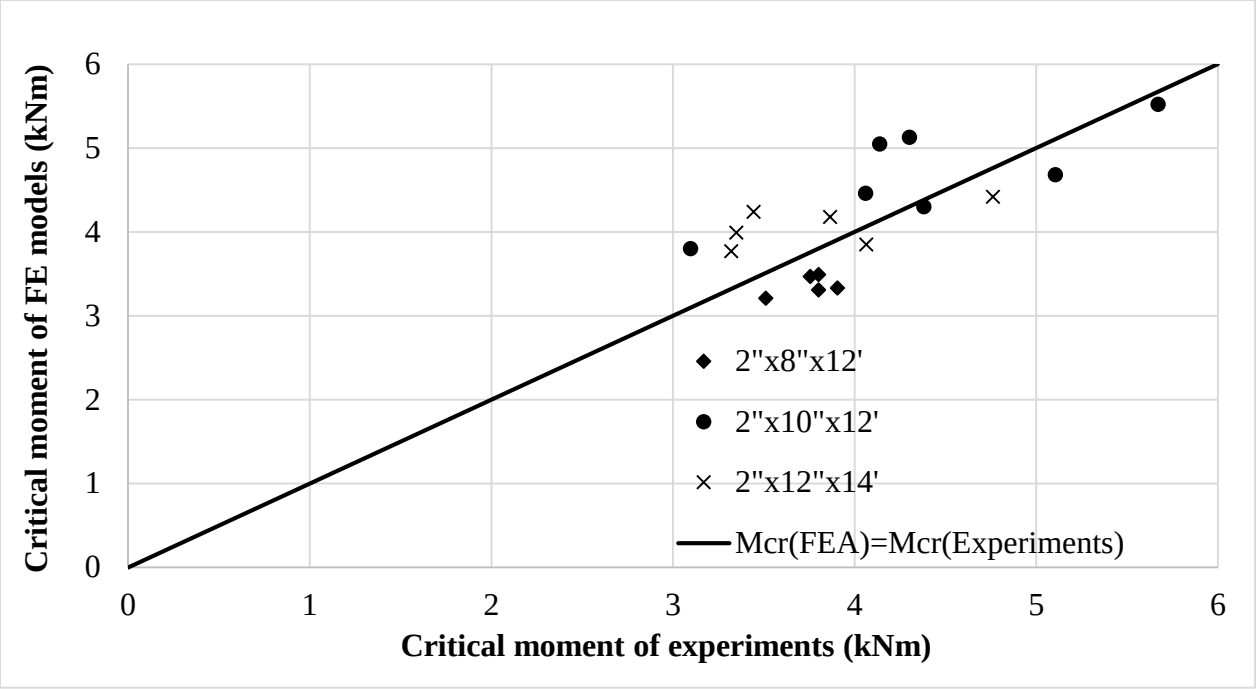

Figure 6.4 Comparison of experiemtnal results and FEA model results

(a)

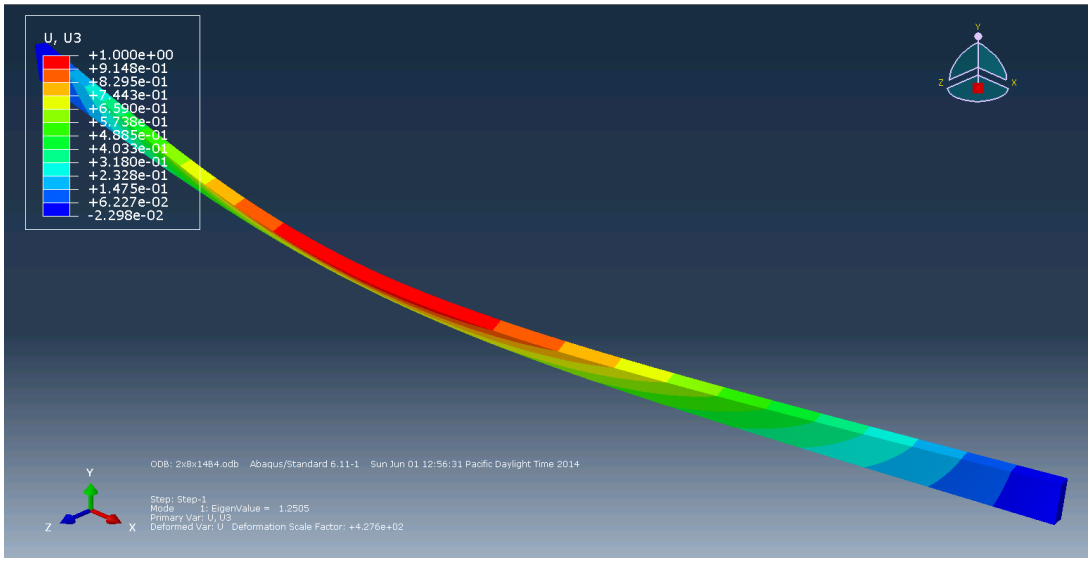

(b)

Figure 6.5 Typical buckling deformation of experiments and FEA models of beam 2”×8”×14’ The experimental buckling deformation, and (b) The FEA model buckling deformation

(a)

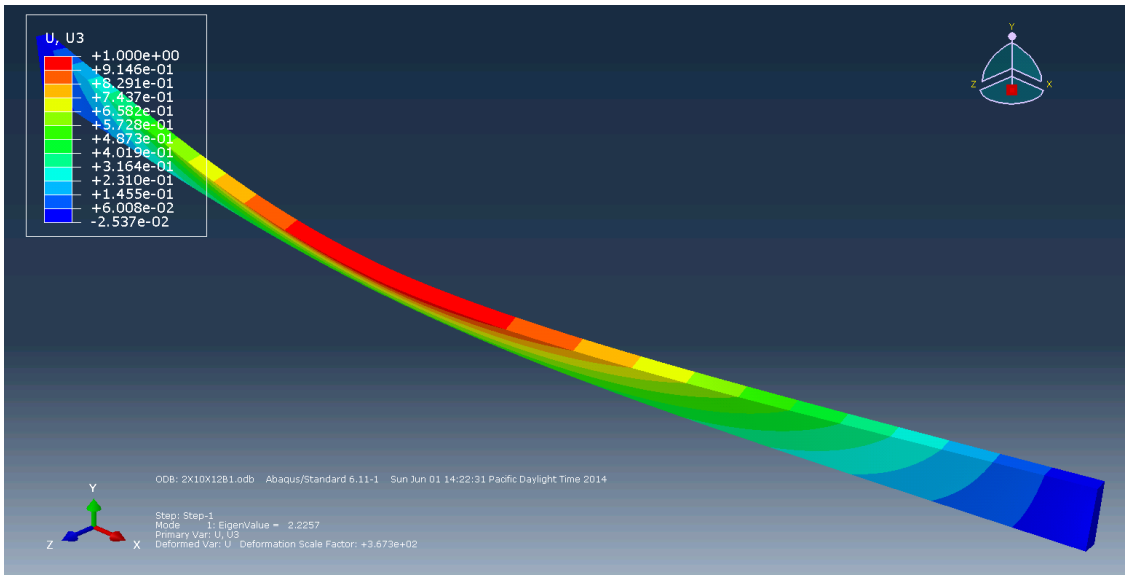

(b)

Figure 6.6 Typical buckling deformation of experiments and FEA models of beam 2”×10”×12’
(a) The experimental buckling deformation, and (b) The FEA buckling deformation

(a)

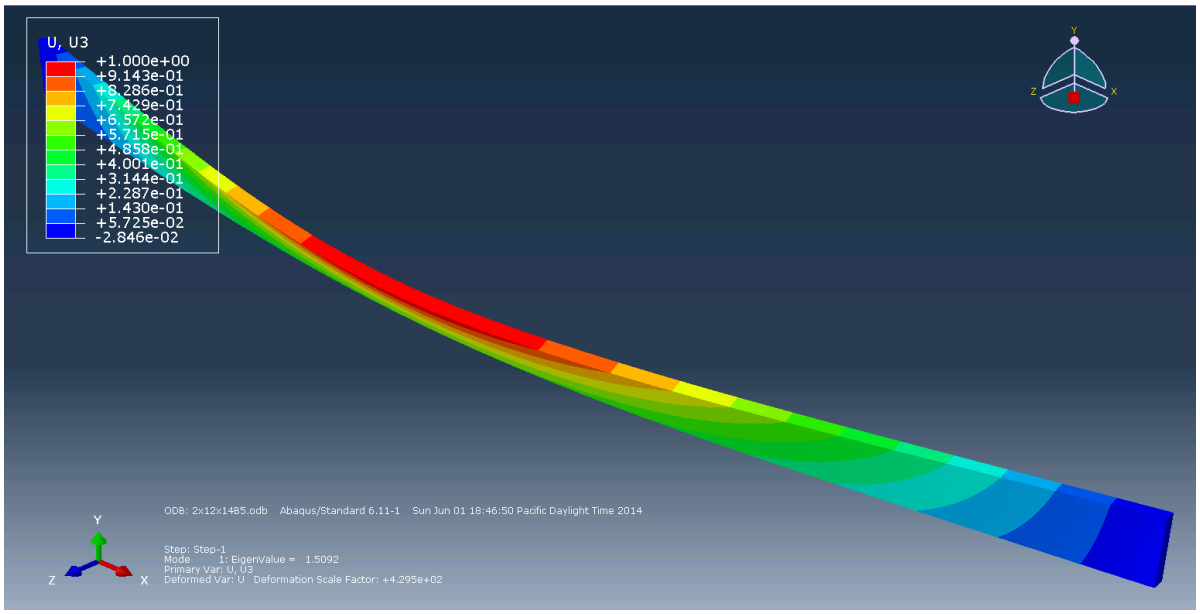

(b)

Figure 6.7 Typical buckling deformation of experiments and FEA models of beam 2”×12”×14’

(a) The experimental buckling deformation, and (b) The FEA buckling deformation

Similar to the experimental buckling shape, there is a significant lateral deformation and twist in the FEA models which decreased gradually towards the end supports. In the models, the same colour presents the same magnitude of displacement, as shown in Figure 6.5 (b), Figure 6.6 (b) and Figure 6.7 (b), the top and bottom of cross-section along the beam have different colours. Based on the displacement label in the top-left corner, the lateral displacement of the top of cross-section is greater than the lateral displacement of the bottom of cross-section. Therefore, the FEA model was successfully able to predict the buckling deformation of all the examined beams correctly.

6.3 Notation for Chapter 6

E_L modulus of elasticity in the longitudinal direction (MPa)

E_R modulus of elasticity in the radial direction (MPa)

E_T modulus of elasticity in the tangential direction (MPa)

G_{RT} shear modulus about radial and tangential direction (MPa)

G_T shear modulus about transverse (MPa)

ν_{LR} Poisson's ratios along longitudinal and radial direction

ν_{LT} Poisson's ratios along longitudinal and tangential direction

ν_{RT} Poisson's ratios along radial and tangential direction

6.4 References

[1] Simulia (2011): ABAQUS analysis user's manual (Version 6.11). Dassault Systemes.

[2] Hooley, R. F. and Madsen, B. (1964). Lateral Buckling of Glued Laminated Beams, Journal of Structural Engineering Division, ASCE, Vol. 90, No. ST3, pp 201-303.

Chapter 7

Parametric Study

7.1 Scope

The comparisons between the finite element and experimental results in Chapter 6 have validated the finite element model. The validated FEA model is used in the present chapter to conduct a parametric study aimed at investigating four effects on the lateral torsional buckling capacity: a) the load height effect, b) the location of end support restraint along the height of the cross-section, c) the effect of beam dimensions and d) the effect of warping contribution in buckling capacity.

7.2 Mesh Details

Similar to the sensitivity analysis in Chapter 3 and FEA model in Chapter 6, the C3D8 eight-noded brick element was used to model the problem. The dimensions of models are 2"×12"×12', 2"×12"×10', 2"×12"×14' and 2"×10"×12'. The mesh is fully defined by the numbers of elements n_1 along height, the number of elements n_2 along the width, and the number of elements n_3 along the span (Figure 7.1). The number of elements n_1 is 76 for the 286 mm deep beams and 62 for 235 mm deep beams. Parameter n_2 take the value 10 in all runs, while parameter n_3 takes the values 562, 482, and 402 for the 4267 mm, 3658 mm, and 3048 mm span beams, respectively.

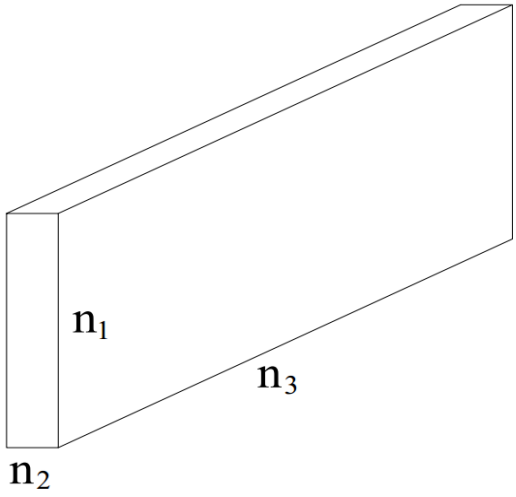

Figure 7.1 Finite Element Mesh

7.3 Mechanical properties

The finite element model was developed for Spruce-pine-fir NO.1/NO.2 grade of wood. The mean value of modulus of elasticity in the longitudinal direction (E_L) reported in (CAN/CSA O86-09, 2009) was chosen as a reference value. Since Spruce-Pine-Fir (SPF) represents a group of wood species with similar characteristics, the properties of Lodgepole Pine (a species of SPF) were chosen to develop the model. CAN/CSA O86-09 does not provide the values of shear modulus and Poisson's ratio. Therefore, the mechanical properties (Modulus of elasticity about radial E_R and tangential direction E_T, Shear modulus about longitudinal and radial direction G_{LR} and about longitudinal and tangential direction G_{LT} and about radial and tangential direction G_{RT}, Poisson's ratios along longitudinal and radial direction v_{LR}, and along longitudinal and radial direction v_{LT}, and along radial and tangential direction v_{RT}) were taken based on the ratio of E_L as reported in Wood handbook (FPL, 2010).

Since the difference between the properties in the radial and tangential direction (modulus of elasticity in radial direction E_R and tangential direction E_T) can be considered insignificant (Isopescu, 2012), it can be assumed that they are equal, i.e., $E_R = E_T = E_t$, where the parameters about the transverse direction should be obtained from experiments. Also, the shear modulus G_{LR}

and G_{LT} can be assumed equal, i.e., $G_{LR} = G_{LT} = G_T$ and Poisson's ratios $\nu_{LR} = \nu_{LT} = \nu_T$. Thus, in the FEA model, the values of the mechanical parameters taken are shown in Table 7.1

Table 7.1 The mechanical parameters of Spruce-Pine-Fir

Parameter	Value
E_L	9500 MPa
E_t	808 MPa
G_T	451 MPa
G_{RT}	47.5 MPa
ν_T	0.332
ν_{RT}	0.469

7.4 Analyses to Investigate Effect of Load Position

In the classical lateral torsional buckling solution, the critical moment is equal to the result of the classical solution multiplied by the load eccentricity factor, as shown in Equation 7.1. When the bending moment is applied on the neutral axis, the load eccentricity factor $C_e = 1.0$.

$$M_{cr} = C_e C_b M_u \tag{7.1}$$

where

$$M_u = \frac{\pi}{L_u}\sqrt{E_L I_y G_T J + \left(\frac{\pi E_L}{L_u}\right)^2 I_y C_w} \tag{7.2}$$

in which C_b is equivalent moment factor which accounts for the moment gradient (Equation 2.6 in Chapter 2), C_e is the load eccentricity factor which accounts for the load position effect. It is provided in (AFPA, 2003) as

$$C_e = \sqrt{\eta^2 + 1} - \eta \tag{7.3}$$

where

$$\eta = \frac{Kd}{2L_u}\sqrt{\frac{E_L I_y}{G_T J}} \tag{7.4}$$

in which d is the depth of the cross-section. Negative values of η mean that the load is applied below the centroid and positive values denote loads applied above the centroid (AFPA, 2003). Symbol L_u is the unbraced span of the beam. Constant K takes the value $K = 1.72$ when the beam is under concentrated load at center of length and the value $K = 1.44$ when the beam is under uniformly distributed load.

7.4.1 Background

The classical lateral torsional buckling solution (Equation 7.2) is based on loads which are applied at the centroid of the rectangular section. However, in practical situations, the load is located on the top face of the beam. In such a case, as discussed in the literature review section, an additional destabilizing twisting moment is induced by the vertical load undergoing a horizontal displacement relative to the section centroid. Conversely, when the load acts on the bottom of the beam, the resulting twisting moments have a stabilizing effect and increase the capacity of the member. Thus section conducts a buckling FEA in which all three loading positions are investigated. A comparison is then made with results based on the load eccentricity factor C_e as determined from Equation (7.3).

7.4.2 Boundary condition and load patterns

The reference model is a simply supported beam, similar to that adopted in the sensitivity analysis. The boundary supports are located on the mid-height of the end cross-section, in a manner similar to the classical solution. The end cross-section was free to rotate about the major and minor axes. In the longitudinal direction, the left end was restrained and the other end was free to move.

Two loading patterns are investigated by the model. The first loading pattern was a concentrated load at the beam mid-span and the second one was a uniformly distributed load. For each loading pattern, three cases were considered concerning to the location of the load relative to the section

centroid. (a) top face loading, (b) centroidal loading, and (c) bottom face loading. For the case of centroidal loading, half of the load was applied to the top face and the other half on the bottom face (Figs. 7.2 a-f)

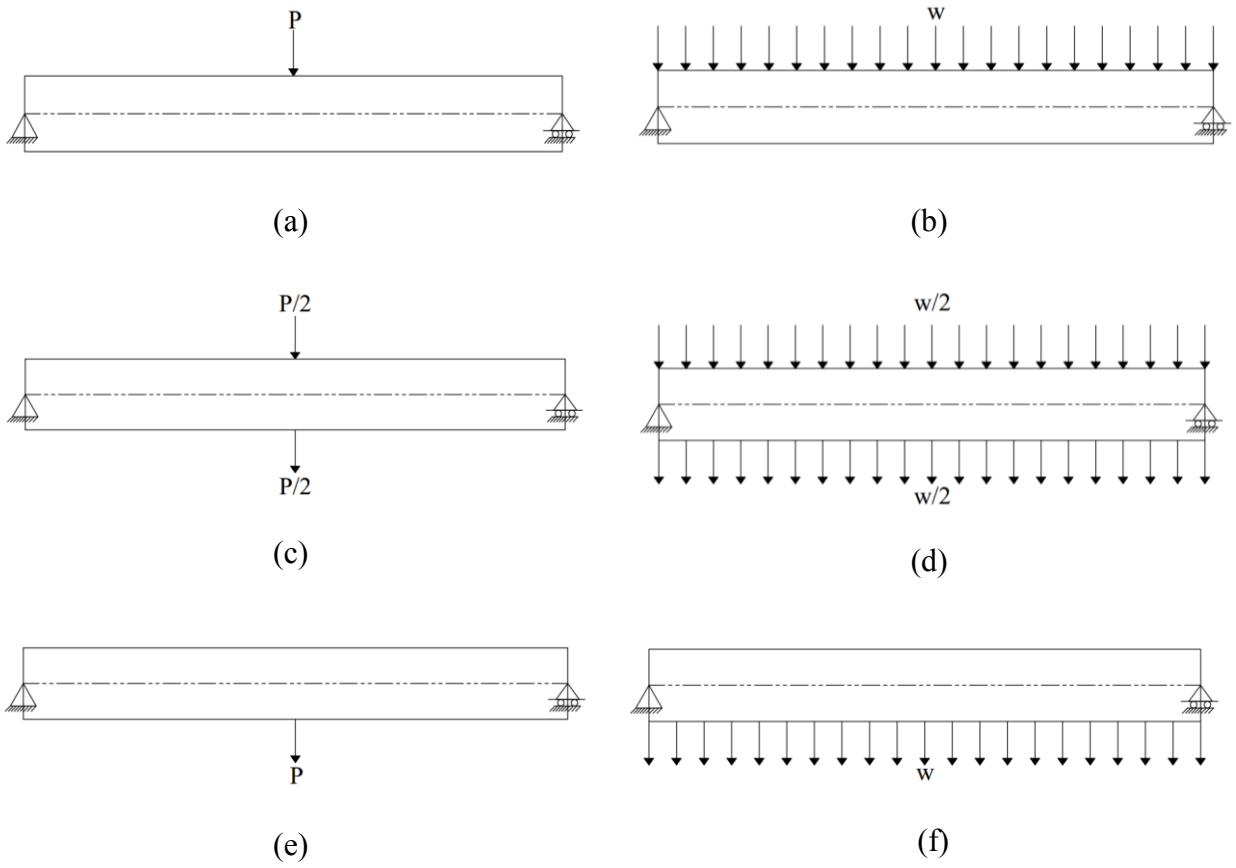

Figure 7.2 Simply supported beam under concentrated load at mid-span and uniformly distributed load acting at (a) (b) top face, (c) (d) centroid, and (e) (f) bottom face.

Similar to the FEA models in Chapter 6, the concentrated load was applied as a series of forty-nine concentrated loads acting on a small area (45.5mm×22.8mm) at the center of span. For the uniformly distributed load, a series of concentrated loads were applied to the middle line of the top and bottom faces (Figure 7.3).

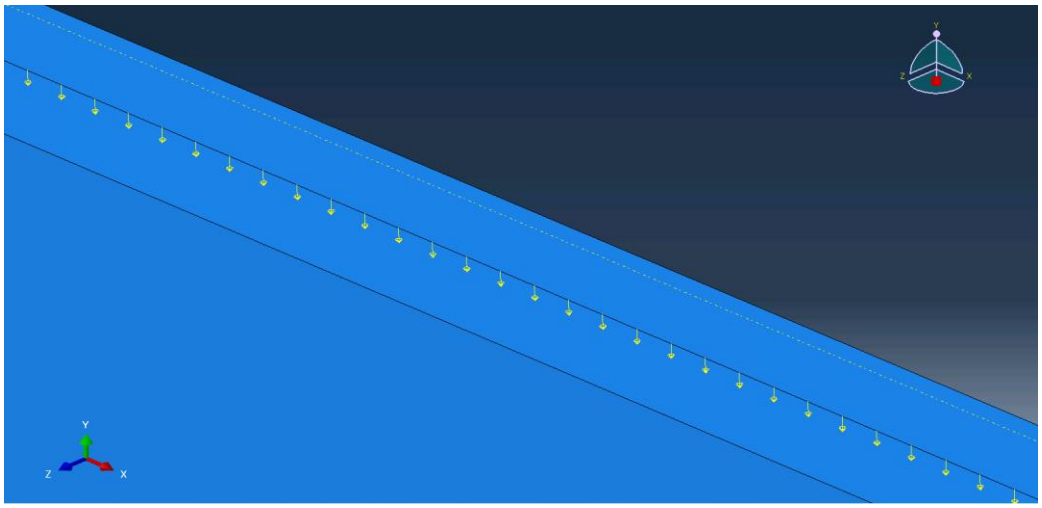

Figure 7.3 The constitution of uniformly distributed load

7.4.3 Load eccentricity factor

For the dimensions of the cross-section of the reference model (38mm on width and 286mm on depth), the values of the eccentricity factor η as determined from Equation (7.3) for different load options and locations are shown in column 13 of Table 7.2 and 7.3.

7.4.4 Observations and results

The critical moments of the FEA model under a concentrated load at the center are presented for the reference beam and beam number A1 and A2 in ninth column of Table 7.2. When the load was applied on the top face (A1), the critical moment decreased, and conversely, when the load was applied on the bottom face (A2), the critical moment increased. In order to compare the eccentricity factors of FEA model with Equation (7.3) and (7.4), a comparison is made between the FEA models and the classical solution (Column 10-13) which includes the equivalent moment factor, load eccentricity factor and critical moment. Based on the ratio between the results of the FEA models and classical solution which is presented in the column 14, the difference of the two methods is insignificant. Therefore, it can be seen that the model is able to capture the eccentricity factors provided in (AFPA, 2003)

Table 7.3 shows the same comparison as Table 7.2, for the FEA models under uniformly distributed load. The same results of Table 7.2 are observed in Table 7.3.

7.5 Analyses to Investigate Effect of Support Height

7.5.1 Motivation

The classical lateral torsional buckling solution is based on supports which are located at the centroid of the end cross-section. However, practically in connection design and construction, the point of restraint may be located above or below than the section centroid. Also, in the tests performed in Chapter 4 and 5, the points of support were located at the bottom face. It is thus of practical interest to investigate the effect of the support location relative to the section centroid.

7.5.2 Loading Patterns and Boundary Condition Details

Two loading cases were considered: a mid-span load and a uniformly distributed load. For each loading, three load positions were considered: top face loading, centroid loading and bottom face loading.

Figure 7.4 (a) shows the reference case where the supports are located at mid-height of the beam, this case is analogous to the classical solution which has been performed in Chapter 3. In Figure 7.4 (b), the supports are located at the bottom, the beam is simply supported and free to rotate about weak and strong axis. The boundary conditions are illustrated in Figure 7.5a-d and include two types of constraints:

a) Those related to displacements within the plane of the cross-section where a set of restraints are enforced on the horizontal lines (AB and A'B') located at the underside of the section and vertical lines (CD and C'D'). Degrees of freedom along vertical direction were restrained at AB and A'B'. Degrees of freedom along lateral direction were restrained at CD and C'D'.

b) Those related to longitudinal displacements at the location of the support. At one end (Point C), the displacement along the longitudinal direction was restrained but at the other end, Point C' was free to move longitudinally.

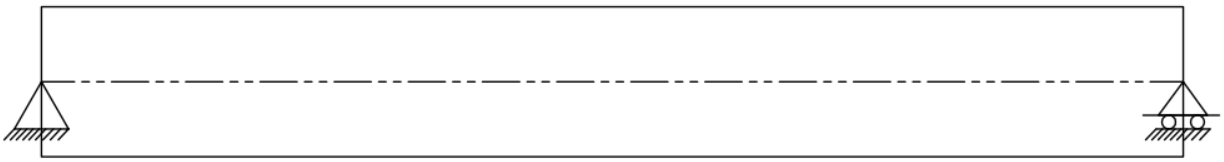

(a)

(b)

Figure 7.4 The location of supports at (a) Mid-height of beam, and (b) bottom of beam.

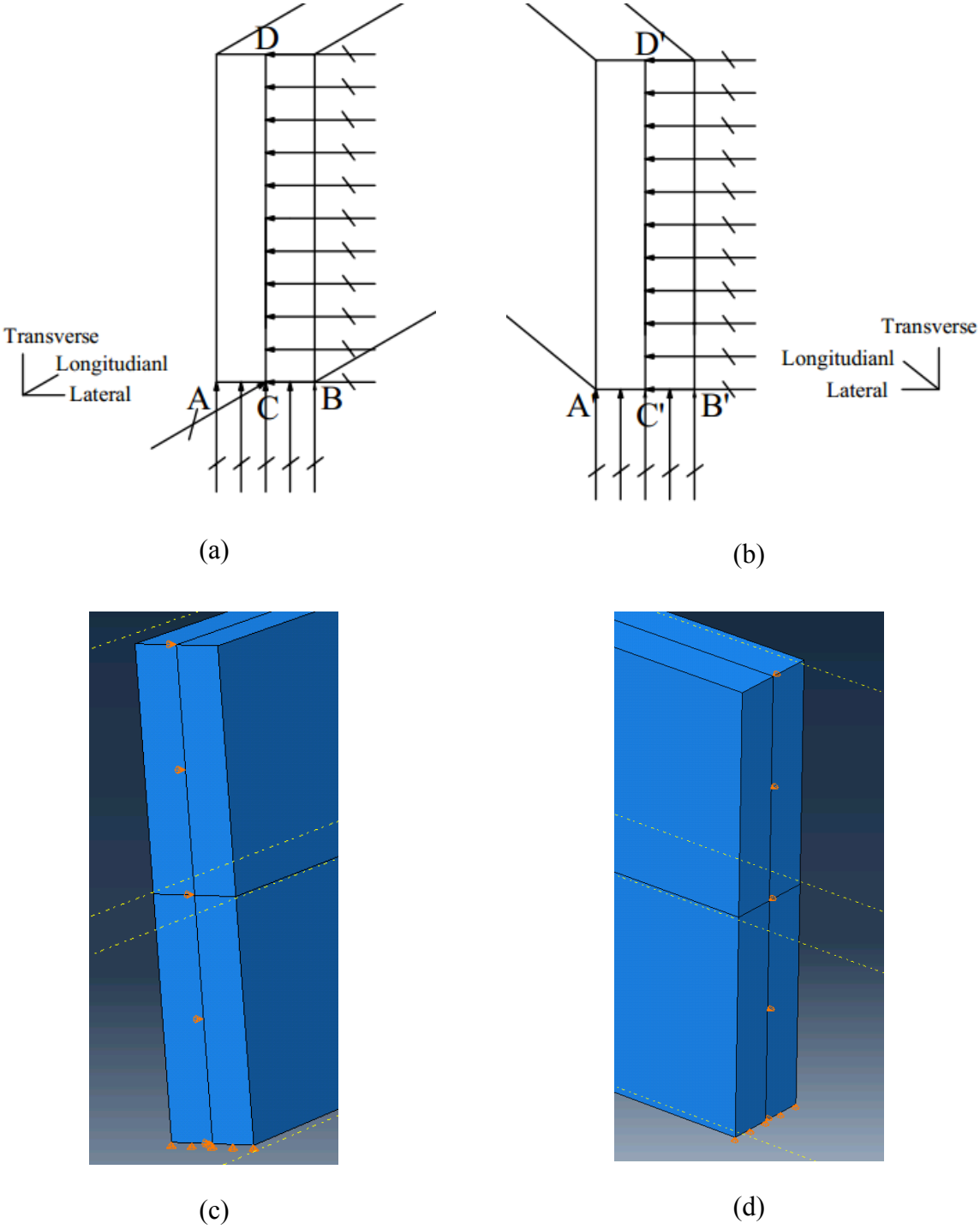

Figure 7.5 The boundary condition located on the bottom (a) restriction of left end cross-section, (b) restriction of right end cross-section, (c) Left end in ABAQUS model, and (d) right end in ABAQUS model

7.5.3 Observations and Results

Beam number A3, A4, A5 in Table 7.2 present the details and results of boundary conditions located at the bottom of beam under concentrated load at mid-span. The lateral torsional buckling capacity of FEA model are shown in column 9. Comparing with the critical moment of column 9 of A0, A1 and A2 (supports located at mid-height), there are no significant changes after moving the supports from middle height to bottom (A0=A3, A1=A4 and A2=A5). Also, the same comparisons are made for the uniformly distributed load (Table 7.3), similar as Table 7.2, the effect of moving the support from mid-height to bottom can be neglected.

7.6 Effect of Dimension

7.6.1 Dimensions

According to the classical lateral torsional buckling solution, the capacity of a beam is not only affected by mechanical properties but also the dimensions of the beam, three models were developed based on changing one dimension of the reference model and then compared the results with the reference case. The first two were varying the length of the reference model from 12 feet (3658mm) to 14 feet (4267mm) and 10 feet (3048mm) while keeping the dimension of cross-section unchanged, the last one was changing the depth of reference model from 12 inch (286mm) to 10 inch (235mm) while keeping the width 2 inch (38mm) and length 12 feet (3658mm) unchanged. The mechanical properties were taken identical to those of the reference model (Table 7.1).

7.6.2 Boundary Condition and Load Patterns

The beam is simply supported and under concentrated load at center of span and uniformly distributed load, the end cross-sections were free to rotate about weak and strong axis and the restrictions were located on the center of the end cross-section.

7.6.3 Observation and Results

A6, A7 and A8 in Column 9 of Table 7.2 presented the details and results models with different

dimensions. The results of A6, and A7 in column 10 show that with the same dimension of cross-section, an inverse relationship occurred between lateral torsional buckling resistance and beam span, the lateral torsional buckling resistance increased with the reduction of span, just the opposite, the resistance decreased with the increase of length. The column 13 (classical solution) of Table 7.2 present the same trend. The same observations are also observed in uniformly distributed load of B6 and B7.

The result of A8 in column 9 of Table 7.2 shows that the identical relationship happened between lateral torsional buckling resistance and depth, the lateral torsional buckling resistance decreased with the reduction of depth. Comparing with classical solution (Column 13), all the observations between buckling resistance and dimensions from FEA model present the same trend of classical solution. The same observations are also observed in the uniformly distributed load of B8.

Table 7.2 Parametric runs of model under concentrated load at mid-span

	Geometric and Loading Parameters				Mesh Parameters			FEA	Classical Solution				Comparison
1	2	3	4	5	6	7	8	9	10	11	12	13	14
#	Load location	Support location	Span	Depth	n1	n2	n3	Critical moment (kNm)	Classical solution (1)	C_b	C_e	M_{cr} (10) ×(11) ×(12)	(9)/(13)
A0	**Centroid**	**Centroid**	**12'**	**12"**	76	10	482	5.90	4.50	1.35	1.00	6.08	0.970
A1	**Top**	Centroid	12'	12"	76	10	482	4.97	4.50	1.35	0.851	5.17	0.961
A2	**Bottom**	Centroid	12'	12"	76	10	482	6.95	4.50	1.35	1.17	7.11	0.977
A3	Centroid	**Bottom**	12'	12"	76	10	482	5.89					
A4	**Top**	**Bottom**	12'	12"	76	10	482	4.96					
A5	**Bottom**	**Bottom**	12'	12"	76	10	482	6.93					
A6	Centroid	Centroid	**10'**	12"	76	10	402	7.11	5.44	1.35	1.00	7.34	0.969
A7	Centroid	Centroid	**14'**	12"	76	10	562	5.04	3.85	1.35	1.00	5.19	0.971
A8	Centroid	Centroid	12'	**10"**	62	10	482	4.78	3.66	1.35	1.00	4.94	0.968

(1) Based on $M_u = \frac{\pi}{L_u}\sqrt{E_L I_y G_T J + \left(\frac{\pi E_L}{L_u}\right)^2 I_y C_w}$ (The solution assuming centroidal support and centroidal load)

Table 7.3 Parametric runs of model under uniformly distributed load

	Geometric and Loading Parameters				Mesh Parameters			FEA	Classical Solution				Comparison
1	2	3	4	5	6	7	8	9	10	11	12	13	14
#	Load location	Support location	Span	Depth	n1	n2	n3	Critical moment (kNm)	Classical solution (1)	C_b	C_e	M_{cr} (10) ×(11) ×(12)	(9) /(13)
B0	**Centroid**	**Centroid**	12'	12"	76	10	482	4.93	4.50	1.13	1.00	5.09	1.00
B1	**Top**	Centroid	12'	12"	76	10	482	4.33	4.50	1.13	0.874	4.44	1.032
B2	**Bottom**	Centroid	12'	12"	76	10	482	5.63	4.50	1.13	1.14	5.80	0.975
B3	Centroid	**Bottom**	12'	12"	76	10	482	4.93					
B4	**Top**	**Bottom**	12'	12"	76	10	482	4.32					
B5	**Bottom**	**Bottom**	12'	12"	76	10	482	5.61					
B6	Centroid	Centroid	**10'**	12"	76	10	402	5.96	5.44	1.13	1.00	6.15	0.969
B7	Centroid	Centroid	**14'**	12"	76	10	562	4.20	3.85	1.13	1.00	4.35	0.966
B8	Centroid	Centroid	12'	**10"**	62	10	482	4.00	3.66	1.13	1.00	4.14	0.966

(1) Based on $M_u = \frac{\pi}{L_u}\sqrt{E_L I_y G_T J + \left(\frac{\pi E_L}{L_u}\right)^2 I_y C_w}$ (The solution assuming centroidal support and centroidal load)

7.7 Effect of Warping Contribution in Buckling Capacity

7.7.1 Motivation

In classical lateral torsional buckling solution, the resistance provided by warping is considered. In order to explore the contribution of warping in buckling capacity of rectangular cross-section, a comparison was made with FEA model, classical solution with and without the resistance provided by warping to investigate the effect of warping.

7.7.2 Boundary Conditions, Load Pattern and Dimension

Since the classical lateral torsional buckling solution is based on loads and boundary conditions which are located at the centroid, the reference cases which is simply supported beam under uniformly distributed load and concentrated load at mid-span were used to investigate the effect of warping in the buckling resistance. The dimensions of reference model are 2"×12"×12' (38mm×286mm×3658mm).

7.7.3 Observation and Results

The mechanical properties have been provided in Table 7.1, substituted the parameters into Equation (7.5) and (7.6), the buckling capacities are 4.50 kNm and 4.44 kNm. Since the reference cases are under uniformly distributed load and concentrated load, the results of Equation (7.5) and (7.6) should multiply the equivalent moment factor C_b. The comparison with classical solution and FEA reference models are shown in Table 7.4

$$M_u = \frac{\pi}{L_u}\sqrt{E_L I_y G_T J + \left(\frac{\pi E_L}{L_u}\right)^2 I_y C_w} \tag{7.5}$$

$$M_u = \frac{\pi}{L_u}\sqrt{E_L I_y G_T J} \tag{7.6}$$

Table 7.4 Comparison with FEA model, classical solution with and without warping constant

	1	2	3	4
Load patterns	C_b	Classical solution with warping constant (kNm) (Equation 7.5)	Classical solution without warping constant (kNm) (Equation 7.6)	FEA model (kNm)
Uniformly distributed load	1.35	6.08	5.99	5.90
Concentrated load	1.13	5.09	5.02	4.93

As shown in Table 7.4, the buckling capacity of the FEA model, classical solution with and without warping constant are similar, the differences are insignificant. Therefore, the warping contribution is negligible for rectangular section in buckling capacity.

7.8 Summary

The finite element model developed in this chapter accounts for the effect of a) load positions (top face, centroid, and bottom face), b) support locations (centroid and bottom), c) dimensions (length and depth), d) warping contribution of buckling capacity for rectangular section.

a) Comparing with the load applied on centroid, the load acts on the top face of beam would decrease the buckling capacity, and in contrast, the buckling capacity would be increased when the load acts on the bottom face. The FEA models are able to capture the eccentricity factors provided in (AFPA, 2003)
b) Comparing with the support locates on the mid-height, the support locates on the bottom has negligible effect of buckling capacity.
c) Comparing with the reference beam case, there is an inverse relationship between buckling capacity with length. However, with the increase in beam depth, an increase in the buckling capacity was observed.
d) Comparing with the reference beam case in FEA model and classical solution, the warping contribution of buckling capacity can be neglected for a rectangular section.

7.9 Notation for Chapter 7

C_b the equivalent moment factor

C_e load eccentricity factor

C_w the warping constant

d beam depth (mm)

E_L modulus of elasticity along the longitudinal direction (MPa)

E_R modulus of elasticity along the radial direction (MPa)

E_T modulus of elasticity along the tangential direction (MPa)

E_t modulus of elasticity about transverse (MPa)

G_{LR} shear modulus about longitudinal and radial direction (MPa)

G_{LT} shear modulus about longitudinal and tangential direction (MPa)

G_{RT} shear modulus about radial and tangential direction (MPa)

I_y moment of initial in weak axis (mm^4)

J Saint Venant torsion constant (mm^4)

K Constant based on loading and boundary conditions

L_u the unbraced length of beam

M_u the critical moment of simply supported beam under constant moment

M_{cr} critical moment of beam

ν_{LR} Poisson's ratios along longitudinal and radial direction

ν_{LT} Poisson's ratios along longitudinal and tangential direction

ν_{RT} Poisson's ratios along radial and tangential direction

ν_T Poisson's ratios about transverse

7.10 References

[1] Canadian Standards Association. (2009). CSA standards O86-09, Engineering design in wood, Mississauga, Ontario, Canada.

[2] Forest Products Labratory. (2010). Wood Handbook-Wood as an Engineering Material. Madison, USA.

[3] Isopescu, D., Stanila, O., and Asatanei, I. (2012). Analysis of Wood Bending Properties on Standardized Samples and Structurals Size Beams Tests, Buletinul Insititutului PolitehnicDIN Din Iasi, Publicat de Universitatea Tehnică „Gheorghe Asachi" din Iaşi.

[4] American Forest and Paper Association. (2003). Technical Report 14: Deisigning for lateral-torsional stability in wood members. Washington, D.C.

Chapter 8

Conclusion and Recommendation

8.1 Summary and Conclusions

Following are the conclusions obtained as the result of the current study;

1) Through the sensitivity analysis, it was shown that only the modulus of elasticity E_L along the longitudinal direction and the shear modulus G_T about the transverse direction affect the critical moment of beam. In contrast, the modulus of elasticity about the transverse direction, E_t, Poisson's ratios ν_T and ν_{RT} and the shear modulus G_{RT} have negligible effect on the critical moment.

2) Through experimental testing, the critical moment of rectangular sawn lumber beam was shown to follow the classical lateral torsional buckling solution.

3) Through detailed Buckling FEA with identical dimensions, mechanical properties, load patterns and boundary condition to those of the experimental specimens, the FEA models were capable to predict the critical moments comparable to those observed in the test and the classical lateral torsional buckling solution.

4) By performing a parametric analysis using the FEA models, several observations were made: 1) loads applied on the top face of the beam decreased the critical moment of the beam. In contrast, loads applied on the bottom face increased its critical moment. 2) The FEA models were shown to provide results in good agreement with those provided by the eccentricity provided in (AFPA, 2003). 3) the critical moment is not greatly influenced by moving the supports from mid-height to bottom of end cross-section. 4) The critical moments decrease with the span of

the beam in agreement with the classical solution. However, the buckling capacity is found to increase with section depth.

8.2 Recommendation for Future Research

1) Wood members (Sawn lumber beams) have higher degree of imperfection compared to steel beam and members of glued-laminated timber. Other than dimension and mechanical properties, the imperfections have an effect on the critical moment of a beam, which the classical solution does not account for. For future investigation, full scale testing can be performed to study the effect of imperfections on the critical moment of the members. The developed FEA model is able to consider the imperfections which can help verifying experimental results with computational and analytical results.

2) The developed FEA model can also be used to investigate actual connections used in typical beam supports.

8.3 Reference

[1] American Forest and Paper Association. (2003). Technical Report 14: Deisigning for lateral-torsional stability in wood members. Washington, D.C.

Appendix A

Lateral Torsional Buckling Modes of Experimental Testing and FEA Models

This appendix provides the buckling shape of seventeen (17) specimens obtained from the experimental program and FEA models.

Observations

It can be seen that there is a significant out-of-plane deformation and twist in both the experimental and FEA models beams, which decreased gradually towards the end supports. The FEA models were able to capture the buckling shape of beams in the experiments.

(a)

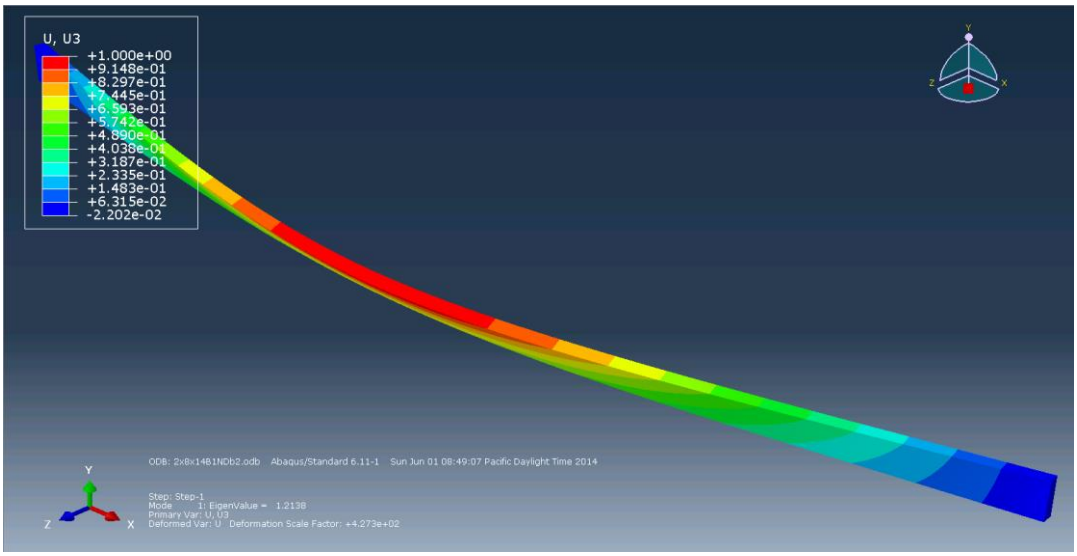

(b)

Figure A.1 Buckling mode of Beam 1 of 2”×8”×14’ specimens
(a) experimentally observed and (b) FEA predicted

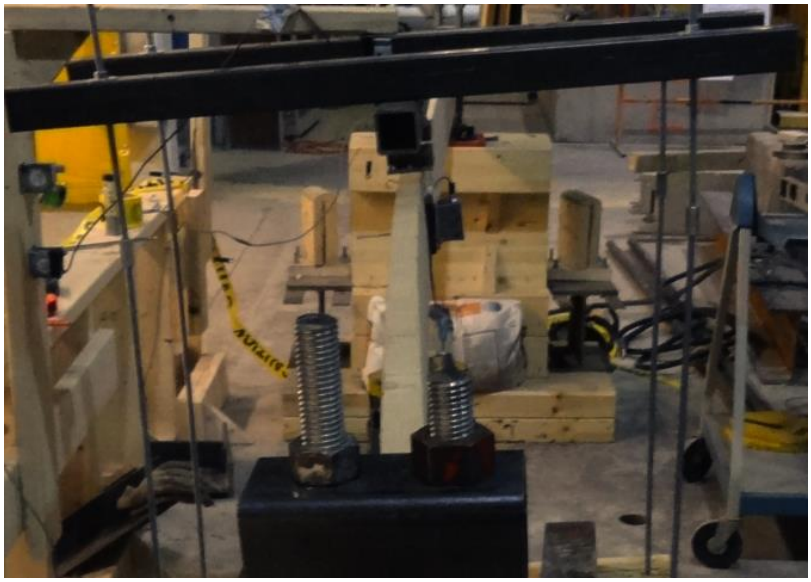

(a)

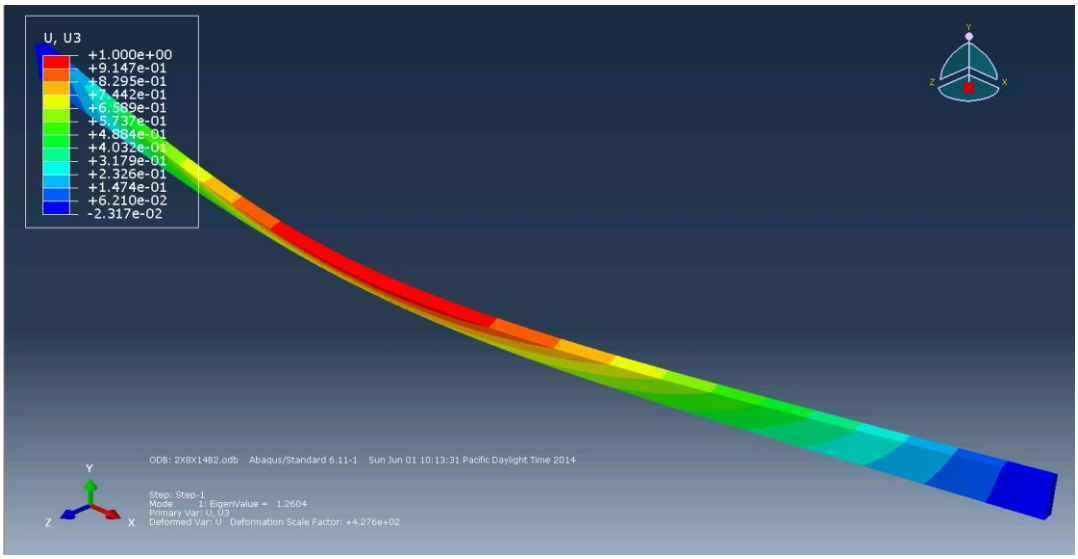

(b)

Figure A.2 Buckling mode of Beam 2 of 2”×8”×14’ specimens

(b) experimentally observed and (b) FEA predicted

(a)

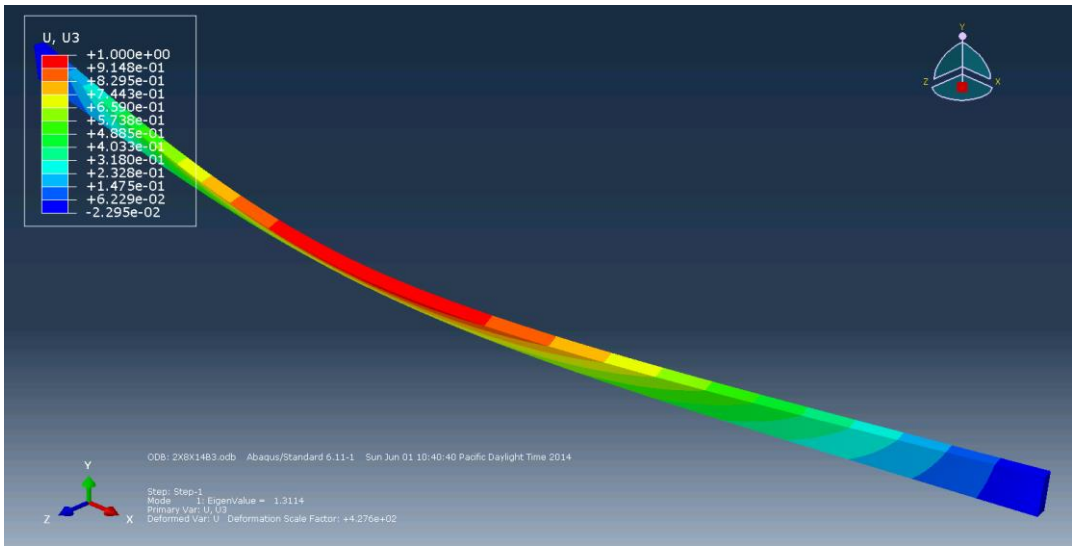

(b)

Figure A.3 Buckling mode of Beam 3 of 2”×8”×14’ specimens

(c) experimentally observed and (b) FEA predicted

(a)

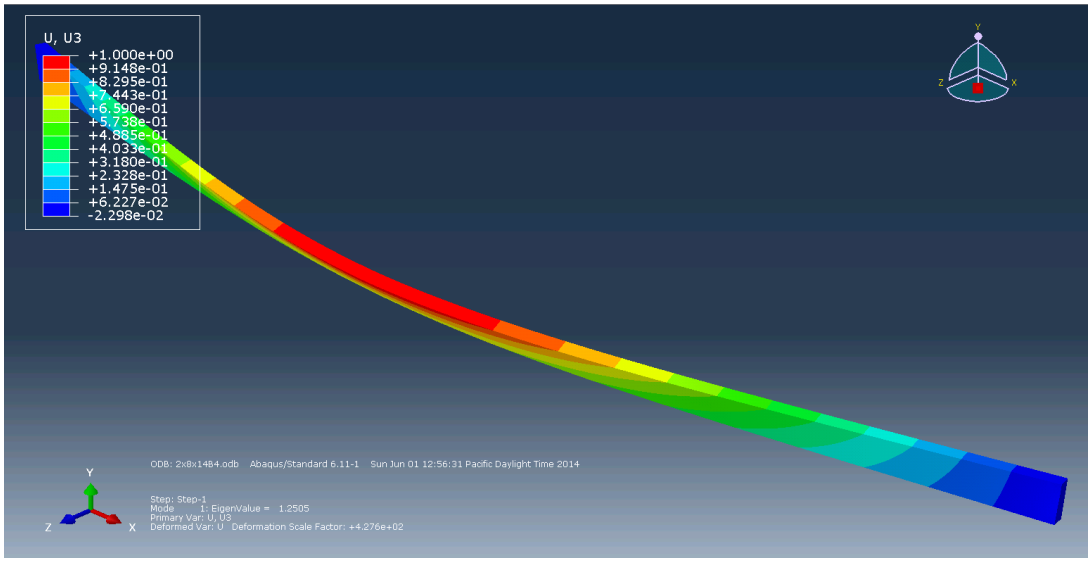

(b)

Figure A.4 Buckling mode of Beam 4 of 2”×8”×14’ specimens

(a) experimentally observed and (b) FEA predicted

(a)

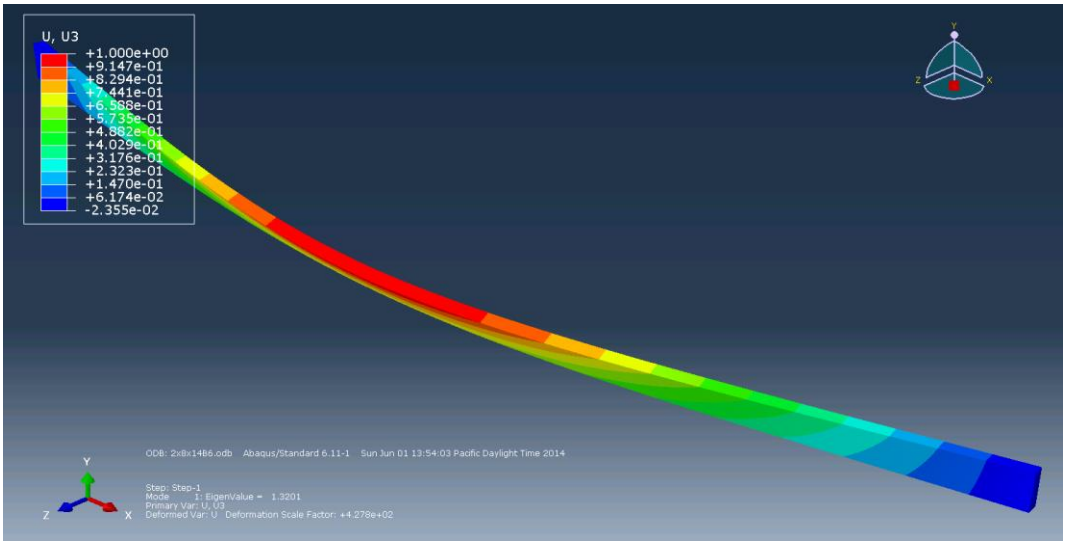

(b)

Figure A.5 Buckling mode of Beam 6 of 2”×8”×14’ specimens

(a) experimentally observed and (b) FEA predicted

(a)

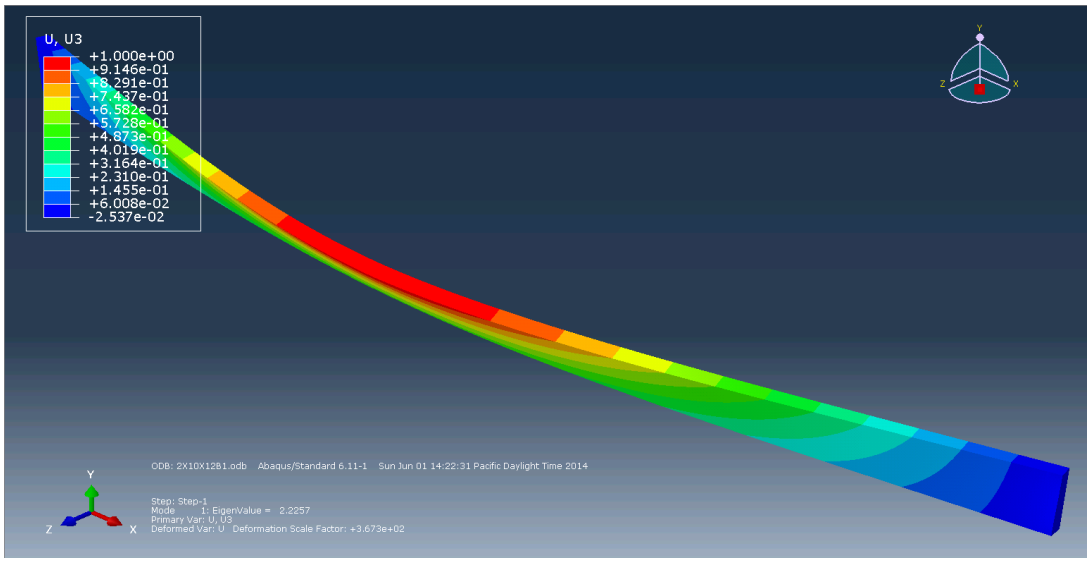

(b)

Figure A.6 Buckling mode of Beam 1 of 2”×10”×12’ specimens

(a) experimentally observed and (b) FEA predicted

(a)

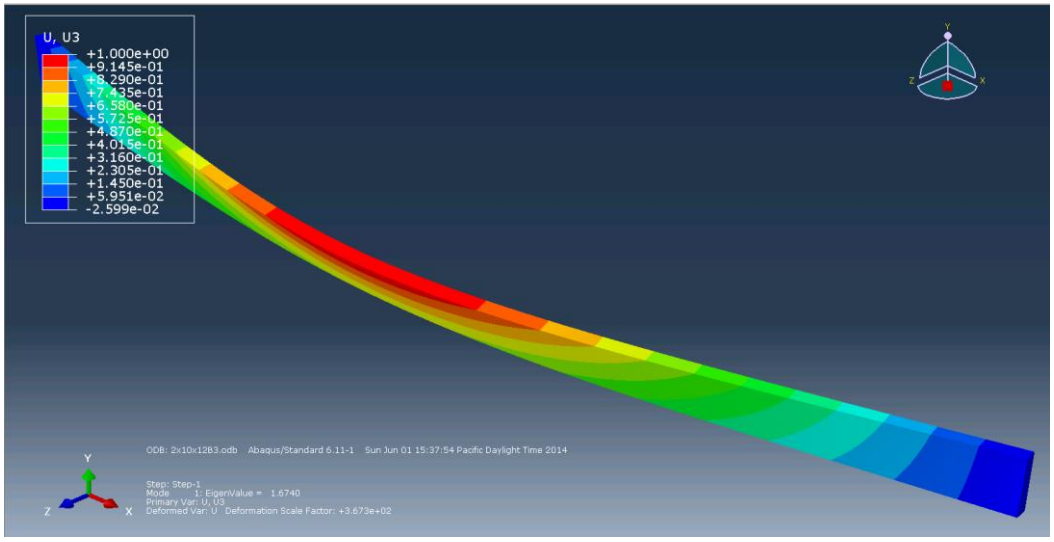

(b)

Figure A.7 Buckling mode of Beam 3 of 2”×10”×12’ specimens

(a) experimentally observed and (b) FEA predicted

(a)

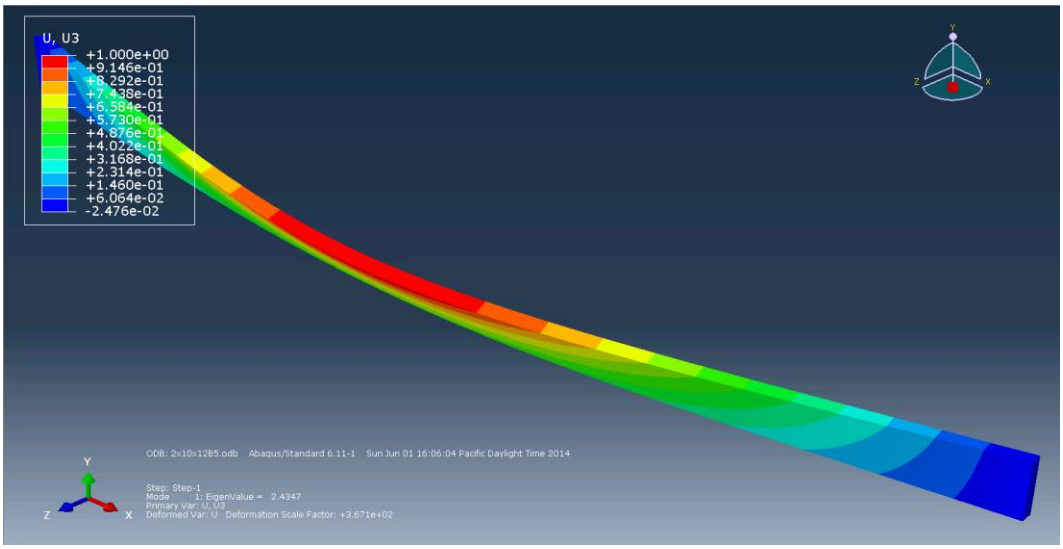

(b)

Figure A.8 Buckling mode of Beam 5 of 2”×10”×12’ specimens

(a) experimentally observed and (b) FEA predicted

(a)

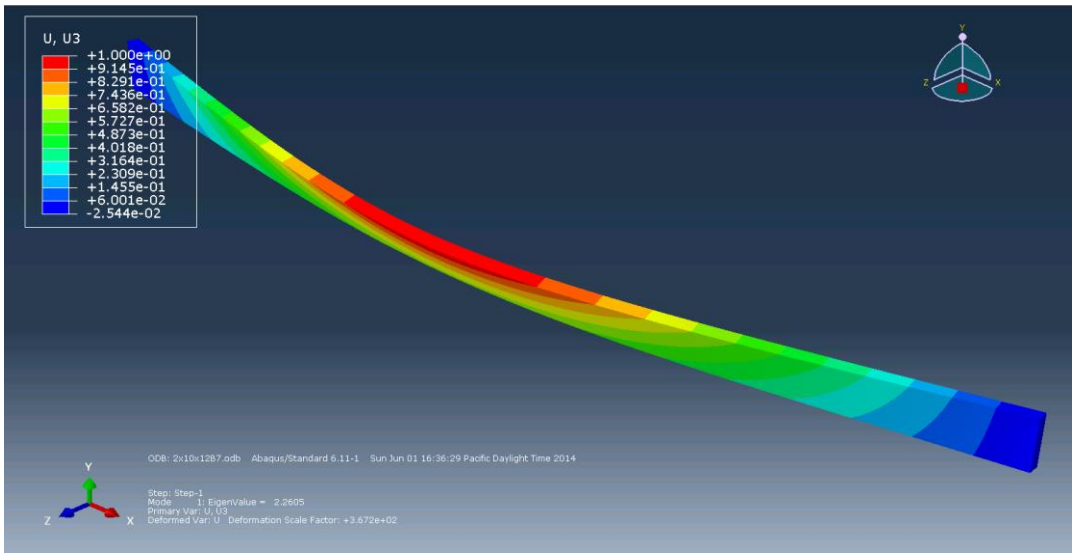

(b)

Figure A.9 Buckling mode of Beam 7 of 2”×10”×12’ specimens

(a) experimentally observed and (b) FEA predicted

(a)

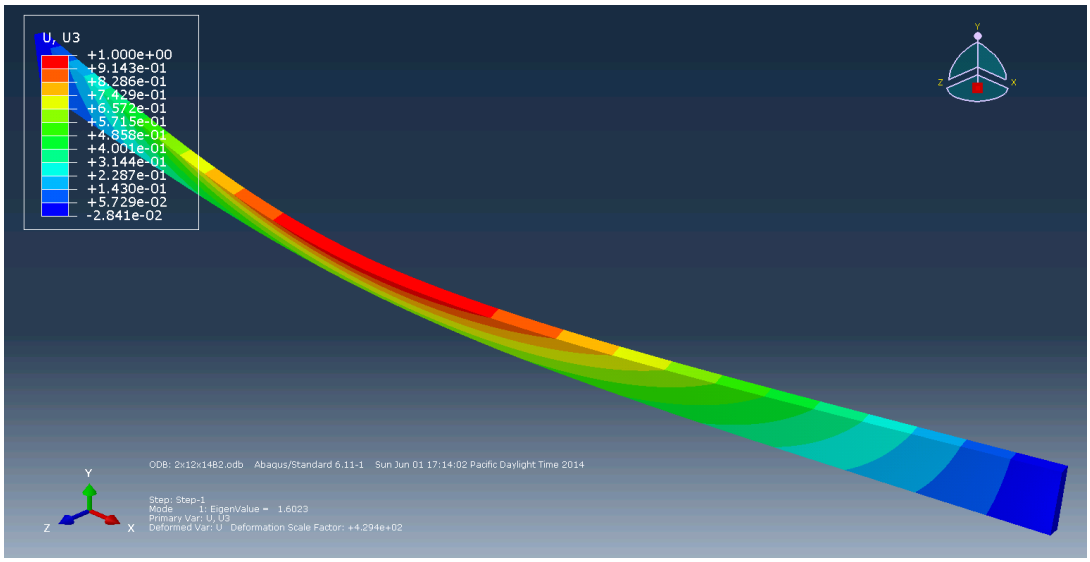

(b)

Figure A.10 Buckling mode of Beam 2 of 2”×12”×14’ specimens

(a) experimentally observed and (b) FEA predicted

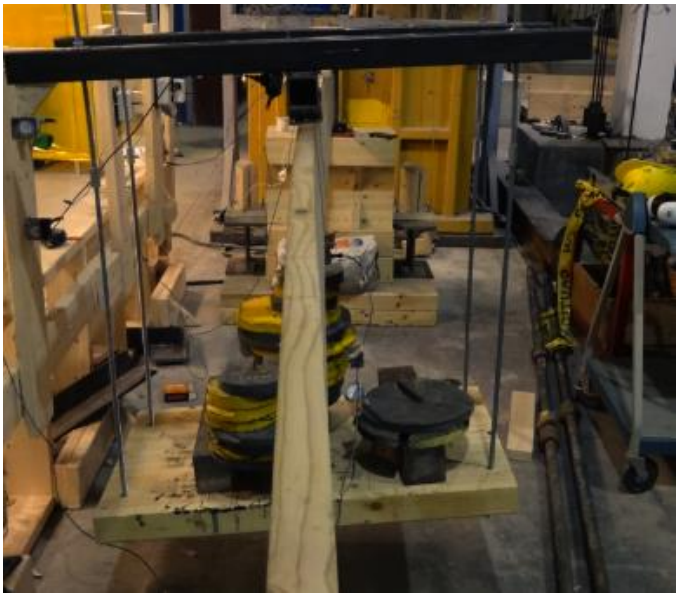

(a)

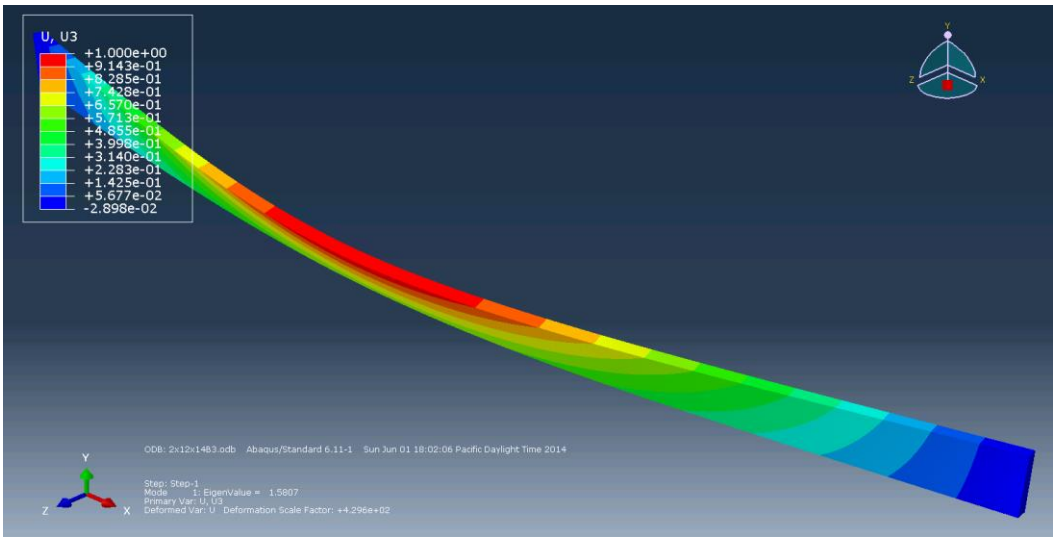

(b)

Figure A.11 Buckling mode of Beam 3 of 2”×12”×14’ specimens

(a) experimentally observed and (b) FEA predicted

(a)

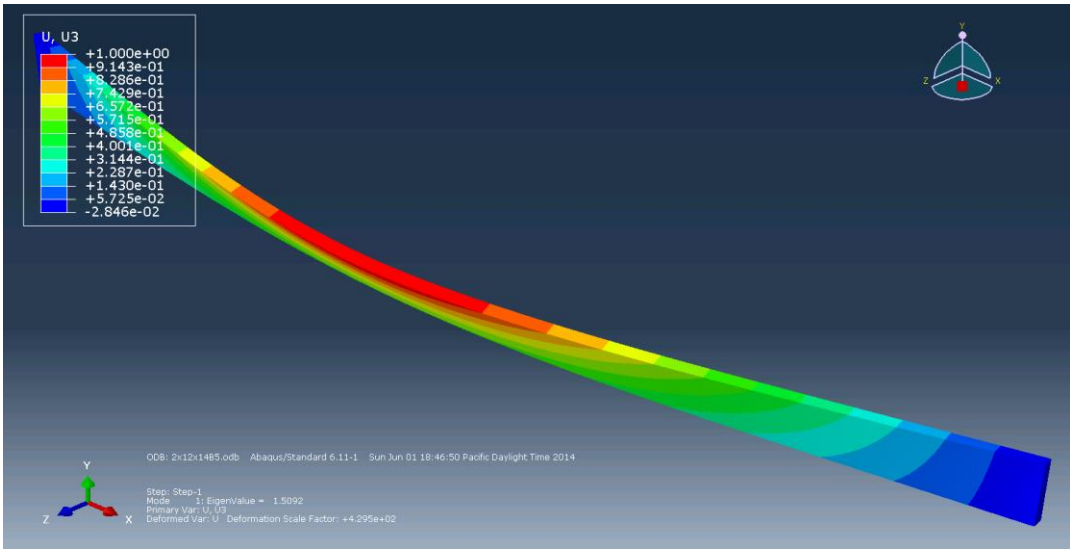

(b)

Figure A.12 Buckling mode of Beam 5 of 2”×12”×14’ specimens

(a) experimentally observed and (b) FEA predicted

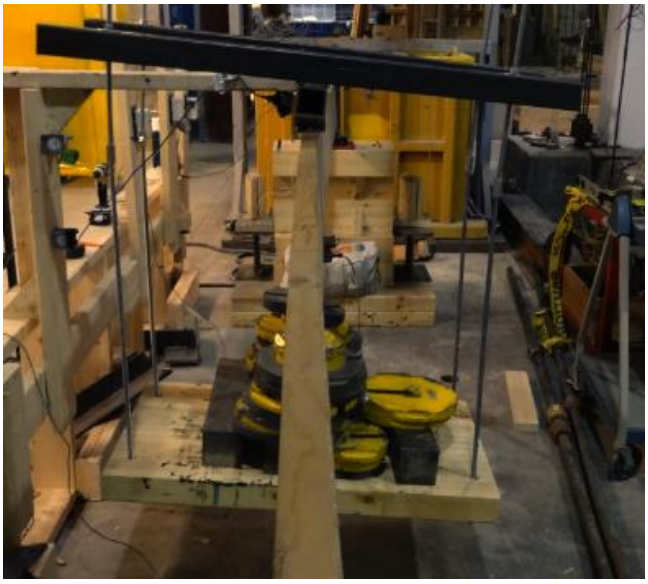

(a)

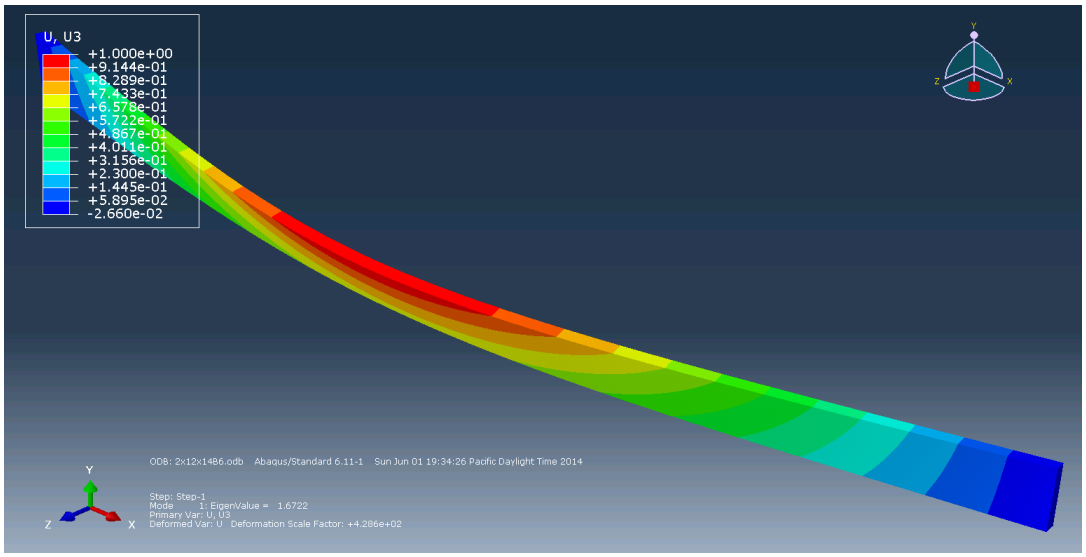

(b)

Figure A.13 Buckling mode of Beam 6 of 2”×12”×14’ specimens

(a) experimentally observed and (b) FEA predicted

Appendix B

Deformation of Lateral Torsional Buckling in Experiments

This appendix provides the applied load with corresponding twist, vertical and lateral displacement of mid-span for eleven (11) specimens form the experimental program. The lateral displacements were the measured at mid-height and at mid-span.

Observations

The tables show a direct relation between the applied load and twist, vertical displacement and lateral displacement of the beams.

Table B.1 Beam 1 of 2”×8”×14’ specimens

Load (N)	Twist (Degree)	Vertical displacement (mm)	Mid-height lateral displacement (mm)
1230	0	0	0
1319	0.00239	0.872	0.875
1408	0.00239	1.50	1.17
1497	0.00756	2.25	1.48
1586	0.0306	3.14	1.80
1675	0.0848	3.92	2.24
1764	0.123	4.85	2.69
1853	0.201	5.73	3.00
1942	0.262	6.59	3.88
2031	0.339	7.46	4.48
2120	0.563	8.76	6.21
2209	0.810	10.1	8.23
2298	1.37	12.0	12.1
2387	2.21	14.8	18.0
2476	3.52	21.2	30.1
3344	----	----	----

Note: ---- means the data was not recorded.

Table B.2 Beam 2 of 2”×8”×14’ specimens

LOAD (N)	Twist (Degree)	Vertical displacement (mm)	Mid-height lateral displacement (mm)
1229	0	0	0
1320	0.116	0.516	0.340
1411	0.100	1.20	0.882
1501	0.162	1.86	1.35
1592	0.185	2.52	1.98
1683	0.231	3.36	2.89
1773	0.301	4.07	3.38
1864	0.324	4.97	4.59
1955	0.301	5.82	5.86
2046	0.440	6.59	6.81
2136	0.532	7.64	8.36
2227	0.694	8.67	9.92
2318	0.887	9.81	11.9
2408	1.19	11.3	14.7
2499	2.19	13.6	20.2
2544	2.10	15.3	23.1
3719	----	----	----

Table B.3 Beam 3 of 2”×8”×14’ specimens

LOAD (N)	Twist (Degree)	Vertical displacement (mm)	Mid-height lateral displacement (mm)
1229	0	0	0
1320	0.031	0.712	0.233
1411	0.131	1.38	0.688
1501	0.278	2.24	1.32
1592	0.362	3.10	1.99
1683	0.447	4.01	2.60
1773	0.609	5.03	3.65
1864	0.733	5.91	4.66
1955	0.925	7.21	6.01
2046	1.15	8.34	7.59
2136	1.33	9.45	8.71
2227	1.61	10.8	10.6
2318	1.80	12.3	12.6
2408	2.11	13.9	15.0
2499	2.41	15.5	17.3
2544	2.58	16.4	18.5
2590	2.79	17.4	20.1
2635	2.99	18.7	22.3
2681	3.24	19.9	23.9
2726	3.42	21.5	26.9
2771	3.68	22.0	29.4
3576	----	----	----

Table B.4 Beam 4 of 2”×8”×14’ specimens

LOAD (N)	Twist (Degree)	Vertical displacement (mm)	Mid-height lateral displacement (mm)
1230	0	0	0
1319	0.00756	0.588	0.262
1408	0.00756	1.32	0.669
1497	0.0466	1.97	1.05
1586	0.185	2.95	1.84
1675	0.239	3.72	2.41
1764	0.333	4.45	2.98
1853	0.386	5.46	3.78
1942	0.789	6.38	4.18
2031	0.609	7.37	5.65
2120	0.694	8.57	7.02
2209	0.836	9.50	7.96
2298	1.04	10.5	9.02
2387	1.14	11.9	11.4
2476	1.47	13.5	13.5
2521	1.40	14.7	15.0
2565	1.51	22.2	23.4
2610	3.70	25.2	35.2
2654	4.23	30.3	41.8
2699	4.89	35.7	49.4
2743	5.87	42.5	55.9
3620	----	----	----

Table B.5 Beam 6 of 2”×8”×14’ specimens

Load (N)	Twist (Degree)	Vertical displacement (mm)	Mid-height lateral displacement (mm)
1229	0	0.00	0
1320	0.00796	0.56	0.0290
1411	0.0155	1.16	0.0775
1501	0.0356	1.82	0.0580
1592	0.077	2.50	0.271
1683	0.100	3.14	0.397
1773	0.131	3.82	0.514
1864	0.146	4.65	0.688
1955	0.185	5.42	0.873
2046	0.278	6.24	1.26
2136	0.316	7.05	1.58
2227	0.255	7.86	1.93
2318	0.439	8.75	2.72
2408	0.524	9.57	3.39
2499	0.640	10.4	4.29
2544	0.702	11.1	4.91
2590	0.826	11.7	5.61
2635	0.941	12.4	6.47
2681	1.10	13.1	7.71
2726	1.24	13.9	9.12
2771	1.38	14.6	10.3
2817	1.54	15.4	11.6
2862	2.00	17.3	15.6
2908	1.91	17.6	15.8
2953	2.35	19.6	19.6
2998	9.33	78.0	82.6
3610	----	----	----

Table B.6 Beam 2 of 2”×10”×12’ specimens

Load (N)	Twist (Degree)	Vertical displacement (mm)	Mid-height lateral displacement (mm)
3444	0	0	0
3533	0.034	0.010	0.116
3622	0.199	0.506	1.06
3711	0.205	0.506	1.05
3800	0.177	0.650	1.02
3889	0.182	0.826	1.07
3978	0.182	1.03	1.09
4067	0.193	1.26	1.12
4156	0.194	1.44	1.14
4245	0.182	1.84	1.07
4334	0.205	1.92	1.16
4423	0.216	2.16	1.28
4512	0.233	2.44	1.35
4601	0.245	2.69	1.42
4690	0.234	2.87	1.42
4779	0.233	3.10	1.41
4868	0.228	3.35	1.43
4957	0.239	3.59	1.59
5046	0.313	4.21	2.05
5135	0.347	4.28	2.26
5224	0.353	4.51	2.35
5313	0.410	4.86	2.69
5402	0.444	5.12	2.95
5491	0.467	5.39	3.12
5672	4.35	10.5	24.9

Table B.7 Beam 3 of 2”×10”×12’ specimens

Load (N)	Twist (Degree)	Vertical displacement (mm)	Mid-height lateral displacement (mm)
1928	0	0	0
2017	0.0059	0.145	0.281
2106	0.0685	0.723	1.07
2195	0.0229	1.02	0.814
2284	0.0737	1.24	1.64
2373	0.310	1.52	3.06
2462	0.367	1.90	4.69
2551	0.524	2.28	6.67
2640	0.688	2.58	8.42
2729	0.928	3.12	11.4
2818	1.27	3.77	14.9
2907	1.60	4.31	18.6
2996	2.29	5.31	25.8
3085	3.19	7.31	36.0
3174	4.36	10.3	46.2
3341	----	----	----

Table B.8 Beam 5 of 2”×10”×12’ specimens

Load (N)	Twist (Degree)	Vertical displacement (mm)	Mid-height lateral displacement (mm)
3485	0	0	0
3576	0.00588	0.010	0.0290
3667	0.0223	0.217	0.0770
3758	0.0341	0.217	0.116
3848	0.0626	0.372	0.243
3939	0.0629	0.496	0.242
4030	0.0740	0.640	0.339
4120	0.103	0.805	0.485
4211	0.0855	0.940	0.495
4302	0.091	1.07	0.485
4392	0.120	1.26	0.669
4483	0.148	1.40	0.872
4574	0.165	1.59	0.979
4665	0.160	1.70	1.05
4755	0.136	1.91	1.11
4846	0.165	2.04	1.27
4937	0.165	2.23	1.29
5027	0.182	2.34	1.42
5073	0.222	2.35	1.64
5118	0.245	2.57	1.77
5163	0.250	2.59	1.88
5209	0.251	2.79	1.96
5254	0.274	2.80	2.02
5299	0.273	2.80	2.04
5345	0.303	3.01	2.09
5390	0.285	3.02	2.17
5436	0.285	3.19	2.19
5481	0.319	3.24	2.52
5526	0.325	3.25	2.53
5572	0.364	3.41	2.89
5685	0.462	3.57	3.60
5784	0.478	3.59	3.88
5875	0.672	3.99	5.37
5965	0.934	3.99	7.11
6030	0.997	3.97	7.72
6111	1.14	3.97	8.94
6191	1.22	3.98	9.53
6300	----	----	----

Table B.9 Beam 8 of 2”×10”×12’ specimens

Load (N)	Twist (Degree)	Vertical displacement (mm)	Mid-height lateral displacement (mm)
3444	0	0	0
3533	0.0570	0.217	0.465
3622	0.148	0.620	1.12
3711	0.228	0.950	1.71
3800	0.290	1.31	2.41
3889	0.398	1.80	3.20
3978	0.524	2.40	4.34
4067	0.626	2.90	5.18
4156	0.688	3.44	6.25
4245	0.831	4.06	7.35
4334	1.031	4.81	8.87
4423	1.720	7.63	14.8
4512	8.799	42.7	61.5

Table B.10 Beam 1 of 2”×12”×14’ specimens

Load (N)	Twist (Degree)	Vertical displacement (mm)	Mid-height lateral displacement (mm)
2540	0	0	0
2629	0.00233	0.929	0.0970
2718	0.0182	1.22	0.155
2807	0.113	2.48	0.514
2896	0.217	4.85	1.11
2985	0.357	8.19	2.01
3074	0.542	11.7	3.06
3163	0.935	17.9	5.53

Table B.11 Beam 2 of 2”×12”×14’ specimens

Load (N)	Twist (Degree)	Vertical displacement (mm)	Mid-height lateral displacement (mm)
1633	0	0	0
1722	0.235	0.0720	1.18
1811	0.375	0.0720	2.06
1900	0.515	0.0310	3.02
1989	0.573	0.134	3.52
2078	0.754	0.238	4.66
2167	0.907	0.314	6.10
2256	1.06	0.475	7.30
2345	1.24	0.712	8.66
2434	1.36	0.878	9.99
2523	1.59	1.04	11.9
2612	1.73	1.24	13.2
2701	1.93	1.71	15.2
2790	2.21	2.12	17.7
2879	2.57	2.54	21.0
2968	2.33	3.02	20.3
3057	2.50	3.46	22.0
3146	3.35	4.99	29.0
3191	4.65	8.13	40.7
3235	5.93	12.7	51.2
3280	6.07	13.9	53.1